PROCESSING-PERFORMANCE RELATIONSHIPS FOR

FIBRE-REINFORCED COMPOSITES

by

AMJED SALEH MAHMOOD

A thesis submitted to the University of Plymouth in partial fulfilment for

the degree of PhD

DOCTOR OF PHILOSOPHY

School of Marine Science and Engineering

Faculty of Science and Engineering

October 2015

PROCESSING-PERFORMANCE RELATIONSHIPS FOR FIBRE-REINFORCED COMPOSITES

Abstract

The present study considers the dependence of mechanical properties in composite laminates on the fibre architecture. The objective is to characterise the mechanical properties of composite plates while varying the fibre distribution but keeping the constituent materials unchanged. Image analysis and fractal dimension have been used to quantify fibre distribution and resin-rich volumes (RRV) and to correlate these with the mechanical properties of the fibre-reinforced composites. The formation, shape and size of RRV in composites with different fabric architectures is discussed. The majority of studies in literatures show a negative effect of the RRV on the mechanical behaviour of composite materials. RRV arise primarily as a result of (a) the clustering of fibres as bundles in textiles, (b) the stacking sequence, and/ or stacking process, (c) the resin properties and flow characteristics, (d) the heating rate as this directly affects viscosity and (e) the consolidation pressure. Woven glass and carbon/epoxy fabric composites were manufactured either by the infusion or the resin transfer moulding (RTM) process. The fractal dimension (D) has been employed to explore the correlation between fabric architecture and mechanical properties (in glass or/ carbon fibre reinforced composites with different weave styles and fibre volume fraction). The fractal dimension was determined using optical microscopy images and ImageJ with FracLac software, and the D has been correlated with the flexural modulus, ultimate flexural strength (UFS), interlaminar shear strength (ILSS) and the fatigue properties of the woven carbon/epoxy fabric composites.

The present study also considers the dependence of fatigue properties in composite laminates on static properties and fibre architecture. Four-point flexural fatigue test was conducted under load control, at sinusoidal frequency of 10 Hz with amplitude control. Using a stress ratio ($R=\sigma_{min}/\sigma_{max}$) of 0.1 for the tension side and 10 for the compression side, specimens were subjected to maximum fatigue stresses of 95% to 82.5% step 2.5% of the ultimate flexural strength (UFS). The fatigue data were correlated with the static properties and the fibre distribution, in order to obtain a useful general description of the laminate behaviour under flexural fatigue load. The analysis of variance (ANOVA) technique was applied to the results obtained to identify statistically the significance of the correlations. Composite strength and ILSS show a clear dependence on the fibre distribution quantified using D. For the carbon fabric architectures considered in this study, the fatigue properties of composite laminates have significant correlations with the fibre distribution and the static properties of the laminates. The loss of 5-6 % in the flexural modulus of composite laminates indicates an increasing risk of failure of the composite laminates under fatigue loads. The endurance limits, based on either the static properties or the fibre distribution, were inversely proportional to the strength for all laminates.

List of contents

List of Figures

[XIV]

List of Tables

Nomenclature (list of symbols)

<u>Acronyms</u>

A	Fatigue strength exponent
A_F	Areal weight of fabric
ANOVA	Analysis of variance
AP	Angle-plied unidirectional laminates composites
B	Fatigue strength coefficient
CFRP	Carbon fibre reinforced polymer
CT	Computerised tomography
D	Fractal dimension
DIC	Digital image correlation
E	Flexural modulus
E_b	Flexural modulus
E_f	Elastic modulus of fibre
E_{ff}	Flexural modulus under fatigue test
E_m	Elastic modulus of matrix
E_o	Original flexural modulus
E_t	Predicted elastic modulus (rules-of-mixtures)
FDI	Fatigue damage index
FERF	Flow-enhancement reinforcement fabric
F_{max}	Maximum load
FRV	Fibre-rich volumes
Fε	Fibre-containing boxes
I	Second moment of area
ILSS (τ)	Interlaminar shear strength
L	Span of the sample
LCM	Liquid compsite moulding
N	Number of cycles of fatigue test
NCF	Non crimp fabric
N_f	Number of cycles at failure
OOA	Out-of-autocalve
P	Plain weave fabric
R	Stress ratio
R	Pearson correlation coefficient
RIFT	Resin infusion under flexible tool
ROI	Region of interest
RRV	Resin-rich volumes
RTM	Resin transfer moulding
S	Fatigue stress
SRCL	Synchrotron radiation computed laminography
SRCT	Synchrotron radiation computed tomography
STDEV	Standard deviation
T	Twill weave fabric
TB	Twill basket weave fabric
UD	Aligned unidirectional laminates composites
UFS	Ultimate flexural strength
UTS	Ultimate tensile strength
V_f	Fibre volume fraction
VOC	Volatile organic components

V_v	Void volume fraction
XP	Cross-plied unidirectional laminates composites
a	Displacement between load point and support point
b	Width of the sample
d	Deflection at mid-point of the sample
h	Thickness of the sample
i	Iteration step in ImageJ software
m	mass
n	Number of fabric layers
n	Sample size
nd	Number of data points
ni	Number of images
p	A value used for testing a statistical hypothesis
t	Laminate thickness
wp	Warp direction
wt	Weft direction
ε	Box size
η_O	Fibre orientation distribution factor
θ	Crimp angle
ρ_f	Density of the faibre
σ_{min}	Minimum stress
σ_{max}	Maximum stress
ω_n	Natural frequency
μCT	Micro computerised tomography
| |	Absolute value

Acknowledgements

Numerous people have greatly contributed to the development of this thesis during the last four years. I want to express now my most sincere thanks to them all.

Grateful thanks are due to the Director of my Studies, Professor M Neil James, Head of School of Marine Science & Engineering/ Associate Dean, Plymouth University for his support and guidance during my study.

The author is grateful to his supervisors, Dr John Summerscales, Associate Professor (Reader) in Composites Engineering, Plymouth University, and Dr Richard Cullen, Senior Technician, Plymouth University, for their expert guidance, advice, support, and encouragement. They have generously provided me with everything I needed. Without their help this work would never have been possible.

The author would especially like to thank Mr. Eric Taylor at Carr Reinforcements for dedicating time and resources to our request for fabrics woven in different styles from consistent batches of carbon fibre, Mr. Terry Richards (testing & microscopy), Dr. Zoltan Gombos (CT scan) and Mr. Peter Bond (image analysis) for their assistance with the experimental work.

Also, the author gratefully acknowledges the financial support provided by the Iraqi government and the Ministry of Higher Education and Scientific Research (MOHESR) for this doctoral study at Plymouth University.

The author is grateful to Plymouth University for research, training and language sessions during his study.

Author's declaration

At no time during the registration for the degree of Doctor of Philosophy has the author has been registered for any other University award without prior agreement of the Graduate Committee.

Relevant scientific seminars and conferences were regularly attended, at which work was often presented; external institutions were visited for consultation purposes and several papers prepared for publication. The details are on the following pages.

Signed...

Date...

Conference papers:

- Processing-performance relationships for fibre-reinforced composites. Presented at the postgraduate society conference 11th March 2013 at Plymouth University (Second prize of the best oral presentation).

- Using Fractal dimension to quantify the microstructure of fibre reinforced composites. Presented at the international conference (CompositesWeek@Leuven and TexComp-11) in KU Leuven, Belgium, 19th September 2013 (Oral presentation).

- Using Fractal dimension to quantify the microstructure of fibre reinforced composites. Presented at the postgraduate society conference 17th June 2014 at Plymouth University (First prize of the best oral presentation).

- Quantification of fibre distribution and the correlation with mechanical properties for woven composites. Presented at the postgraduate society conference 23rd June 2015 at Plymouth University (Oral presentation).

External training attended:

- GRADSchool: residential development opportunity for PhD researchers 1st – 4th July 2013. Buckland Hall, Brecon Beacons, Wales

- A course for PhD students "Analysis and Design Optimisation of Laminated Composite Structures" at Aalborg University_ Denmark 19th - 23rd May 2014.

- 2nd Annual Conference of the ACCIS Doctoral Training Centre at University of Bristol.

- The Cumberland Lodge Conference: 'Life Beyond the PhD' 15th - 18th August 2015. (Oral and poster presentations).

External Contacts:

- Word count of the thesis: 36924

Chapter 1 INTRODUCTION

1.1 Introduction

The increasing demand for high performance materials, (i.e. those which have high modulus- and/or high strength-to-weight ratio combined with improved fatigue performance and high toughness) has led to rapid advances in the field of fibre–reinforced composites. The global estimated demand could reach 146,000 tonnes of carbon fibre composites produced annually by 2020 for different applications [1]. Composite materials are widely used in the transportation sector, especially in aerospace where, for example, >50% of the structural weight in the Airbus A350XWB and Boeing B787 Dreamliner are manufactured from epoxy composites. Generally, fibre-reinforced polymer composites consist of two materials, fibre-reinforcement (e.g. glass, carbon and aramid) in a resin matrix (epoxy or other polymers); consolidated together to produce a material that has different and enhanced properties compared with its constituent materials. Composite material properties depend on various parameters such as the type of each material, the volume fraction of each material, the geometrical orientation and distribution of fibres and the manufacturing process.

High-performance composites often use autoclave consolidation to improve their mechanical properties by increasing the fibre volume fraction, and hence reducing the defect population. Autoclaves are, however, both an expensive capital equipment cost and a significant constraint on the rate of production. There is therefore increasing interest in composite manufacturing processes which do not require the autoclave stage, e.g. the resin transfer moulding process (RTM). Whilst elimination of the autoclave stage during manufacturing can increase the production rate of composite components and significantly

[3]

reduce the energy consumption, it can also lead to lower fibre volume fractions (V_f) due to the compressibility characteristics of the fibres [2-5]. The lower V_f, obtained at reduced pressure, may lead to resin-rich volumes (RRV) in the composite and a consequent disproportionate reduction in the mechanical properties of the composite laminates[1]. The level of RRV is highest in spray-up and hand-lamination techniques (no consolidation pressure), less common in out-of-autoclave (OOA) and liquid composite moulding (LCM) procedures, and lowest in autoclave and compression moulding processes. Hence increasing the pressure during manufacturing reduces the RRV especially with autoclave consolidation [6, 7] due to the nesting of fibres, and that leads to improved mechanical properties (both static and fatigue).

The author cautions against studying only the effect of fibre volume fraction on the performance of composite laminates unless the effect of changing the fibre architectures and the consequent RRV are fully understood for the reinforcement system in use. Therefore, the manufacture of different laminates with similar manufacturing parameters and different fibre architectures could be useful to correlate the effect of the fibre architectures and the consequent RRV to the static and the fatigue properties of fibre-reinforced composites.

Improvements in mechanical properties and especially fatigue properties of fibre-reinforced composites are desirable [8] for the reason that most failures that occur in composite materials are due to fatigue where cyclic stress occurs [9]. The anisotropic properties of composites give rise to various damage mechanisms [10]. Failure is therefore difficult to predict in composites due to their inhomogeneous and anisotropic properties. Furthermore, the prediction of

---

[1] Mahmood, A.S., James, M.N. and Summerscales, J. The influence of resin-rich volumes (RRV) on the performance of fibre-reinforced composites, a draft of a review paper.

composite life is of great interest to researchers due to the possibility of reduced production cost through proper design, and to reduced risk in transportation vehicles and civil structures. For that reason, the fatigue life and the degradation of the mechanical properties of composites are issues of great importance. However, developments in the fatigue properties and life prediction in composite materials remains complex due to the anisotropic properties of composites. In addition, the fatigue life and the mechanical properties of composite materials depend on many factors, including matrix material, fibre material, volume fractions, fibre orientation, moisture content, voids and porosity, applied stress, strain rate, and stress amplitude [10, 11].

Due to the complexity of the problem, research in this area and the amount of experimental data and information available are relatively limited. Most researchers have studied the effect of different parameters on the mechanical properties of composite laminates. However, no study has had a primary focus on the effect of the uniformity of the fibre distribution and RRV on the fatigue properties of fibre-reinforced composites[2]. Furthermore, using fibre volume fraction (V_f) alone to calculate the mechanical properties of the laminates does not account for the effects of different fibre architectures. New research should seek to understand why there are different mechanical properties in laminates that are manufactured with similar manufacturing parameters and different fibre architectures.

Consider three laminates which have identical manufacturing parameters (unidirectional fibre, resin type, thickness, fibre volume fraction….etc.), but different fibre distributions. Figure 1.1 shows idealised microstructure images

---

[2] I offer my apologies to the authors of any studies that might have been missed despite searching up to the time of writing this thesis.

for ten fibre bundles occupying the same area fraction. The distribution of the bundles is obviously different in each case and the fractal dimension quantifies the microstructure variations from left to right as 1.7198, 1.722 and 1.7366.

So, this raises the questions of (a) are the mechanical properties of laminate 1 higher than laminates 2 and 3 or lower? …. and (b) what is the effect of using woven fabric or any other type of fabric instead of unidirectional fabric?

Laminate 1   Laminate 2   Laminate 3
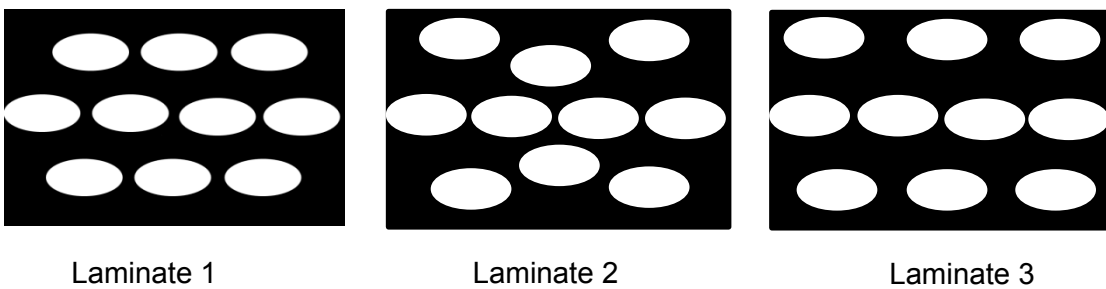
Figure 1-1: Three idealised composite microstructures with ten fibre bundles (i.e. similar fibre volume fraction) and different fractal dimension.

This study considers experimental static and fatigue tests. Fractal dimension will be employed to explore the correlation between fabric architecture and mechanical properties (in glass or carbon fibre reinforced composites with different weave styles and fibre volume fraction), in order to answer the following questions:

- Why are there different mechanical properties (static and fatigue) for laminates that are manufactured with similar manufacturing parameters and different fibre architectures?

- Is there any correlation between the static properties and the uniformity of the fibre distribution of the composite laminates and, if so, what is it?

[6]

- Is there any correlation between the fatigue properties and the uniformity of the fibre distribution of the composite laminates and, if so, what is it?

- Is there any correlation between the fatigue properties and the static properties of the fibre-reinforced composites laminates and, if so, what is it?

- Is it possible to predict the fatigue life of the composite laminates based on the static properties and the fibre distribution of the laminates?

- Is it possible to use the above-mentioned correlations for various types of fabric?

1.2 Motivation of the research

Many researchers have studied the effect of processing parameters on the properties of composites, but few have focused on the effect of the uniformity of the fibre distribution on the fatigue of composite laminates. Therefore, this project is believed to be the first to correlate fractal dimensions of sections of continuous woven reinforcement fabric laminates with the fatigue properties. In addition, this study will contribute to knowledge of the following issues:

- Correlations that may exist between the uniformity of the fibre distribution and the mechanical properties of the composite laminates and that could lead to improved performance of the composites.

- Whether using fractal dimension (D) can sensibly reduce an image of the key aspects of the microstructure to a single real number and hence assist in characterising the microstructure.

[7]

- Whether predicting the mechanical properties of woven fabrics from specific microscopic images will allow a reduction in the time and the cost of mechanical tests (static and fatigue) necessary to characterise a composite material.

- Explaining the difference between the mechanical properties of laminates with similar fibre volume fraction and differing fibre bundle architecture.

- Improving theoretical approaches to characterising the static and the fatigue properties of composite laminates.

- Predicting the life of composite laminates based on either the static properties or the analysis of the microstructural images and hence could lead to reduced risk of failure of the composite structures.

- Modifying fibre architectures to improve the performance of fibre-reinforced composites.

In addition to other researchers in this aspect of composite materials, the most direct beneficiaries from this project could be manufacturers of the composite laminates (e.g. companies that manufacture aircraft, spacecraft, cars, ships, boats and sports equipment) because they may be able to manufacture composite laminates without an autoclave stage, and this may contribute significantly to increasing the production rate and reducing the energy consumption of the production stages. In turn this would save significant money and time. Therefore, this could foster the global economic performance, and specifically the economic competitiveness of the United Kingdom. In addition, it may increase the effectiveness of public services and enhance the quality of life, health and creative output.

1.3 Objectives

The overall aim of the project is to understand the effect of the fibre distribution and RRV on the mechanical properties of composites, and the contribution arising from process parameters such as the fibre distribution, the RRV size and shape, the manufacturing process type, infusion pressure, and number of laminate layers. The desired outcome is that the properties of advanced composites can be predicted using appropriate formulae based on newly developed relationships between measured properties and microstructures. The initial study will determine whether using the fractal dimension with the box-counting method has the ability to describe the fibre distribution effect and then, whether the fractal dimension is suitable to distinguish the differences between various fibre architectures. Therefore, the research will follow the methodology below to reach its aims:

a-   Glass fibre-reinforced composites will be manufactured by an infusion process using several different infusion pressure levels.

b-   The microstructure of the samples will be quantified using optical microscopy with Olympus and ImageJ with FracLac software software for image processing and analysis to quantify features using fractal dimension.

c-   Samples will be tested for static mechanical properties such as tensile modulus, strength and strain to failure and interlaminar shear strength, ILSS.

d-   Correlations will be sought between:

[9]

    i.   Measured properties and microstructures quantified as fractal dimension.

    ii.   Measured properties and fibre volume fraction and compare them to the fractal dimension correlations.

e-   Carbon fibre-reinforced composites will then be manufactured by resin transfer moulding, RTM, with various fibre distributions and number of layers.

f-   Samples will be tested for static mechanical properties such as flexural modulus, strength and strain to failure and interlaminar shear strength, ILSS.

g-   Samples will be tested in fatigue using 4-point bending tests to determine S/N curves for the various composite laminates.

h-   Correlations will then be sought between measured properties (static and fatigue) and microstructures quantified as fractal dimension.

i-   Finally, an empirical model will be identified for the fatigue behaviour of composites in terms of the uniformity of the fibre distribution and static properties.

j-   Attempts will be made to use X-ray computerised tomography (CT) to understand and predict the initiation of failure in the woven carbon/epoxy laminates under fatigue load.

k-   The validity of the static and fatigue models will be checked by applying them to other types of laminate.

Figure 1.2 is a flowchart indicating research activities and the path required to complete the study.

1.4 Structure of the thesis

Chapter One provides an introduction to the research topic and the principal research questions. It explains the significance and the motivation of the research, the primary aims, objectives and the structure of the thesis.

Chapter Two systematically reviews the existing literature relating to composite mesostructure, including the RRV and fibre distribution effects, static and fatigue properties of fibre-reinforced composites and the various numerical and experimental techniques that have been used in these studies. A key concept is the quantification of mesostructural images using fractal dimension.

In Chapter Three the experimental methodology that was employed is presented. This includes details of the laminate manufacturing process and the resulting laminates (materials used plus process parameters), microstructural characterisation: preparation, image capture, analysis (including an investigation of the suitability of the box counting method as a route to fractal dimension in composite laminates), static mechanical properties, fatigue properties and failure analysis. In Chapter Four, the results are presented for all the materials and processing parameters studied as detailed in Chapter Three. Chapter Five considers applying the observed correlations to a different (basket weave) fabric. Finally, Chapter Six presents some general conclusions and a discussion of the study's findings, leading to some appropriate recommendations for future work.

[11]
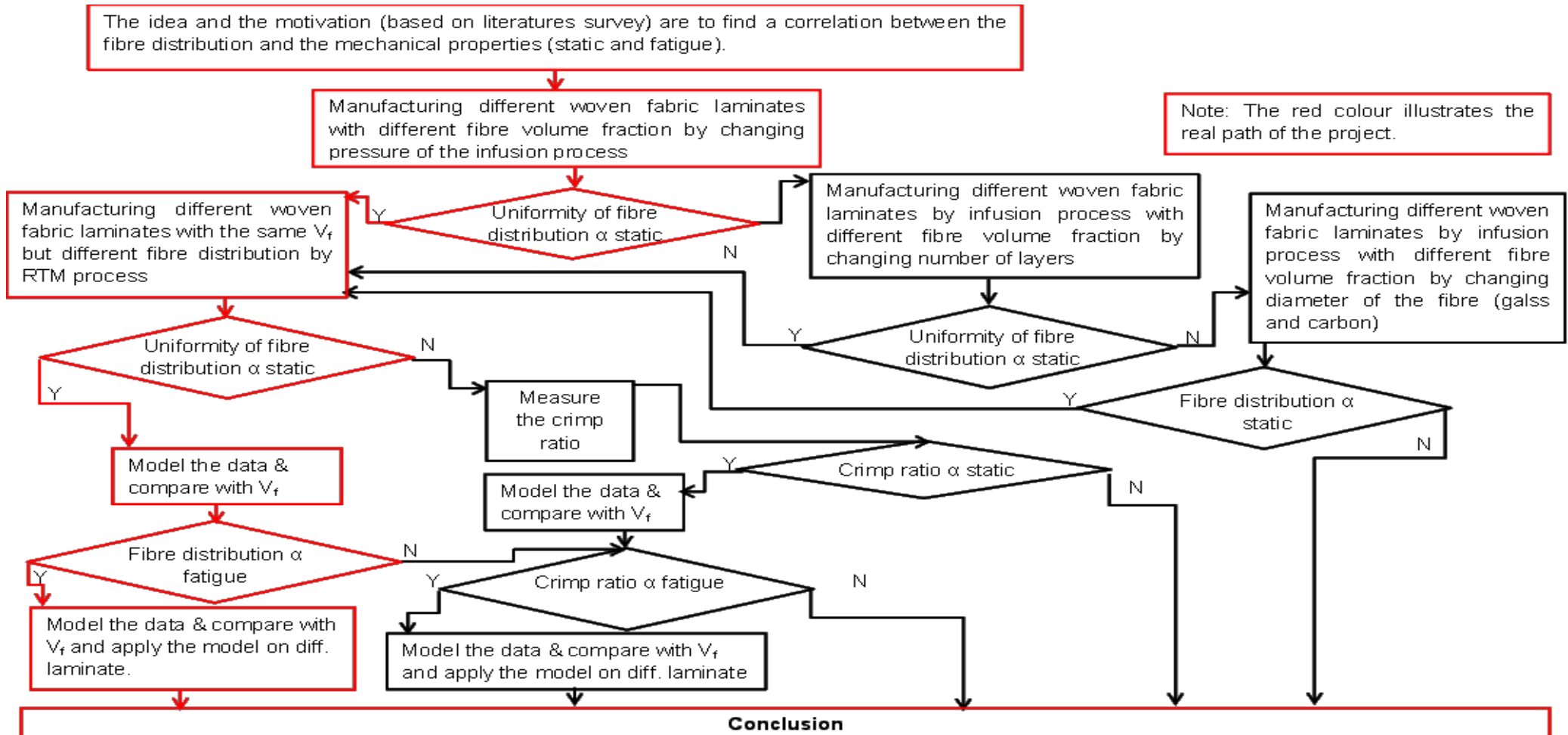
Figure 1-2: The research activities and the path required to complete the study.

Chapter 2 LITERATURE REVIEW

2.1 Introduction

This chapter reviews the literature relating to composite mesostructure, including the RRV and fibre distribution effects, static and fatigue properties of fibre-reinforced composites and the various numerical and experimental techniques that have been used in these studies. A key concept is the quantification of images, i.e. mesostructures, using fractal dimension.

2.2 Mesostructure analysis for fibre-reinforced composites

Characterising a multiphase material can involve an analysis at a micro-, meso- or macro-structural level, as all of these can influence the properties and performance of the material. In the case of a composite laminate it is most effective in terms of time and information to perform a mesoscale analysis (see Figure 2.1) that deals with millimetre length scales and describes the fibre volume fraction, the fibre distribution and variations of the fibre direction inside the laminate. Previous research has used mesostructural information to analyse and simulate the behaviour of composite materials [12-17], and found it to be an effective tool for the analysis of fibre reinforced composites, since tow distributions take the form of repeated arrangements for many types of composite fabrics (e.g. woven, non-crimp and braided fabrics). Furthermore, it is time consuming and complex to model the behaviour of composite laminates at the micro level, because the fibres may be irregularly distributed both within the tow and through the laminate and the fibres may have different shapes and diameters.

Micro (µm)   meso (mm)   macro (m)

Length scale
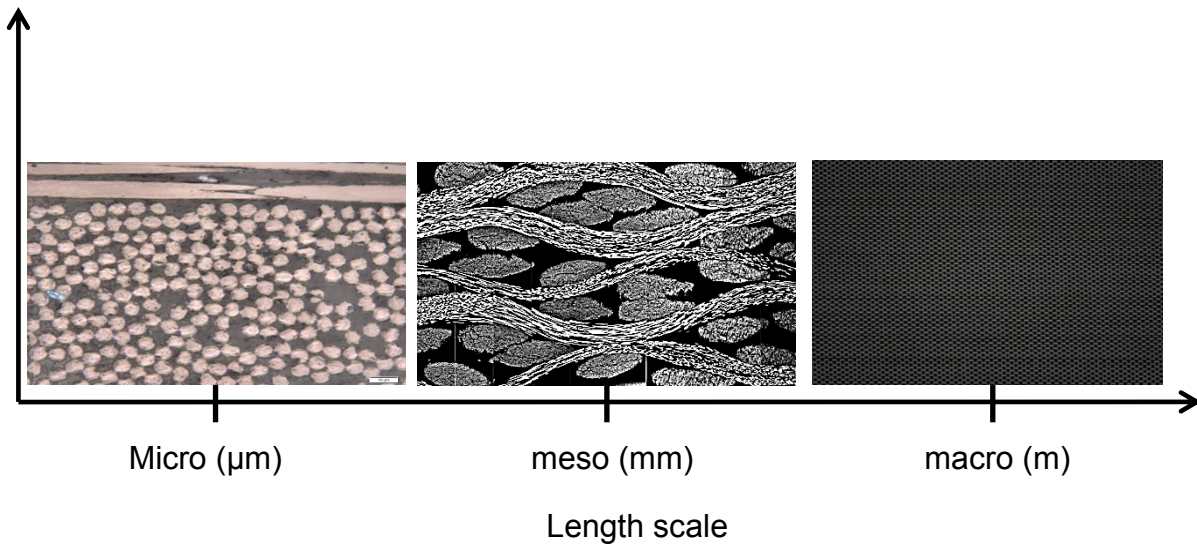
Figure 2-1: The composite laminates of this study at different structural scales: from micro through meso to macro.

To achieve the required objectives of the study, the literature review is focused on three main technical areas:

- The effect of the RRV and the uniformity of the fibre distribution on the mechanical properties of fibre-reinforced composites;

- A review of the fatigue properties of fibre-reinforced composites, and the main factors that affect this property;

- The measurement of features in microscopic images for composites and homogeneous materials, and the best method to measure the uniformity of the fibre distribution in the mesostructure analysis.

2.3 The effect of the RRV and fibre distribution on the performance of composites

Using fibre volume fraction (V_f) alone to characterise the mechanical properties of laminates does not provide an adequate account of the effects of different fibre architectures. Uniform distribution of fibre minimises resin-rich volumes

[16]

while fibre clustering inevitably creates RRV. Most studies discuss RRV in the context of different processing parameters. No known published work has a primary focus on controlling their size, shape or distribution within the laminate.

2.3.1 Overview

For an increasing number of layers of a specific reinforcement in a constant thickness laminate, as the fibre volume fraction increases, there will inevitably be a decrease in RRV measured as their number, individual volume and total volume. The level of RRV will be highest in spray-up and hand-lamination (no consolidation pressure), less common in out-of-autoclave (OOA) and liquid composite moulding (LCM), and lowest in autoclave and compression moulding processes as shown in Figure 2.2.

This section considers the effect of the RRV and the fibre distribution, on the mechanical and physical behaviour of composites, in order to understand the performance of composite materials. It reviews published work in the context of its relevance to the following questions:

- What is the influence of processing parameters on the formation, shape and size of RRV in composites with different fabric architectures?

- What procedures and techniques can be used to measure RRV?

- What is the effect of voids within RRV?

- What is the effect of the RRV on the behaviour of fibre-reinforced composite materials?

[17]
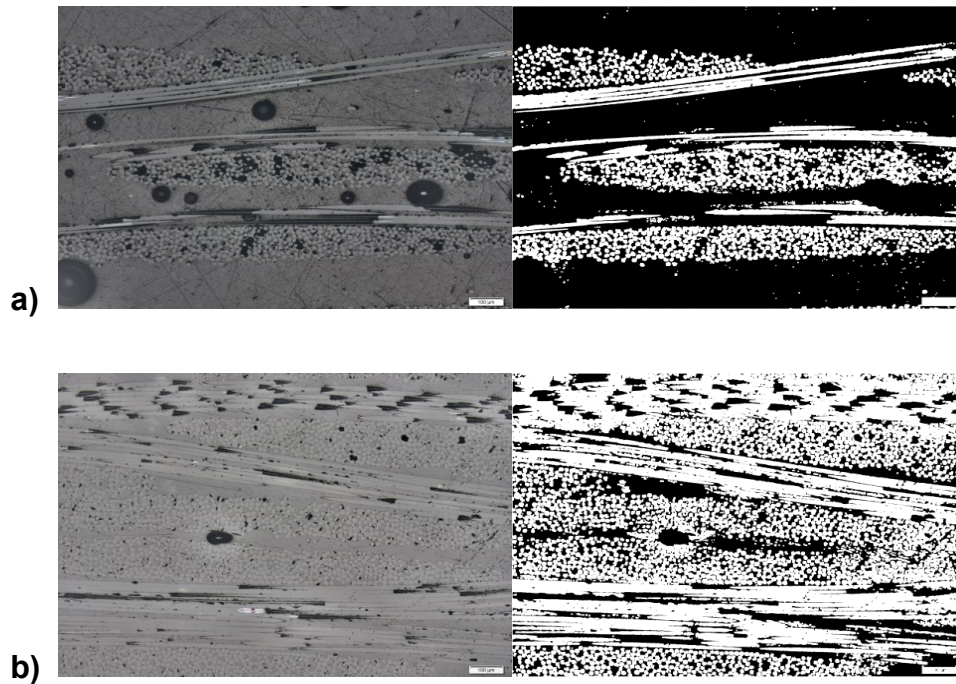
Figure 2-2: Typical micrographs (original (left) & binary (right)). (a) Hand lamination composite (V_f=27 %) and (b) Vacuum infused composite (V_f=66 %). The same reinforcement shows increased RRV (black in the image) at top (no) consolidation pressure.

2.3.2 Production of composites and consequent RRV

This section considers the influence of processing parameters on the formation, shape and size of RRV for (i) aligned and cross/angle-plied unidirectional (UD) composites, (ii) two-dimensional (2D) woven fabric, (iii) three dimensional (3D) woven fabric, and (iv) stitched Non Crimp Fabric (NCF). Conclusions regarding composites manufacture and RRV are then presented.

Lower compression pressure will reduce V_f and uncured resin flow; increase the RRV and the void fraction [18]. Furthermore, *the pore spaces* are filled with resin during the flow, consolidation and cure process to create the RRV [19]. The resin flow in some consolidation processes can displace fibres and create gaps which fill with resin to form the RRV [20]. Gaps are also created due to *clustering of fibres* to create a space which becomes the RRV [21]. Increasing

[18]

the *manufacturing pressure* as mentioned in section 2.3.1 will reduce the RRV especially with autoclave consolidation [6, 7] due to the nesting of fibres. The RRV amount depends on *the design of the product, fibre layout and the stacking sequence*.

RRV have been found to be proportional to *resin viscosity* changes by adding nano particles [22] or by varying *the heating rate* of the manufacturing process [23].

2.3.2.1 Aligned unidirectional (UD), cross-plied (XP), and angle-plied (AP) unidirectional laminae composites

The RRV in UD, XP and AP unidirectional laminae composites are caused by different processing parameters which are related.

Costa et al. [24] consolidated prepreg carbon fibre laminates in a stacking sequence $[0,90]_{14}$. They showed that the RRV with voids are distributed at ply interfaces and that cracks in the RRV initiate at the *void tips*.

Chensong [25] tried to model the formation of the RRV in glass fibre (351 g/m^2) angled composite parts using applied mechanics. It was shown that RRV thickness was inversely proportional to radius of a corner and fibre volume fraction. The RRV thickness in unidirectional (UD) composites was found to be larger than that for cross-plied laminates due to the better compressibility of the UD material. The study used open channel moulds, and the experimental results show an average of 20% difference with the model.

2.3.2.2 Two-dimensional (2D) woven fabric

The difference between the processing parameters that create the RRV in 2D woven fabric and UD fabric are related to *fabric architecture*. Furthermore, Cartié et al. [26] studied the delamination of Z-pinned carbon fibre reinforced laminates and found that the RRV surround the Z-pin. In manufacturing U-beams the reinforcement pulls tight around the inner corners and results in the RRV on the outer surface [27].

2.3.2.3 Three dimensional (3D) woven fabric

In 3D woven fabric, additional parameters are present to those in UD and 2D woven fabric, which have a great effect on distribution and size of the RRV including weave style and distribution of *the out-of-plane binder yarn* reinforcement [28, 29], *binder yarn path* [30, 31] and *level of compaction* [28, 30].

2.3.2.4 Stitched Non Crimp Fabric (NCF)

Mouritz et al. [32] reviewed the effect of stitching on the in-plane mechanical properties of fibre reinforced composites and found that the stitching causes the RRV. According to different researchers, *the stitches* of the NCF create the RRV [33-39] as shown in Figure 2.3. The shape of the RRV depends on the stacking sequence of the composite laminates [37, 38]. The size of the RRV are controlled by the yarn size and stacking sequence [37].
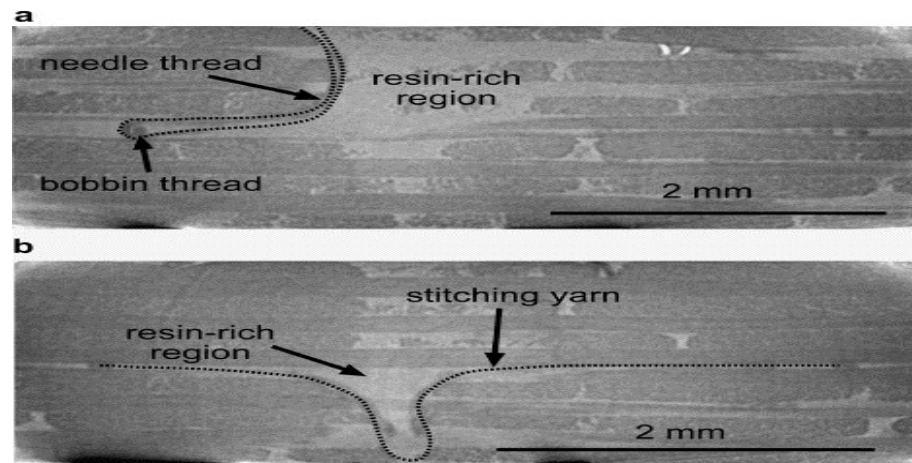
Figure 2-3: (a) the stitching seam direction perpendicular to the image plane, and (b) the stitching seam laying in the image plane. (reproduced from [39] with the permission of the authors and the publishers).

2.3.2.5 Conclusions regarding composites manufacture and RRV

The literature clearly indicates that consolidation increases fibre volume fraction and in consequence reduces the size of RRV. For a given reinforcement, and a constant reinforcement, the change from (i) autoclave or compression moulding to (ii) out - of – autoclave, vacuum bagging, RTM or RIFT to (iii) hand lay-up (or spray-up) will increase the extent of RRV. Figure 2.4 illustrates the influence of processing parameters on formation, shape and size of RRV with different fabric architectures. The main causes of the RRV are the fibre layout, the resin properties and the processing parameters. Therefore, this study will try to characterise the mechanical properties of composite plates by varying the fibre layout but keeping the other parameters unchanged.

2.4 Identification and measurement of RRV

The three principal techniques used to measure RRV in fibre-reinforced composites are: (i) X-ray transmission, (ii) computerised tomography (CT) and,

(iii) microscopy with image analysis. Techniques (i) and (ii) may be non-destructive testing (NDT) while (iii) normally requires cut sections.

2.4.1 X-ray transmission

In this technique X-rays are projected toward the composite laminate surface, then captured on the other side by a detector which gives a 2D image through the thickness of the laminate structure.

Tan et al. [40] used X-radiography to examine damage characteristics in NCF stitched composites subjected to impact loading. They consolidated either 32-ply $[45^{\circ}/90^{\circ}/-45^{\circ}/0^{\circ}/(0^{\circ}/45^{\circ}/90^{\circ}/90^{\circ}/-45^{\circ}/0^{\circ})_2]_S$ or 20-ply $[45^{\circ}/90^{\circ}/-45^{\circ}/0^{\circ}_2/45^{\circ}/90^{\circ}_2/-45^{\circ}/0^{\circ}]_S$ stacking sequences and found that the RRV around stitch threads acted as crack initiation sites.
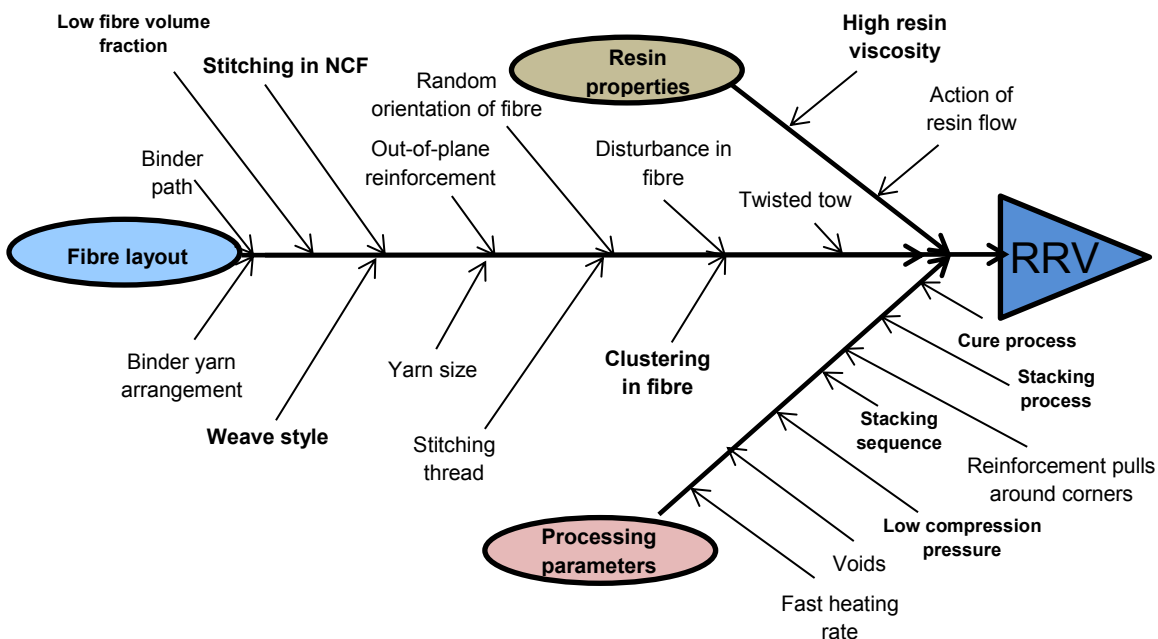
Figure 2-4: Summary of all causes of the RRV with significant influences in bold.

[22]

2.4.2 Computerised tomography (CT)

In CT scanning the X-ray passes through a composite laminate from different angles to create multiple images. These images can be reconstructed to yield a 3D image of the laminate showing the size and distribution of the RRV or the voids.

Mahadik et al. [28] measured the size and shape of the RRV in a resin transfer moulded (RTM) composite using CT. They consolidated samples with fibre volume fractions from 50% to 65% step 5%. The authors found that the RRV size (0.2 mm^3 to 0.5 mm^3 for different fabrics) was inversely proportional to *the level of compaction* and heavily dependent on fibre architecture. For a fabric used in their study, when the fibre volume fraction was increased by 10%, the RRV height decreased by 83% due to the flattening of the yarn and the RRV length reduced by 67%. However, the width of the RRV remained unchanged. Liotier et al. [37] claimed that CT can be successfully used to measure composite defects. They used a circular sample with a radius of 10 mm and 2000 projections per full rotation (i.e. every 0.18°). This procedure maximises the contrast between carbon fibres and epoxy, and hence improves determination of the RRV. The RRV in multi-axial multi-ply stitched carbon composites manufactured by liquid resin infusion averaged 3.0 ± 0.5% of the overall laminate volume. Tan et al. [40] used CT to analyse defects and examine damage characteristics in stitched epoxy composites subjected to impact loading. They showed that *the cracks* were initiated at the RRV. Bull et al. [41] claimed that synchrotron radiation computed tomography (SRCT) and computed laminography (SRCL) offer clear images with details of individual fibres and the RRV. The crack bridging within the RRV is shown in Figure 2.5.
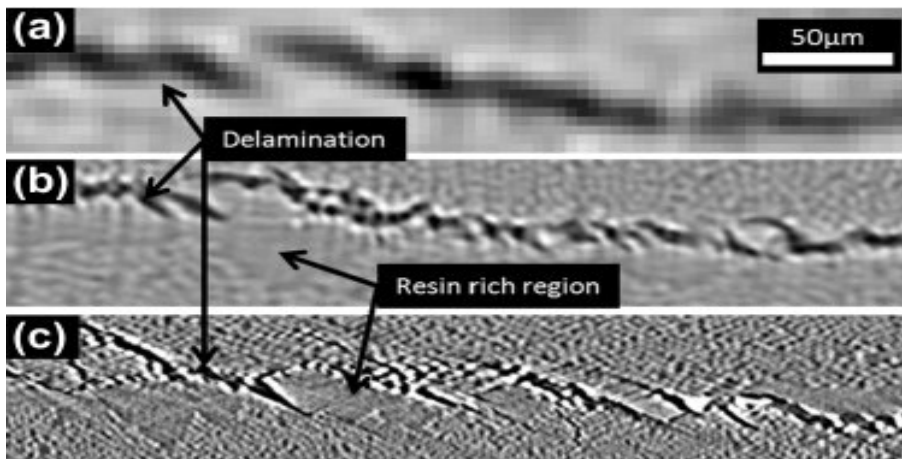
Figure 2-5: Close up of a delaminated region obtained using (a) µCT (b) SRCT (c) and SRCL. (a and b) are of the same specimen at approximately the same location, (c) is representative of similar damage on a separate specimen [41].

2.4.3 Microscopic image analysis

Microscopic image analysis provides access to spatial information on fibre distribution in addition to volume fraction data. Hayes [42] has reviewed optical microscopy of fibre-reinforced composites. Guild and Summerscales [13], Summerscales [43] and Summerscales et al. [44] reviewed the use of computer-based image analysis in the microscopical study of fibre-reinforced composites.

Summerscales et al. [45] manufactured composite plates from nine-layer unidirectional carbon stitched fabric with cold-curing epoxy. They used different dwell times (0, 90 or 180 min.) before applying vacuum pressure (0.8 bar), and found that fibres clustered more and RRV were reduced the most for the 90 minutes dwell specimen. They supported a hypothesis that the mechanical properties depend on the fibre distribution in addition to the fibre volume fraction.

Griffin et al. [46] and [47] studied commercial flow-enhancement reinforcement fabrics (FERF), from Carr Reinforcements, woven with specially designed mesoscale architecture for RTM processes. Image analysis of optical

micrographs was used to quantify the micro-/mesostructures as statistical distributions of pore space areas and perimeters. *Increased flow rate* was shown to be related to the presence of both modest-sized and large pore space in the reinforcement architecture. The pore spaces became resin-rich volumes in the composites. These authors noted that the RRV may be implicated in premature mechanical failure of the laminate.

Pearce et al. [48] studied three Brochier (now Hexcel) fabrics: 5-harness satin (5HS) , Injectex 5HS FERF and a 2x2 twill (Figure 2.6 and Table 2.1), with the same fibre type, surface treatment and fibre volume fractions, to relate variations in permeability and mechanical performance to differences in the composite microstructures. The satin fabric (Figure 2.6), had the highest proportion of small flow areas (<0.06 mm^2). The twill fabric had the smallest number of flow areas, but also contained a significant number of very large pore spaces (>0.5 mm^2). The Injectex fabric (Figure 2.6) had significant numbers of pore space areas in the range 0.08-0.30 mm^2. The proportion of larger pore spaces, and the consequent fabric permeability was ranked twill>Injectex>satin with the ranking of interlaminar shear strength (ILSS) being in *reverse order*. Pearce et al. [49] continued to analyse the above data set using automated image analysis, specifically fractal dimension to quantify the microstructure.

Canal et al. [50] consolidated 14-layer unidirectional laminates from prepreg sheets of E-glass/MTM57 epoxy resin at 120°C under 640 kPa autoclave pressure. Compression tests were carried out within a scanning electron microscope, and a digital image correlation technique (DIC) with various magnifications (250x, 2000x, and 6000x) was used to examine differences in strains between the RRV and the fibre rich volumes (FRV). They found that the

calculated strains from DIC measurement were in a good agreement with the

numerical results from a finite element model.

Twill   Satin   Injectex
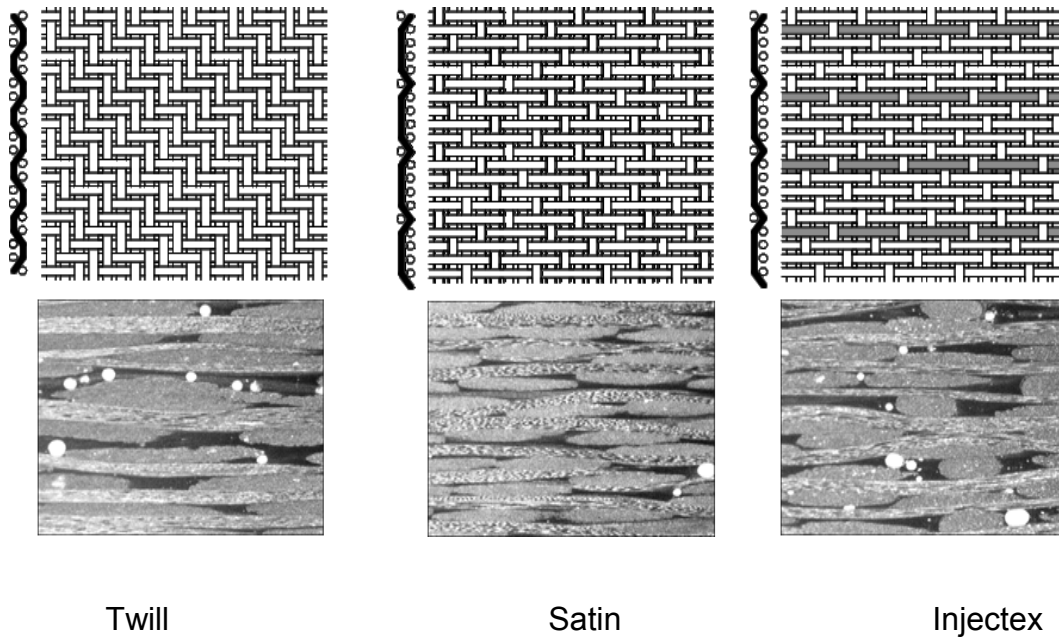
Figure 2-6: Schematics and transverse micrographs of Brochier weave. Image frame is 3.6 x 3.0 mm showing the different RRV dependent on weave style. (Reproduced from [44] with the permission of the authors and the publishers).

Table 2-1: Fabric description and the pore space area of Brochier (now Hexcel) woven carbon fibre fabrics.

Group	Fabric designation	Description	%bound tows	Source reference	Pore space area (mm^2)	The Rank of ILSS
I	Brochier E3853 G986 6K carbon fibre fabric	290 g/m^2 Standard 2x2 twill weave	0%	Pearce et al. [33]	>0.5	Lowest
I	Brochier E3833 G963 6K carbon fibre fabric	290 g/m^2 5-harness satin Injectex weave with one in five bound tows	20%	Pearce et al. [33]	0.08-0.30	Middle
I	Brochier E3795 6K carbon fibre fabric	290 g/m2 Standard 5-harness satin weave	0%	Pearce et al. [33]	<0.06	Highest

[26]

2.5 Voids

The pore space within a dry fabric may, during infusion with resin, become a resin rich volume which can include voids (closed spaces) or porosity (inter-connected channels). Voids/porosity may contain included air, or other volatile organic components (VOC). Subject to the resolution of the detection system, and the extent of sampling, the accuracy of void volume fraction (V_v) determination is probably ± 0.5% [51]. Stone and Clarke [52] reported that below void volume fraction (V_v) = 1.5%, voids tend to be volatile-induced and hence spherical with diameters in the range 5-20 µm, while above V_v = 1.5% the voids are flattened and elongated in the in-plane direction due to the limitation of space between the fibre bundles. They are also significantly larger than those voids at a lower V_v. Mayr et al. [53] have recently reported that small pores in CFRP with porosity levels <1.8% often have roughly circular cross-sections and found an abrupt increase in the out-of-plane shape factors above this percentage porosity.

Judd and Wright [54] reviewed 47 papers and concluded that "although there is a considerable scatter in results (reflecting in part the difficulties of accurate void content determination) the available data show that the interlaminar shear strength of composites decreases by about 7 per cent for each 1 per cent voids up to at least the 4 per cent void content level, beyond which the rate of decrease diminishes. Other mechanical properties may be affected to a similar extent. This is true for all composites regardless of the resin, fibre or fibre surface treatment used in their fabrication". Similar findings were reported by Ghiorse [55].

[27]

Purslow [56] proposed a novel classification system for voids to replace the previous system which was only applicable to fairly uniformly distributed voids. For example, to quote a V_v (void volume fraction) of 0.5% for a composite of generally high quality (voids < 0.2%) but with an occasional very large void could be very misleading and potentially dangerous. He suggested that the void content should be quoted as "0<voids<0.2%; infrequent local voids > 0.5%". His studies have suggested that when V_v < 0.5%, the voids are spherical with a diameter of 10 µm and are due to trapped volatiles. As V_v increases, the voids due to trapped volatiles decrease in number and are replaced by large intra-tow/intra-lamina voids. The results suggested a linear relationship between V_v and void thickness, where the thickness is related to fibre diameter.

Stringer [57] used hand lay-up to manufacture composite laminates with woven carbon fibre (340 g/m^2). The laminate layers were XP $[0^0/90^0]_7$ to produce 2-3 mm laminate thickness. Increasing epoxy viscosity by a dwell period before applying the vacuum pressure could reduce the voids and hence improve the mechanical properties of the laminates. Well-chosen dwell periods could also reduce the RRV [45] as mentioned above.

Santulli et al. [51] used microscopic image analysis to measure the void content in twill weave E-glass/polypropylene composites. They found that coplanar voids (voids that spread over the same plane, commonly corresponding to interlayer boundaries) exist when RRV are detected between the laminae.

The extent to which voids affect the mechanical properties of the fibre-reinforced composites is dependent on void content, void distribution and void shape. A high void content minimises the mechanical properties of composites.

2.6 Evaluation of the effects of RRV on composite performance

Studies normally show a negative effect of increasing RRV on all mechanical properties of fibre-reinforced composites. This section is therefore divided into four parts dealing with (i) stress concentrations arising from RRV, (ii) crack initiation and propagation, (iii) static properties and (iv) dynamic properties.

2.6.1 Stress concentration

The study of stress concentration is very important in composite laminates, because failure normally starts from sites of stress concentration. Mikhaluk et al. [36] claimed that the RRV could influence the mechanical behaviour of carbon/epoxy NCF laminates, and cause stress concentrations. Iarve et al. [58] analysed stresses in three dimensions for textile composites both numerically (using the finite element method) and experimentally (using Moiré interferometry). Their experiments measured strain distributions which characterised with well-localised high strain bands corresponding to the RRV between the fibre tows. The RRV cause a difference in stresses from region to region in composite laminates which leads to the stress concentration.

2.6.2 Crack initiation and propagation

In addition to its effect on the mechanical properties of composites, it is useful to investigate the effect of RRV on crack behaviour. As indicated above, the RRV are strongly implicated in creating initiation sites and propagation paths for crack growth [31, 59-63] as shown in Figure 2.7. Tan et al. [40] showed that *the cracks* were initiated at the RRV. Bull et al. [41] used synchrotron radiation computed tomography (SRCT) and showed that the cracks connected with the

RRV as mentioned earlier. Dyer et al. [64] studied the fatigue behaviour of continuous glass fibre reinforced composites with XP stacking sequence $[90^o/0^o]_{2s}$. They found that failure occurred from cracks which had initiated and grown in RRV. Therefore, the RRV are the weak link between cracks. In addition, some studies stated that the cracks move from one ply to another through the RRV [38, 60]. Furthermore, more RRV means a greater number of micro-cracks [38], and coherent fracture of the laminates through the RRV [65]. However, Liang et al. [66] stated that all cracks observed in their study were located at fibre/matrix interfaces, in fibre rich volumes. Thus, almost no transverse cracks were found in RRV due to a weak transverse strength of flax/epoxy.
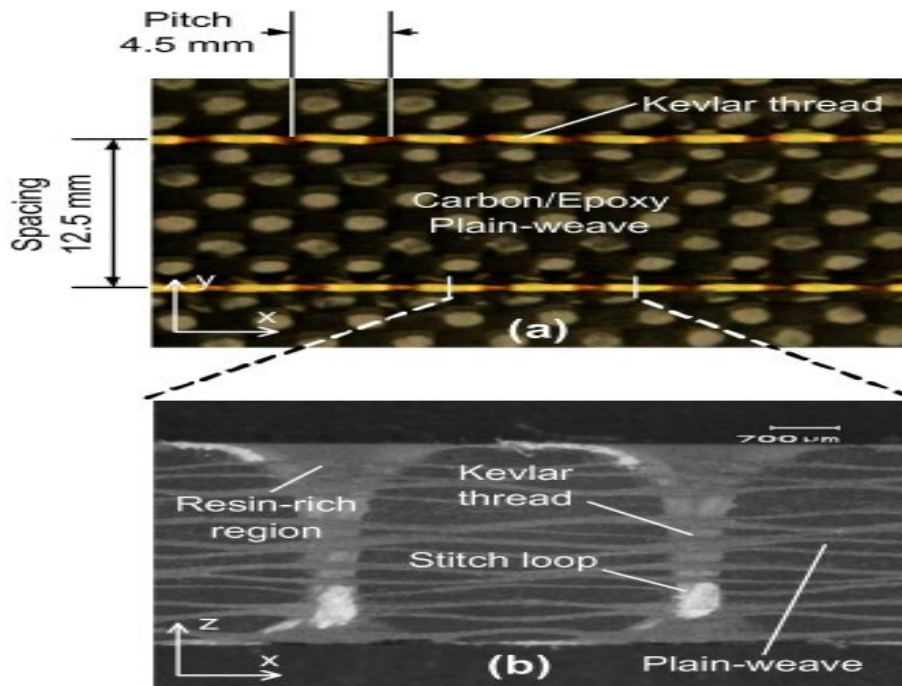
Figure 2-7: *(a) top view and (b) cross-sectional view of lock stitch pattern. (reproduced from [63] with the permission of the authors and the publishers).*

[30]

2.6.3 Static properties

Numerous articles describe the effect of the RRV on the mechanical properties of composites. Basford et al. [67] measured the compression and inter-laminar shear strengths of carbon fibre/epoxy composite laminates reinforced with either normal 5-harness satin (5HS) or Injectex 5HS FERF woven fabrics at constant fabric areal weight and V_f. The strength of both fabrics was found to decrease as the proportion of flow-enhancement tows increased. The presence of *the twisted tow* (used to enhance flow rates in Injectex) was found to cause large RRV adjacent to the tow.

Hale [29] investigated the in-plane and out-of-plane strains in woven carbon textile composites experimentally (using Moiré interferometry) and found that the RRV have high local/ microstructural distortions which differ from theoretical predictions (using finite element analysis) for these sites.

Aziz and Ansell [68] investigated the effect of fibre alignment on the flexural properties of either kenaf or hemp bast fibre composites. They found that the fibre alignment and the location of RRV both have a large negative effect on the flexural strength.

Gojny et al. [69] studied the effect of carbon nanotubes on the mechanical properties of glass fibre reinforced composites. They claimed that the RRV had a large local deformation relative to the reinforcement. The RRV are estimated from the formation of the observed shear-bands of the microscopic image.

Tzetzis and Hogg [70] investigated an infusion repair technique that could increase the toughness of carbon fibre laminates and reported a small reduction in load for crack growth under mode I (opening), due to the damage in the RRV.

[31]

Dhakal et al. [71] analysed the effect of water absorption on the tensile and flexural properties of hemp fibre reinforced composites. They found that the random orientation of fibres can produce RRV which can reduce the mechanical properties. Lomov et al. [72] claimed that the RRV has a lowest tensile strain, when they used meso-finite element analysis of carbon fabric textile composites. However they neglected the nesting of layers in their models. Sudarisman and Davies [18] investigated the effect of processing parameters such as epoxy concentration (within an acetone solution for wetting the carbon fibres), compressive pressure and holding time on the flexural properties of composites. They showed that the RRV produce poor bonding between individual prepreg layers. Colin de Verdiere et al. [73] showed that the RRV reduced the in-plane stiffness of tufted Non-Crimp Fabric (NCF) composite materials by 13% relative to non-tufted reinforcement. Liu and Liang [74] consolidated prepreg carbon/epoxy with a stacking sequence $[0^{o}/-45^{o}/45^{o}/90^{o}]_{s}$ and reported RRV in the layers adjacent to an embedded optical fibre.

Heß and Himmel [75] simulated the experimental results of non-crimp fabric (NCF) carbon fibre/epoxy laminates under in-plane tension, compression and shear loading using finite element method. Their overall mean deviation was 8% to 13% between experiment and simulation. Fibre dislocation and RRV were found to reduce the laminate strength. Vaughan and McCarthy [76] investigated transverse shear fracture in carbon fibre-epoxy laminates at micro-scale and found that shear bands propagated at the RRV.

2.6.4 Dynamic properties

(wave propagation, fatigue, impact)

2.6.4.1 Wave propagation properties

The RRV have a large effect on the dynamic properties of composites. Jeong and Hsu [77] analysed wave propagation in carbon fibre reinforced composites and found that the ultrasonic velocity was inversely proportional to the void content. They discovered that voids are localised in the RRV.

2.6.4.2 Fatigue properties

This section reviews the main parameters that affect the fatigue properties of composite laminates, and indicates methods that have been used to improve them. In addition to reviewing the prediction of fatigue life of fibre-reinforced composites, it will explore correlations that have been observed between fatigue properties and the static properties or the fibre distribution of fibre-reinforced composites.

The mechanical properties of composites have been extensively considered in analytical and experimental investigations for the last four decades [78]. Kalam et al. [79] studied the fatigue behaviour of oil palm fruit bunch fibre/epoxy and carbon fibre/epoxy composites and found that damage had started in the RRV. Kawai et al. [80] manufactured unidirectional carbon-fibre-reinforced composites with different resin matrices using the autoclave method. They concluded that there was a degradation of the fatigue performance of carbon-polyimide composites. Because in comparison with the other two systems used in the study, carbon-polyimide had very large RRV, which were produced during the

manufacturing process. Aymerich et al. [33] studied the effect of stitching on the mechanical behaviour of graphite-epoxy laminates and observed that the stitching caused a reduction in the fatigue performance due to the misalignment of fibres, damage of fibers (because of the needle penetration) and the RRV surrounding the stitches. Chambers et al. [60] discovered that the distribution, size and shape of voids have a greater effect on the flexural fatigue of composites than the void volume fraction. This was due to effect of the voids on the crack propagation in the RRV at the inter-ply regions.

Ferreira et al. [81] investigated the fatigue performance of polypropylene-glass fibre thermoplastic composites. They observed that in their composites the loss of stiffness was proportional to the temperature rise during testing of all laminates used in their study. Bertin et al. [82] found that the stacking sequence has a great impact on the mechanical behaviour of composites under thermal-cyclic loading. De Monte et al. [83] studied the effect of sample thickness and temperature with different fibre orientations of short glass fibre and found that the fatigue properties were inversely proportional with temperature, and the degree of anisotropy was increased by reducing the thickness, because varying the thickness could affect the fibre orientation across the thickness. Ferreira et al. [84] concluded that the fatigue strength was strongly influenced by the stacking sequence.

Fuqiang and Weixing [85] concluded that internal defects are the common cause of the random distributions of the static and the fatigue properties of composite laminates. By studying statistically the correlation between the fatigue loading and the fatigue life, their model describes the distributions of fatigue life of composites based on their distributions of static strength. Caprino and D'Amore [86] said that the scatter in S-N curves was due to the variability in

static properties, so that a lower fatigue life was related to a lower ultimate static strength, and it has been observed that fatigue and static–fatigue interaction has a considerable effect on the fatigue lives of GFRP composites [87].

From all the factors mentioned above, one could conclude that the fibre distribution is the common link to other parameters such as the RRV and internal defects, the stacking sequence, the stiffness and the anisotropic properties of the composite laminates. Therefore, the fibre distribution might be one of the main factors that affect the fatigue performance of the fibre-reinforced composite. In this thesis, an empirical model will be identified for the fatigue behaviour of composites in terms of the uniformity of the fibre distribution and static properties, while keeping the other processing parameters unchanged.

The initiation of fatigue damage was identified by Clark et al. [88]. The composite laminates were expected to fail when accumulated damage exceeds a critical level of damage. Accumulation may be used as a more suitable approach to predict the fatigue life of composite laminates. However, fatigue damage cannot be measured directly [89]. The fatigue damage in fibre-reinforced composites has often been modelled by using the degradation in modulus of elasticity [90]. Abbadi et al. [91] addressed fatigue behaviour of composite sandwich materials using nonlinear fatigue models verified from experimental data, which are based on the degradation of the fatigue modulus. Li et al. [92] showed that stiffness degradation in the laminates due to cyclic fatigue loading is a direct consequence of multiple damage events, and cumulative damage growth can be directly evaluated from the stiffness degradation of the samples. Mao and Mahadevan [89] developed a mathematical model for fatigue damage evolution in composite materials, which

is based on continuum damage mechanics concepts of experimental data. Adden and Horst [93] showed degradation of the Young's modulus and the shear modulus, under biaxial tension and torsion fatigue, of non-crimp-fabric GFRP tube specimens. Ferreira et al. [94] studied notch and test condition effects on the fatigue of glass fibre-reinforced composites at ambient temperatures, and observed a sudden drop of stiffness (for unnotched specimens) during the first 10-20% of the fatigue life then the stiffness remained constant until failure. Gude et al. [95] investigated damage evolution of novel 3D textile-reinforced composites under fatigue loading conditions. They claimed that the degradation in composite stiffness under cyclic tensile and shear stresses was due to the creation and propagation of visible cracks. However, compression fatigue loading does not cause development of visible cracks and thus no loss in stiffness during the life cycle. Gagel et al. [96] concluded that location of final failure, of glass fibre NCF reinforced epoxy under tensile fatigue, can be detected via thermography. However, the location of the final failure cannot be related to the local crack density, and the stiffness degradation is governed by different mechanisms of failure. Harris [97] stated that twenty or more fatigue models have been proposed, and the differences between them are quite small. Due to the complexity and test procedures for such experiments and cost of the fatigue samples, the validity of fatigue models can only be tested over limited ranges of combined stresses. Furthemore, according to some authors, an endurance limit for composites actually exists, and is mainly controlled by matrix, but verifying whether the endurance limit actually exists will require a costly and time-consuming testing stage.

Wu and Yao [98] stated that the fatigue damage and failure mechanism of composites is very complex. The five types of failure in fibre reinforced

composites under fatigue and static loading are matrix cracking, fibre breakage, debonding, delamination and fibre pullout. However, the behaviour of fibre reinforced composites under fatigue loading is mainly controlled by the matrix [66, 99], and the micro-voids have no great effect on the fatigue properties of E-glass polypropylene composites [51]. Böger et al. [8] improved the fatigue life of glass fibre-reinforced epoxy under fatigue load by the incorporation of nanoparticles in the matrix. The addition of the nanoparticles improved the fracture toughness of the bulk epoxy, and the inter fibre fracture strength increased by up to 16%. For multiaxial multi-ply stitched carbon, the type of stitching yarn and the size of RRV have a main effect on laminate microcracking under fatigue load [38]. Furthermore, the tensile fatigue behaviour is reduced as a result of localised fibre undulations [39], and crack growth depends on both the fatigue properties of the fibres and of the matrix, with both occurring on different time and space scales [100].

To sum up the results of the work reported in this section, modelling and prediction of the fatigue life requires a significant amount of experimental S-N data for each type of composite [11, 101], as well as critical experiments designed to elucidate the underlying mechanisms and relationships in the composite materials. Most of the researchers have selected fatigue data from published literature as an experimental shortcut. The matrix and the fibre type and the fibre distribution in the fibre-reinforced composites, have been shown to be the main factors that affect the fatigue properties, where the fibre distribution and the RRV are related to each other. The stiffness degradation can be used for measuring the damage that is occurring in the laminates. Failure mechanisms are very complex to unpick, and therefore, analytical models are in short supply and of limited applicability. Given the complexity of the problem, it

[37]

is clear that further research in this area would be both useful and timely. The present project aims to contribute to further understanding in the area of RRV in composite laminates in terms of characterising their distribution and effect on mechanical properties.

2.6.4.3 Impact properties

Azouaoui et al. [102] manufactured XP glass/epoxy laminates with stacking sequence $[0^o/90^o]_{4s}$. They evaluated damage parameter, visually and by scanning electron microscope inspection, against number of impacts according to reduction of material bending stiffness. They found that RRV in their materials had a low resistance to impact fatigue and that the cracks followed the RRV distribution in the glass-epoxy laminates. Tan et al.[40] used X-ray micro-computed tomography (µCT), and X-ray radiography to characterise impact damage in stitched carbon composites. They applied low-velocity impact tests with a normalised impact energy from 1.6-10 (J/mm) to different specimen thicknesses. They showed that the RRV around the stitches in NCF composites are the weakest sites and were the site of impact crack initiation.

2.6.5 Summary

Figure 2.8 summarises the effects of RRV on the static and dynamic mechanical properties, on crack behaviour and on the stress concentrations in fibre-reinforced composites that arise from RRV. One could conclude that reducing the size of the RRV might lead to improved mechanical properties in terms of increasing the static and dynamic properties, and decreasing the crack growth and the stress concentration within the fibre-reinforced composites. The RRV depend on the fibre distribution within the laminates as mentioned earlier.

Therefore, this project investigates the effect of the fibre distribution on the mechanical (static and fatigue) properties of composites but keeping other processing parameters constant.

2.7 Fractal dimension

In terms of understanding the influences of RRV on the properties and performance of composite laminates, and devising models that describe these relationships, it is necessary to be able to correlate the mechanical properties of the composite laminates with quantitative parameters that describe aspects of the microstructure. In common with other materials, the microstructure and its defects govern the properties of the composite material. This section has reviewed a number of published experimental and numerical studies to clarify answers to the following questions:

- How did these previous studies quantify the microstructure features of composite laminates or homogenous materials?

- Is it possible to use the fractal dimension to characterise the microstructure of fibre-reinforced composites?

- How might the fractal dimension be used in correlating the mechanical properties and the microstructural features?
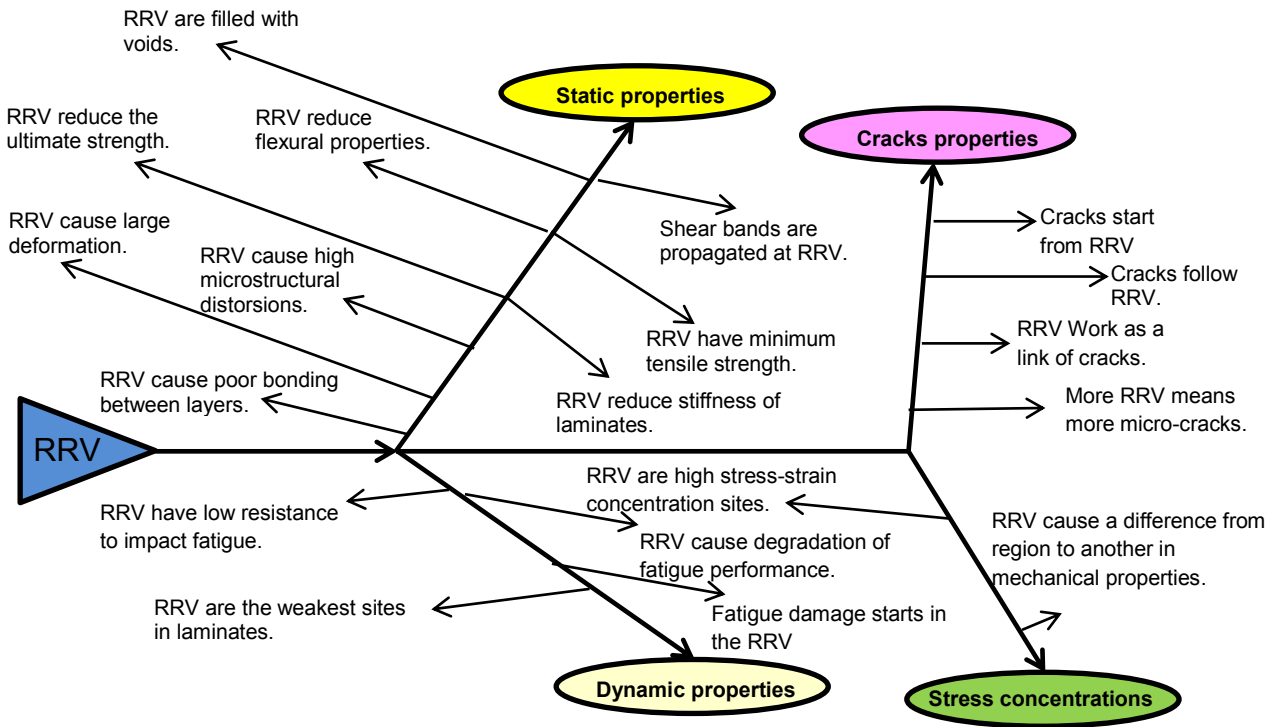
Figure 2-8: The effects of the RRV on the mechanical behaviour of fibre-reinforced composites.

Plane geometry describes regular objects such as points, lines, areas, and volumes using integer dimensions 0, 1, 2, and 3, respectively. However, a variety of natural objects and engineering constructs do not conform to the plane geometry description since their length, area and volume are scale-dependent. Such objects are called fractals, and are described using a non-integer dimension called the fractal dimension (D) [103].

Measuring the fractal dimension of complex objects was popularised in scientific fields about three decades ago [104]. A fractal is a natural phenomenon, or a mathematical set, that exhibits a statistically similar repeating pattern at every scale. Fractals are useful in modelling complex structures (such as eroded coastlines, snowflakes or microstructures) which are spatially correlated, i.e. similar patterns recur at progressively smaller scales. Composite

microstructures are normally quantified using fibre volume fraction, fibre length distribution and fibre orientation distribution. The quantification of distribution within a microstructure requires image processing and analysis. This can be achieved using the D (a non-integer physical dimension) which reduces the key aspects of the microstructure, as seen in representative images, to a single real number.

The characterisation of composite microstructure with the fractal dimension has evolved over the past two decades [44, 48, 105-107]. Picu et al. [108] have provided a useful recent discussion on composites whose microstructures had either a fractal distribution of inclusions, or a random distribution of inclusions. They observed that microstructures that could be described by a fractal dimension always led to stiffer composites, with higher strain hardening rates. D is now also seen as a useful tool to characterise self-similar fracture surfaces occurring at different scales [109] and, as noted by Allen et al. [110] is extremely useful in quantifying the degree of roughness of highly irregular objects, whilst there are also a large number of analysis strategies that have been developed to measure the fractal dimension of composite and homogeneous materials.

Celli et al. [111] used fractal geometry to examine crack paths in alumina–zirconia composites. The cracks observed by scanning electron microscope, all taken at the same magnification, had a relationship between fracture toughness and fractal dimension, and showed the potential of fractal analysis to clarify complex mechanisms such as those involved in the fracture of brittle materials. Biancolini et al. [112] investigated fractal dimension by using the box counting method (described in Section 2.7.1) to study fatigue cracks in steel by characterising the spatial distribution of acoustic emission sources. They found

that the fractal dimension decreased with increase in the number of fatigue loading cycles until the failure point. The authors concluded that they could use the fractal dimension as a damage characterisation parameter. Kuznetsov et al. [113] derived the fractal dimension of a deformed specimen using surface relief images obtained from a scanning electron microscope. The austenitic stainless steel specimen was subjected to a step-wise increase in load. With increasing strain, the curve shows three levels for the fractal dimension: (i) a slight decrease in the fractal dimension is noticed before (ii) the onset of necking in the interval of strain 0.48–0.52, then (iii) the fractal dimension increases to a critical value corresponding to the start of specimen fracture as shown in Figure 2.9. Venkatesh et al. [114] observed that the fractal dimension of fracture surfaces of Ti–6Al–4V extra-low interstitial alloy subjected to different heat treatments was proportional to the fracture surface roughness and hence D could be used as a measure of fracture surface roughness. Yield strength and ultimate tensile strength both decreased, while ductility increased, with increasing fractal dimension. This was attributed to the change in the fracture mode being dependent on the microstructure induced by the heat treatment. Wang et al. [115] analysed fracture surfaces of aluminium alloy by using the fractal dimension. Their results showed the ultimate tensile strength to be proportional to the fractal dimension of the fracture surface roughness, due to different fracture modes that depend on the level of interface reaction status generated by heat treatment. Yuan et al. [116] claimed that D can be extremely useful when applied to tribological work. They calculated the D before and after tin coating and found that the value of D after the coating was larger than before coating in some cases, and the difference was due to various machined

surfaces. They did not find a big difference between D values measured using the slit island or box counting methods.
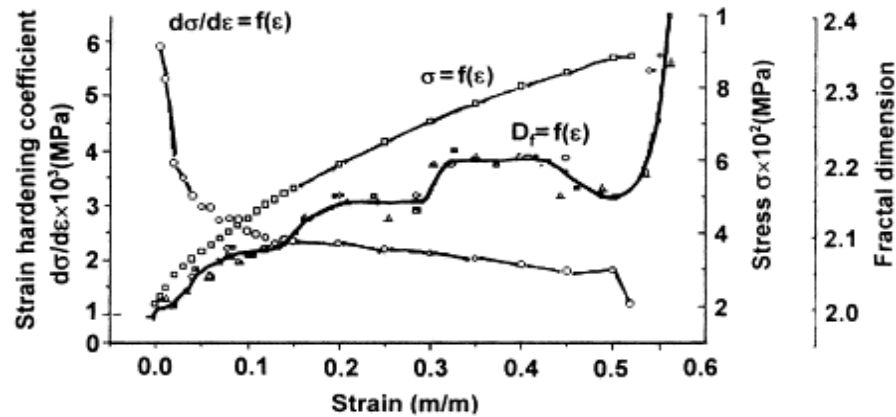
Figure 2-9: The straining diagram for the austenitic stainless steel specimen from Kuznetsov et al. [112].

The fractal dimension has also been applied to characterise particular aspects of polymer matrix composites, in particular, links between their fracture surface topography and toughening mechanisms, e.g. [104, 117], the evolution of defects in composite materials [118], and the microstructural influence on mechanical and other properties, e.g. [108, 109, 119]. A clustered distribution of the reinforcement fibres can result in resin-rich volumes and consequent stress concentrations [107]. Therefore, it would be useful to find a technique that could characterise the fibre distribution within the laminates. Furthermore, such techniques may contribute to the understanding of the "manufacturing process-properties dilemma" in composites where clustered fibre distributions have high permeability in liquid composite moulding (RTM/RIFT) processes but uniform fibre distributions confer better mechanical properties [120].

2.7.1 Box counting method

One of the techniques used to calculate the fractal dimension is the box-counting method which has been widely used in D research [103, 112, 121, 122], because it is easy to use and amenable to simple automated computation.

It can be applied to both linear and non-linear fractal images, and is applicable to microstructural patterns with or without self-similarity [103, 122]. The box counting method has been modified, e.g. [123], to eliminate problems found with the computerised method such as the border effect and non-integer values of box size. Furthermore, it has been applied in various fields due to its simplicity in use [124]. In many situations, one quarter of the shorter image side may provide a proper value for largest box size [122]. Even with the same approach, different scale ranges chosen for the computation of the fractal dimension may lead to different values [125, 126]. In addition, Buczkowski et al. [127] claimed that large box sizes usually characterise the embedding surface of the whole object and that small box sizes approximate the dimension of the substructure for discontinuous objects. In application of composites, the large box size might cover the fibres bundles and the small box sizes could cover the fibres theirselves.

To sum up, the fractal dimension concept has been widely used to characterise homogeneous and composite materials, and provides a link between the structure and the mechanical properties; the box counting D method is a useful way to measure the fibre distribution within composite laminates.

2.8 Summary

The fibre distribution could be one of the main factors that affect the performance of fibre-reinforced composites. It is clear that there is a gap in research related to quantitatively characterising the fibre distribution and RRV, and in terms of then correlating the fatigue properties with the fibre distribution and RRV for fibre-reinforced composites.

The RRV and the fibre distribution have a significant effect on the mechanical behaviour of fibre-reinforced composites. RRV arise primarily as a result of (a) the clustering of fibres as bundles in textiles, (b) the stacking sequence, and/or stacking process, (c) the resin properties and flow characteristics, (d) the heating rate as this directly affects viscosity and (e) the consolidation pressure. The main techniques used to measure the RRV in fibre-reinforced composites are X-ray transmission, computerised tomography (CT) and microscopic image analysis. The formation, shape and size of RRV in composites with different fabric architectures has been briefly discussed above. The majority of studies have shown a negative effect of the RRV on the mechanical behaviour of composite materials.

Further in-depth studies are required that examine the RRV and/or the fibre distribution as a main influential factor on the mechanical (static and dynamic) properties of fibre-reinforced composites.

As a consequence of the literature review above, the present author cautions against reducing laminate consolidation pressure or changing the fibre architecture for high performance composite structures, unless the effect of reduced fibre volume fraction and the consequent fibre distribution and RRV are fully understood for the reinforcement system in use.

Fractal dimension looks promising for quantification of the fibre distribution given that researchers have already used D to correlate some mechanical properties and processing parameters. This aspect has been explored further in the work described in this thesis.

Chapter 3 EXPERIMENTAL METHODOLOGY

3.1 Overview

This chapter presents the experimental methodology employed for the work described in this thesis. It describes the materials used and laminate manufacture, microstructural characterisation of the laminates (preparation of specimens, image capture and fractal dimension analysis), static mechanical properties, fatigue properties and fractography.

3.2 Resin Transfer Moulding (RTM) process

RTM is a process of producing composite laminates by clamping the reinforcement between the upper and lower parts of a fitted mould tool (Figure 3.1). The RTM process (Ciject® One, Composites Integration, Saltash UK) was used in this study for CFRP for the following reasons;

- The RTM mould has a fixed cavity which maintains constant fibre volume fraction V_f for all laminates. This is useful when investigating the uniformity of the fibre distribution effect, for a constant fibre volume fraction, on the performance of the composite laminates. Ideally, the processing parameters will be kept constant.

- The RTM process reduces the thickness variation between specimens and within a specimen (fixed cavity), and the laminates produced by this method have a good surface finish on both side surfaces [128].

- The process does not require high injection pressure.

- The laminates will have a high fibre volume fraction and good mechanical properties.
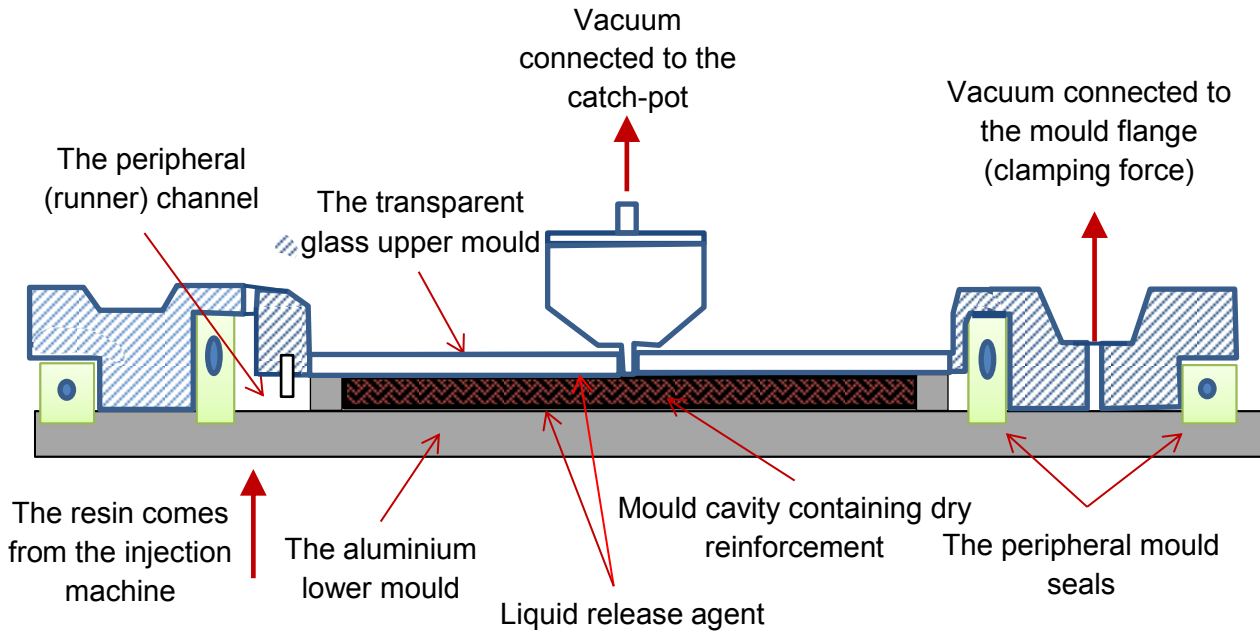
Figure 3-1: The RTM process as implemented in this doctoral study.

 A schematic of the RTM process is given in Figure 3.1. A liquid release agent is applied to the mould surfaces to facilitate easy removal of the laminates. The clamping force may be produced through a number of different techniques such as applying pressure on the upper mould, mechanical clamping methods or vacuum pressure, i.e. one atmospheric net pressure. The latter method was used in this study. After closing the mould, fitting the vacuum catch-pot at the vent position, and connecting the vacuum pump to the catch-pot and flange, the vacuum pump closes the mould and compresses the double seals (an inner resin seal and an outer vacuum seal) to prevent air ingress into the vacuum space. The product of the mould flange area and the external atmospheric pressure gives the clamping force. Resin is injected into the mould through an

injection valve and the peripheral (runner) channel. The mould continues to fill and the resin percolates through the reinforcement fibres until the resin reaches the catch-pot at the mould centre. A transparent glass upper mould allows full observation of the flow of the resin through the fibre-reinforcement. The vacuum is maintained until the resin has cured. At that point, the vacuum is disconnected, the catch-pot is removed, and the mould is then opened to extract the composite laminate plate. The peripheral injection technique offers the most useful route to fill the mould, giving a minimum of reaction pressure against the clamping force, it can also be used to mould large structures and offers the shortcut fill time for a given area.

3.3 Infusion process

Unlike the RTM process that uses a semi-rigid upper mould, the infusion process uses a vacuum bag [129], and hence produces variable laminate thicknesses, due to the variation of cavity size that results from using a vacuum bag instead of an upper mould part. The infusion process is a technique that normally uses only vacuum pressure to draw resin into the mould cavity. Compressing the laminate and hence increasing fibre-to-resin ratio increases the modulus and strength-to-weight ratios and leaves minimal void content in the composite laminates. Fabrics are assembled as a dry stack of materials as in the case of the RTM process. The dry reinforcement is then covered with peel ply[3] and a distribution medium as shown in Figure 3.2. The whole dry stack is then vacuum bagged, and after eliminating bag leaks, resin is allowed to flow into the laminate. The resin distribution over the whole laminate is

---

[3] A release fabric that prevents foreign materials from becoming integrated into the finished laminate.

assisted by the transport/flow medium/mesh, leading to wetting of the dry reinforcement from above.

Like the RTM process, the infusion process offers all the advantages of a closed system process [130, 131]. However, the cavity of the mould is not fixed, but depends on the processing parameters and there is consequently a variation in laminate thickness. The process is controlled by the principles of D'Arcy's equation [132], which describes the resin flow rate as governed by only three factors: (i) resin viscosity, (ii) pressure differential in the cavity, and (iii) permeability of the laminate. If the three parameters are unchanged, then the resin will always flow in a similar manner for every composite laminate.
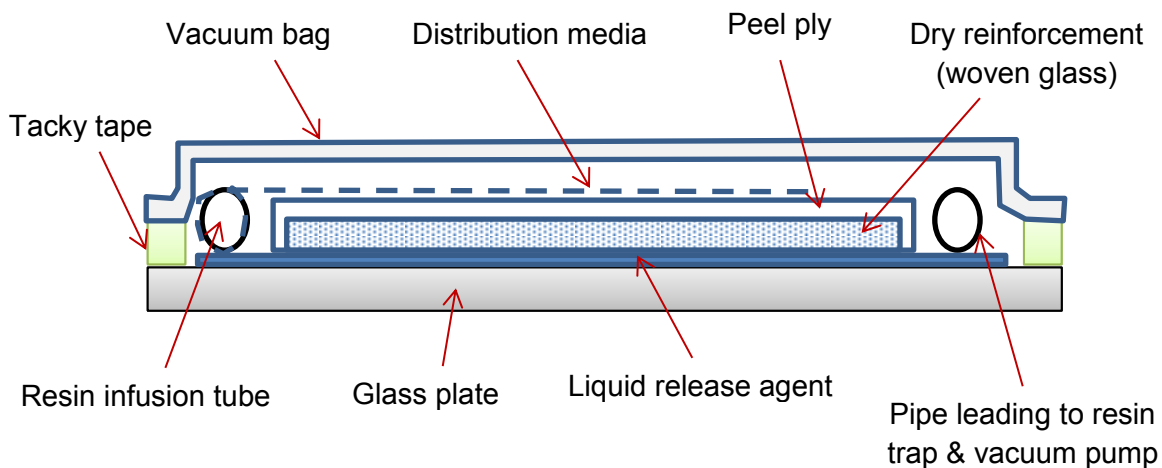
Figure 3-2: The infusion process as implemented in this doctoral study.

3.4 Woven glass composite panels manufactured by the infusion process

One of the objectives of this study, as illustrated in Figure 1.2, are to study the effect of the uniformity of fibre distribution on the mechanical properties of the composite laminates. The initial study started by manufacturing different woven fabric laminates with a range of fibre volume fractions. These composite

laminates were manufactured by the infusion process with different level of consolidations.

The infusion process was used to manufacture $[(90/0)_2]_s$ woven composite panels as shown in Figure (3.3) with a range of levels of consolidation. Three levels of consolidation were chosen: hand lay-up, infusion under 600 mbar and infusion under 900 mbar. The reinforcement comprised eight layers of plain weave 290 g/m^2 glass fabric and the resin was Sicomin SR8100 (properties given in Appendix A-1). Three plates were manufactured under each consolidation condition in order to ensure that the experimental data were statistically meaningful.

In an infusion process, the vacuum bag is sealed with tape, so it is essential to use a pressure gauge to check that there are no leaks which would affect consolidation. Pressure regulation utilised a pressure gauge on the vacuum pump tube. Consolidation pressure was measured via a pressure gauge on the resin inlet tube before the start of the infusion process. Resin was infused in one direction (rectilinear flow) through the laminate as shown in Figure 3.3, which was the 0° direction of the surface laminate layers. The plates were cured under vacuum for 24 hours at ambient temperature according to the resin manufacturer's recommendations (Appendix A-1) before post-curing was performed in an oven at 60 ^{o}C with time-temperature profile shown in Figure 3.4. Subsequently samples were prepared for image analysis and mechanical testing.
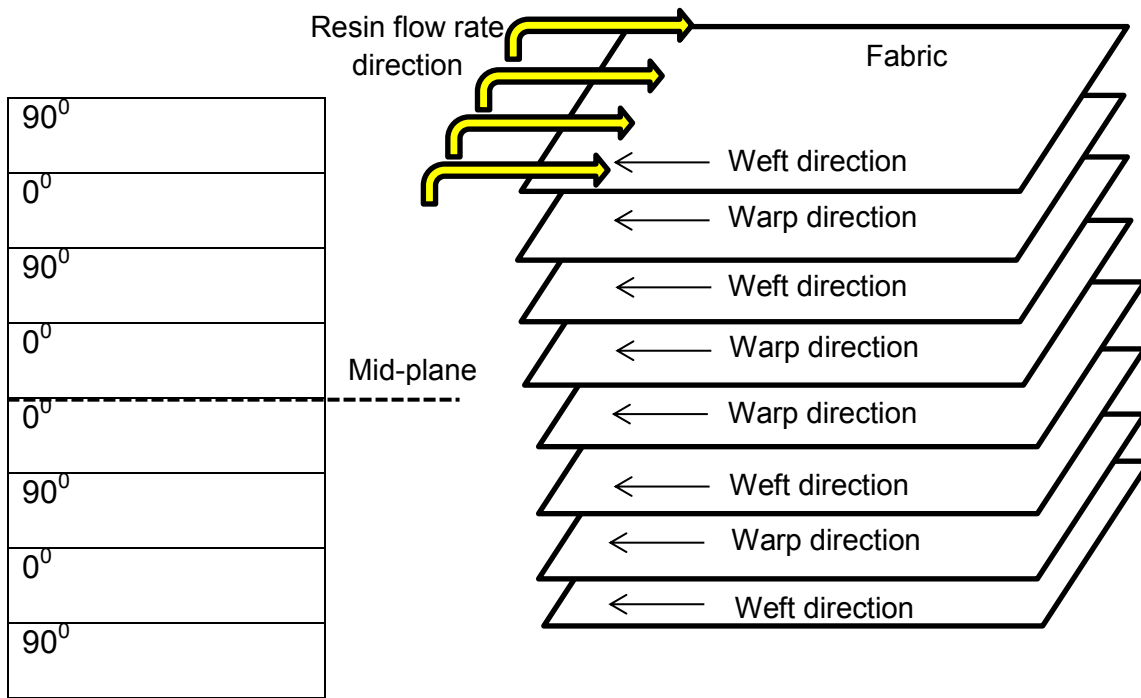
Figure 3-3: The stacking sequence of laminates, 0° is the direction of warp tows & 90° is the direction of weft tows, i.e. [(90/0)$_2$]$_s$.
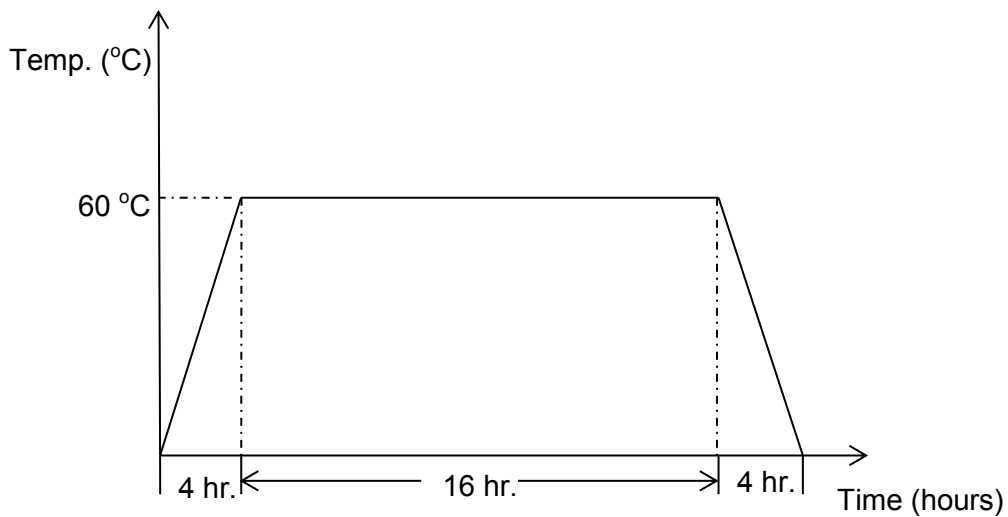
Figure 3-4: The post-curing cycle of the resin used in the infusion process.

3.5 Carbon fibre composite panels manufactured by the RTM process

After initial investigations into the effect of the uniformity of the fibre distribution, on the performance of the glass fibre reinforced composites, with various fibre volume fractions, a study was conducted into the mechanical properties of composite laminates with a similar fibre volume fraction. These composite laminates were manufactured by the RTM process.

Figure 3.5 illustrates the RTM process used to manufacture these woven composite laminates and also illustrates the relative location in each laminate plate, of the various test specimens used in the experimental work. Two (of three) 6K[4] carbon fibre fabric architectures woven by Carr Reinforcements were using the same batches of fibre for both warp and weft. The modulus of elasticity of the carbon fibres was 235 GPa. The areal densities of the two fabrics used in this work were: plain weave 300 g/m^2 and twill weave 320 g/m^2. Yarn counts were 380 tows/m for both warp and weft in the plain weave, and for the warp in the twill weave, while the weft yarn count for the twill weave was 420 tows/m. The resin was Sicomin SR8100 epoxy with Sicomin SD8824 hardener and a weight mix ratio of 100:22. A standard RTM process (Ciject® One, Composites Integration, Saltash UK) was used to manufacture laminates for the experimental work, with a fixed 2 mm cavity and vacuum closing of the mould. The injection pressure was +500 mbar.

---

[4] The 6K tow is formed from approximately 6,000 bundled carbon fibre filaments.

[55]
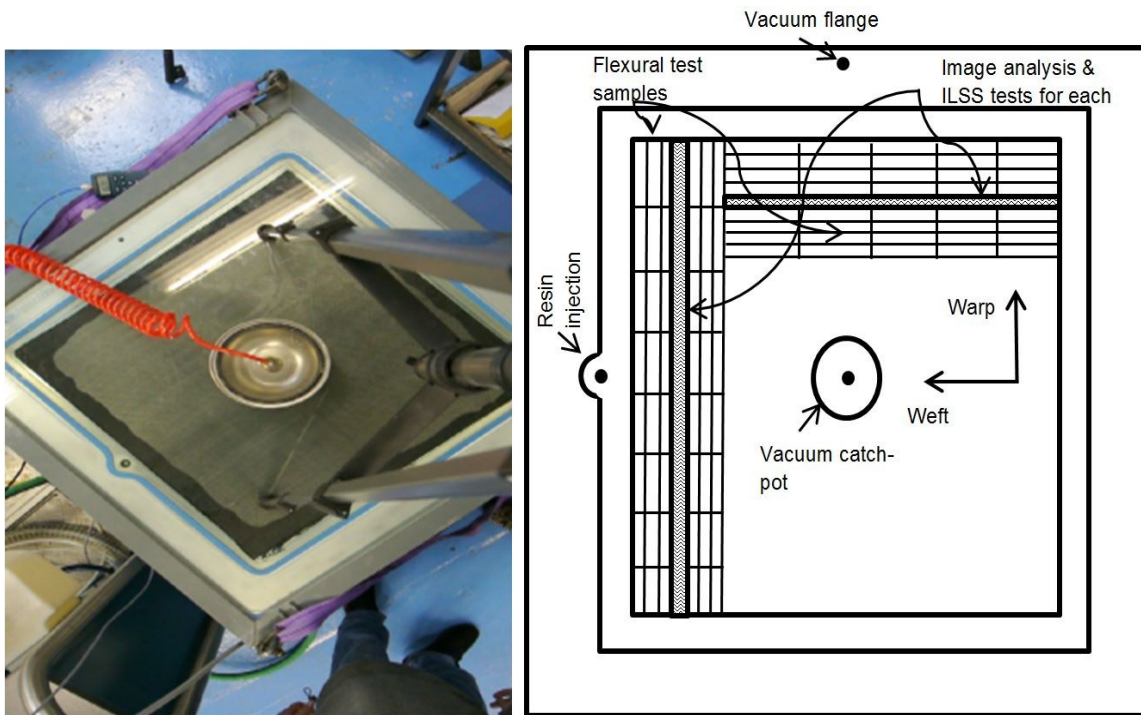
Figure 3-5: The RTM process mould.

Initial problems were experienced with the presence of small bubbles and variable laminate thickness arising from the high vacuum at the middle of the plate, leading to a maximum laminate thickness at the mould edges and a minimum at the centre. This was resolved by reducing the vacuum at the cavity from 1000 mbar absolute to 100 mbar absolute at the end of the injection process to allow the mould tool and laminate deformation to relax.

The plates were then cured under vacuum for 24 hours at ambient temperature. Full peripheral clamping vacuum (1000 mbar absolute) was maintained whilst the resin was cured. The plates were then post-cured in an oven for 8 hours at 60 $^{\circ}$C according to the resin manufacturer's guidelines (Appendix A-2).

Six different composite laminate plates were manufactured for this work, comprising:

- 3 plain weave plates, one each with 4 layers, 5 layers or 6 layers of fabric.

- 3 twill weave plates, one each with 4 layers, 5 layers or 6 layers of fabric.

The target fibre volume fractions were 33.3 % (four layers), 41.67% (five layers) and 50 % (six layers). Samples for mechanical testing and image analysis were cut from the laminate plates according to the layout shown in Figure 3.5.

3.6 Microstructural characterisation: preparation, image capture and analysis

Images of the microstructure were captured using an Olympus BX60 microscope with Olympus Stream image analysis software (SM04733) and analysed using the ImageJ package with FracLac add-in (open source image analysis software written in Java by the US National Institute of Health in Bethesda, Maryland). One of the techniques used to calculate the fractal dimension in ImageJ software is the box-counting method which has been widely used in D research [103, 121]. It is applicable to both linear and non-linear fractal images, and applicable to patterns with or without self-similarity [103, 122]. Furthermore, it has been applied to measurements in various application fields due to its simplicity in use [124].

For consistent image analysis, all images should have (a) the same pixel size, (b) uniform assignment of colours to different parts of the microstructure (e.g. resin as black background), and (c) the ImageJ software options set to obtain the same size of sampling grid area in each case. For these composite two-phase materials, all images were converted into binary images using ImageJ. Each binary image was divided into non-overlapping boxes as shown in Figure 3.6 using variable numbers of boxes, as required to cover the image with 12

grid positions[5], i.e. for each of the 240 images, the analysis was conducted with 12 separate starting co-ordinates, and the results were averaged. In this study, the quantification of the microstructural D was performed with the resin background made black and the fibres made white (see Figure 3.9).
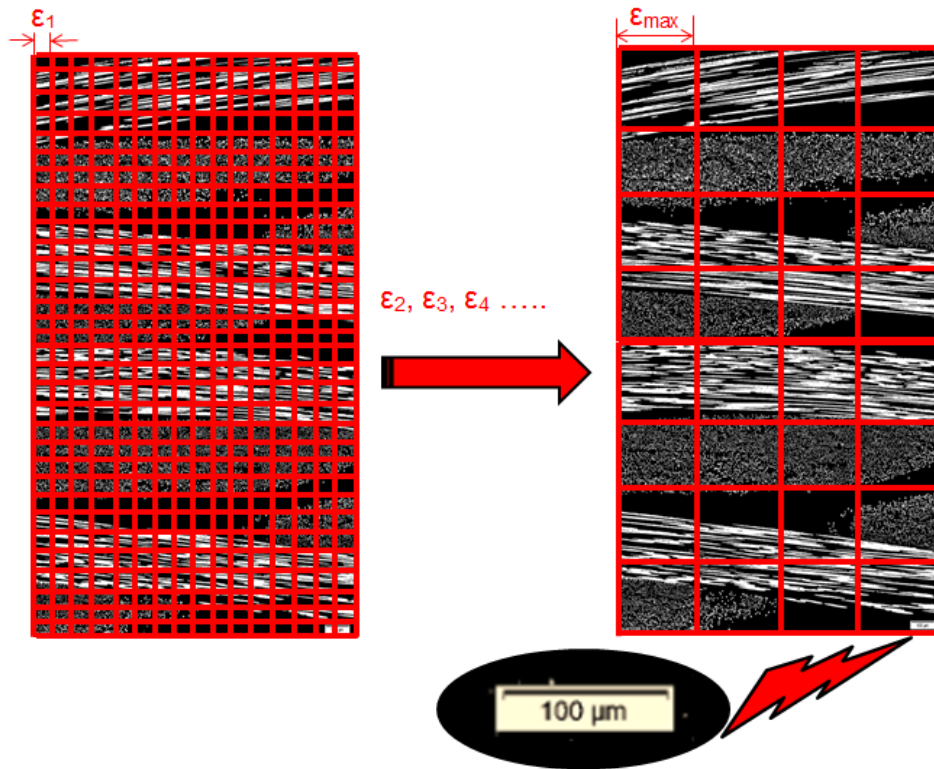
Figure 3-6: Illustration of an increase in box size and decrease in box number in the box counting method (the red boxes are just for illustrative purposes and, in reality, they are 'virtual'). Note that all boxes contain at least one fibre at ε_{max} but a lot of boxes at ε_1 contain no fibre.

ImageJ with FracLac software creates an imaginary network of boxes over the binary image of the sampling region of the laminate with an initial box size (ε_1). It then iteratively creates other networks with different box sizes (ε_2, ε_3, ε_4 .... ε_{max}). This procedure starts from the minimum resolution of 1 pixel and continues until the box size reaches maximum box size (taken as 25% of the shorter side of the image [122]). At every step *i*, the program counts the number of boxes that contain fibre, count $F\varepsilon_i$. A log-log plot of number of fibre-

---

[5] The number of boxes needed to cover all of the foreground pixels depends on where the grid is positioned, hence the grids laid at 12 different locations.

containing boxes, Fε, against box size ε is produced as the output from this process. Each iteration gives a point in this plot. The slope of the regression line equals the negative estimated fractal dimension of the laminate under consideration. Figure 3.7 illustrates the procedure. The slope of the regression line can be calculated using Equation (3.1) for each grid position. The mean fractal dimension of different grid positions has been calculated by using Equation (3.2).
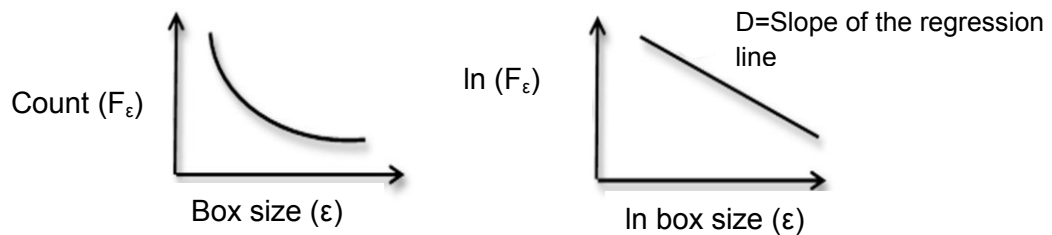
Figure 3-7: Illustration of calculation of the fractal dimension using the box counting method.

$$D = \text{slope} \left[\ln(\text{ number of boxes with detected features})/\ln(\varepsilon) \right] \qquad (3.1)$$

$$\text{Mean } D = \Sigma(D)/\text{grids} \qquad (3.2)$$

For clustered fibres, the tow centres will be further from the surface of the material, whereas for uniformly distributed fibres there will be more reinforcement adjacent to the sample surface (further from the neutral axis in bending) with an expectation of a higher flexural modulus in the latter case. However, the RRV between fibres are larger and more likely to be contiguous in uniform fibre distributions compared with the case for clustered distributions. A larger RRV will reduce the flexural strength. However, for real woven composites, it is difficult to assess uniformity or clustering by eye, and use of the D permits quantification in an objective systematic manner (Figure 3.8).

3.6.1 Image analysis of the infusion glass laminates

Optical image analysis of the microstructure is an important destructive characterising test for composite laminates. One can measure fibre, the resin and void areal fractions in the laminates from 2-D images and hence infer the respective volume fraction for each component. It is very important to choose the correct direction in the samples to perform this D characterisation because that controls the appearance of the samples under optical microscopy. The cut composite samples are embedded in a resin to prepare them for the polishing process. The polishing procedure is described in Appendix A-3 and affects the resolution of the images, especially when image analysis is needed.

At this stage of the research, using samples of the laminates that were manufactured by the infusion process, the D specimens were cut parallel to the cross section of the mechanical test samples, so that the woven weft glass fibres appeared as circles and the warp fibres had an elongated oval form or vice versa dependent on the stacking sequence. Ninety images were analysed at each level of consolidation (30 images from each of the three laminate plates). In this optical microscopy process, the problem of broken fibres, especially those elongated during the cutting procedure should be noted, because they have the same contrast as the voids as shown in Figure 3.8 and this would affect the results of automated image analysis. To avoid this problem, the region of interest (ROI)[6] technique was used, which is illustrated in Figures 3.8 for the three different phases of fibre (Aqua colour), resin (Deep Pink colour) and voids (Dark Blue colour). This problem could subsequently be avoided by changing the cutting procedure using an angle greater than 0° to reduce the

---

[6] In ROI, the user of Olympus Stream image analysis software can define thresholds for multi-phase analysis directly from the image, then the software automatically calculates area and area fraction, and the number of objects and the results can be exported to Excel file.

effect of broken fibres, by improving the polishing process and improving the laminates quality by reducing the voids. The latter two are used in this project.
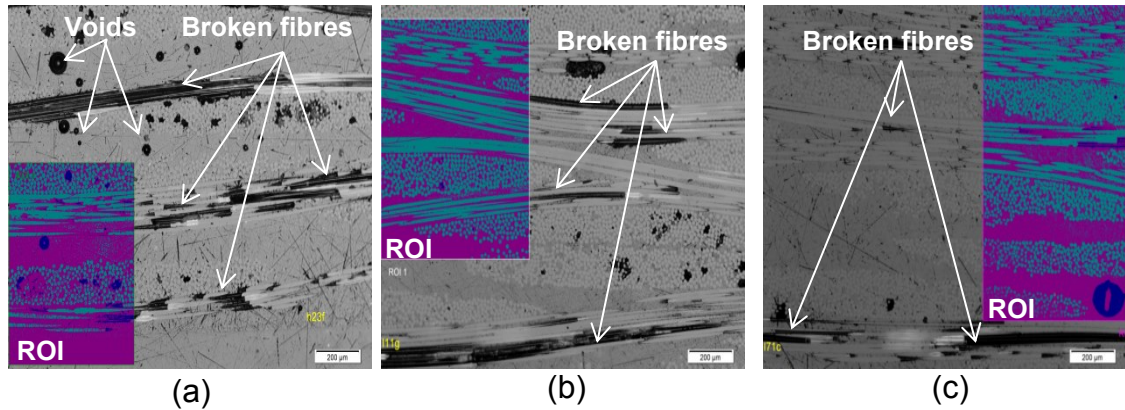
Figure 3-8: Microscopic image analysis of glass fibre – epoxy composite, (a) hand lay-up,(b) 600 and (b) 900 mbar.

The cavity in the infusion process is variable and depends on the level of consolidation and this gives constancy in the fibre volume fraction across the thickness. Therefore, there is no need to analyse the whole thickness of the laminate in order to characterise the D. ImageJ with FracLac software was used to determine the D for each woven glass fibre laminate. The process involved capturing five images, at (10x) magnification, from each of the three replicate plates made using the three different levels of consolidation. This provided 15 images for each consolidation pressure giving 45 images in total for analysis. All the captured images were converted to binary form, as shown in Figure 3.9, which is essential to reduce the computational time [133] necessary to determine the D. Figure 3.9 demonstrates that increasing the level of consolidation (increasing the applied vacuum) results in smaller RRV.
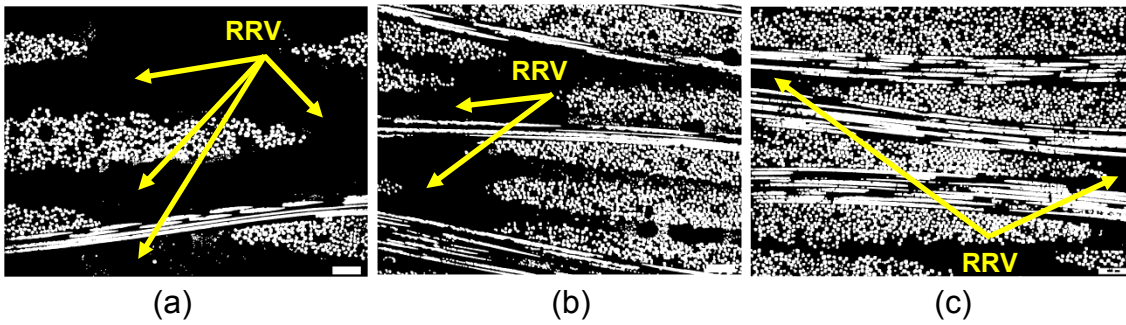
Figure 3-9: Binary images of glass fibre – epoxy composite, (a) hand lay-up, (b) 600 mbar and (b) 900 mbar.

3.6.2 Image analysis of the RTM carbon laminates

Image analysis of mounted microstructural specimens was performed to obtain the D for the laminates that were manufactured by RTM. Samples were cut normal to both the warp and the weft directions shown in Figure 3.5. Accurate determination of the D required 40-60 images from both warp and weft directions in each of the six laminates plates giving 560 images for analysis. The variation in number of images required arises from the variable RTM laminate thickness and the constant 10x magnification factor used in this work. Thus in a thicker sample at the magnification used in this work (10x), a single image does not cover the full laminate thickness (which is necessary for characterising the fibre distribution and D), and it was necessary to overlap several images and move them into digital registration (Figure 3.10) to generate a single merged image for analysis.

raw   first section   merged   raw   second section   merged
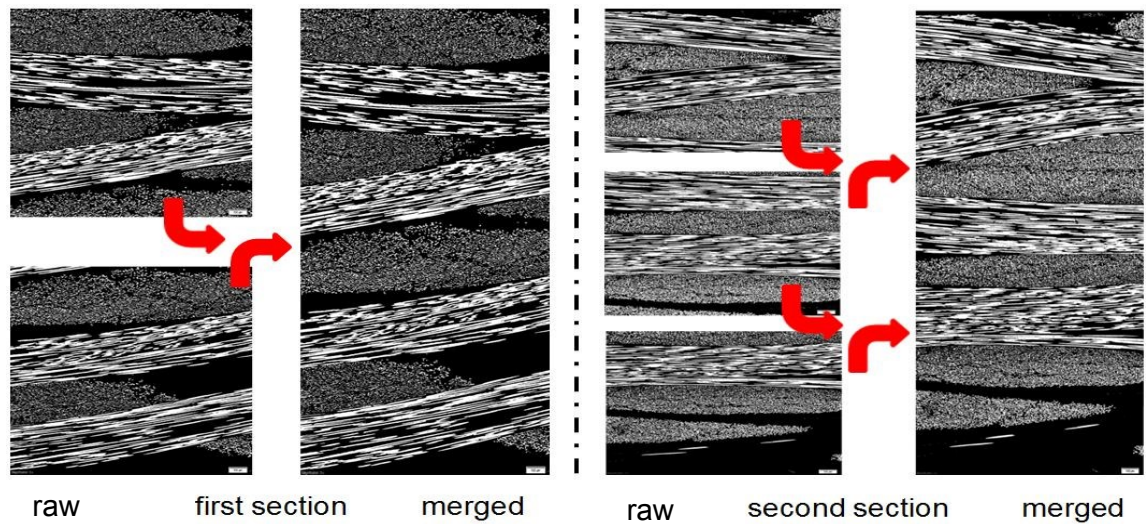
Figure 3-10: Illustration of merging the microstructural images to cover the complete thickness of the laminate (2080x2800) pixels for the first image and (2080x3400) pixels for the second image.

After merging the microstructural images, ImageJ with FracLac software was used to calculate the fractal dimension for 20 samples from each of the 12 cases considered (warp and weft directions in six different RTM laminate plates) giving a total of 240 images to be analysed. Figures 3.11 and 3.12 show the experimental technique used to determine the value of the D of the weft direction of the twill weave plate containing 4 layers of fabric (data shown for only 1 of the 20 values sampled for this case and the D = 1.8504 which equals the slope of the line).
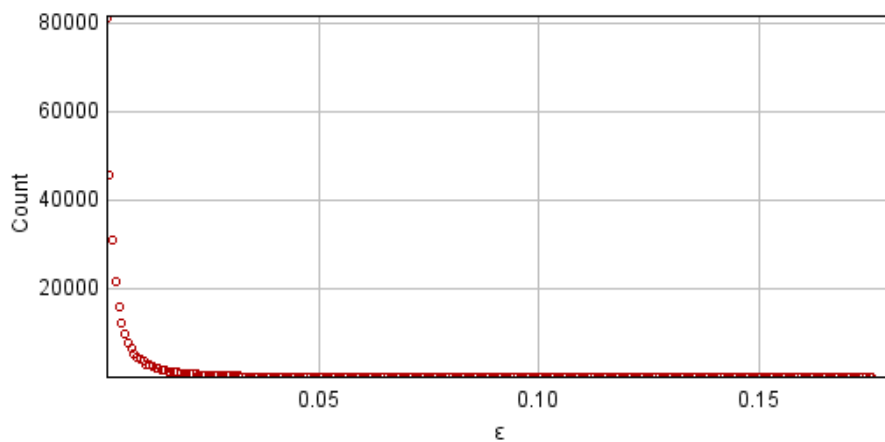
Figure 3-11: Plot of counts against box size for the weft direction of the four layer twill weave laminate.
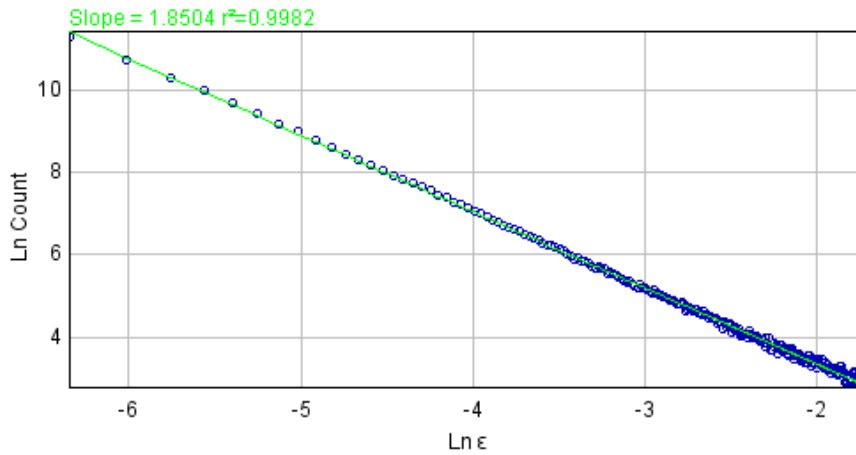
Figure 3-12: Log-log plot of the data in Figure 3.11.

3.7 Fractal dimension box counting method.

It is essential to check the validity of the box counting method when calculating the D for the composite laminates. The estimation of fractal dimension is not straightforward, especially for shapes without self-similarity. The accuracy of the results depends on various factors such as the maximum box size and the grid position relative to the microstructure. Ideally, the effect of each of these factors should be assessed using validated cases with known solutions. The box counting method has been validated in this project with images (shown in Figure 3.13) of known fractal dimensions such as Sierpinksi carpet (D=1.893), an area (D=2), Kock island (D=1.5), Sierpinski gasket (D= 1.585) and Koch snowflake (D=1.262).

Sierpinksi
carpet

An area

Kock island

Sierpinski
gasket

Koch
snowflake
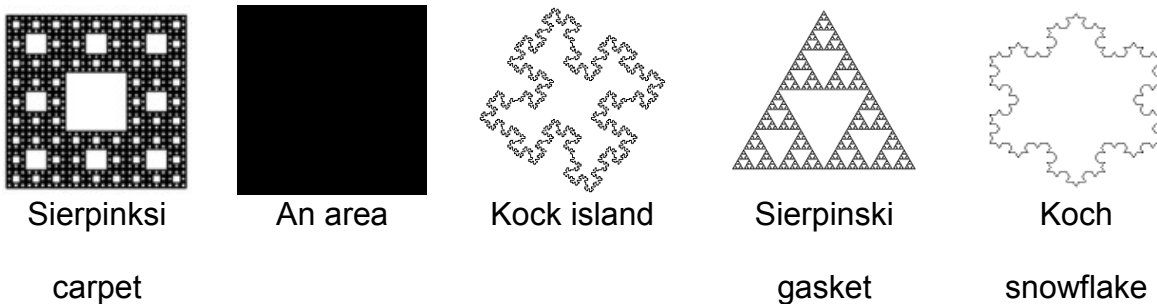
Figure 3-13: Different fractal images.

The box counting method was implemented in ImageJ with FracLac software. The method was validated with actual fractal dimension values that lie in the range 1.262 - 2.0. In order to improve the accuracy of D determination in the present work, the binary images shown in Figure 3.13 were used to investigate the effect of the maximum box size (which was varied from 1-45% of the shorter side of the image) and the effect of the grid position (which was varied from 1-40).

Figures 3.14-3.18 illustrate the effect that maximum box size and grid position have on the calculated D. For most exemplar images, the calculated D approached a stable value as the grid position value increased from 1 to 40, except Sierpinksi carpet and solid image (i.e. Area), and as the maximum box size became > 15% and < 30% of the shorter side of the image. Therefore, in this study, the maximum box size was taken as 25% of the shorter side of the image, which is the value used in the work reported by Foroutan-Pour et al. [122].

In choosing the grid position number, there is trade-off between increasing stability of the D as grid number increases and the additional time required for the calculations. The microstructural images in this study of composite laminates are similar to the Sierpinksi carpet and solid images and both are square shapes. It is essential to increase the grid position number in order to increase the accuracy of the D especially when using a large box size.

The box counting method was used in the work for this thesis to determine the D with the maximum box size and taking 12 grid positions. These parameters were checked with the standard fractal images discussed above. Once a combination of factors was found that appeared to give an acceptable

percentage of error between the actual and the estimated values of D (see Table 3.1), these factors (maximum box size and grid positions) were then applied to calculate the D of all the composite laminate specimens used in this work.
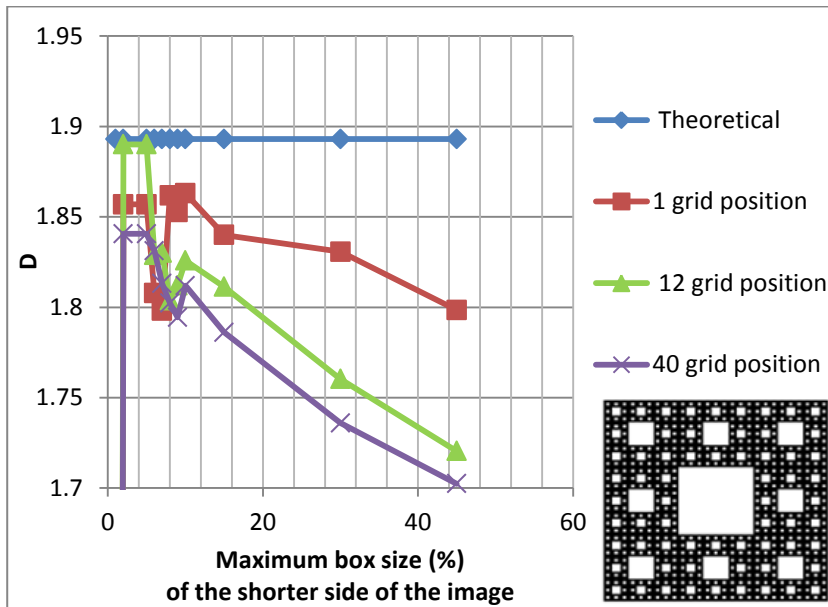
Figure 3-14: The D versus the maximum box size for the Sierpinksi carpet image with various grid positions.
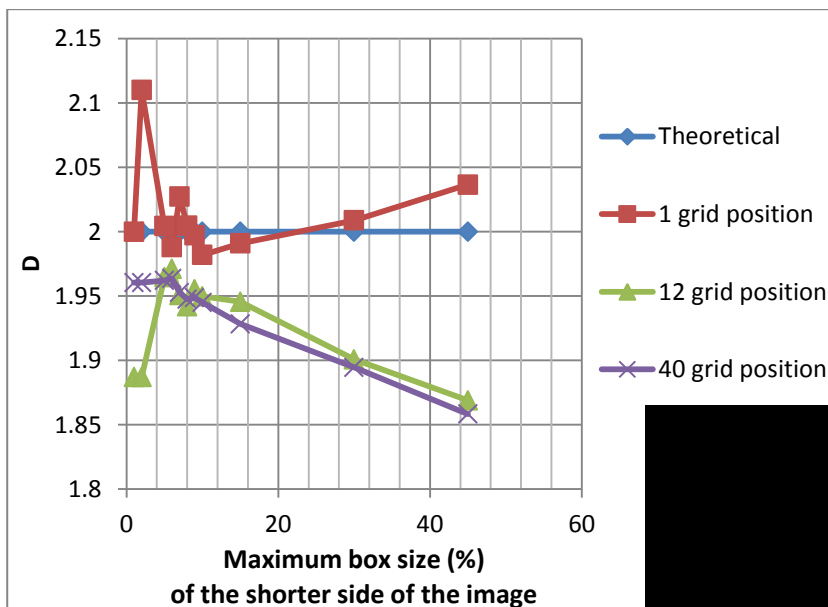
Figure 3-15: The D versus the maximum box size for the Solid image with various grid positions.
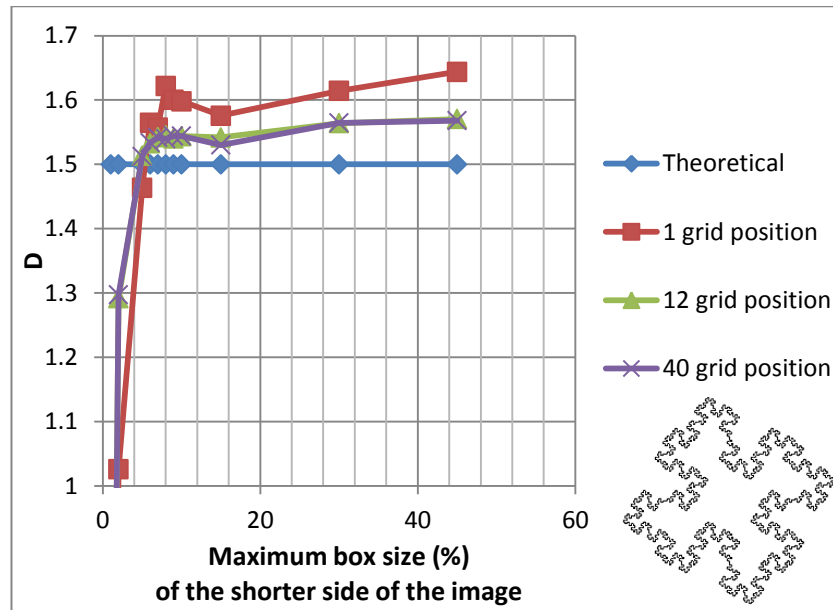
Figure 3-16: The D versus the maximum box size for the Kock island image with various grid positions.
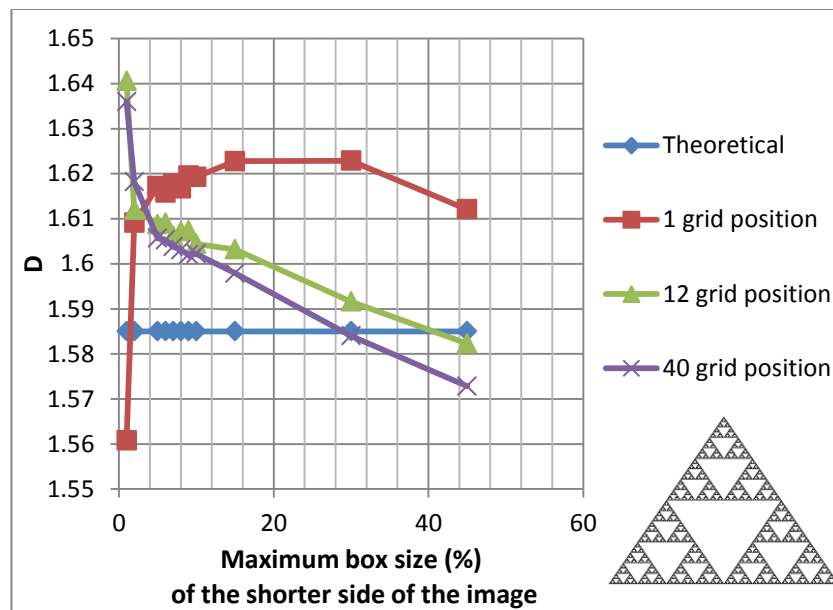
Figure 3-17: The D versus the maximum box size for the Sierpinski Gasket image with various grid positions.
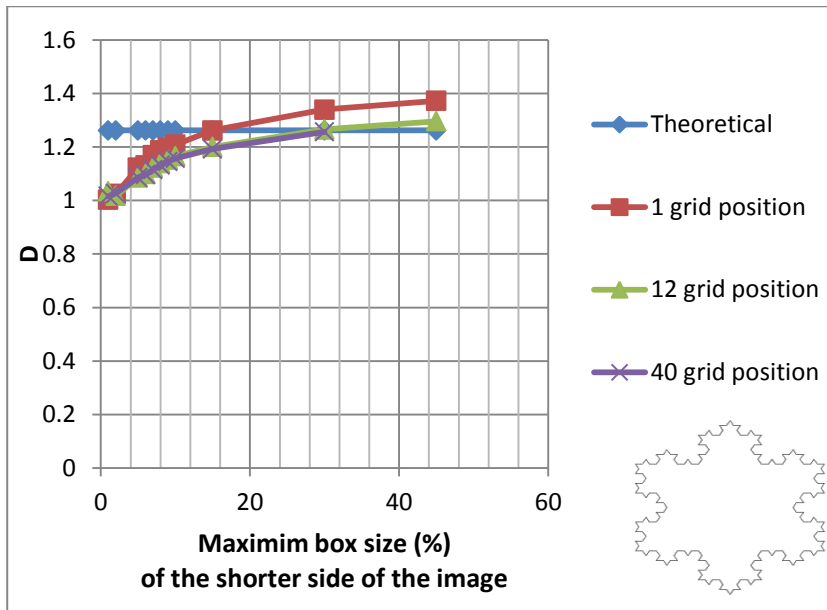
Figure 3-18: The D versus the maximum box size for the Koch snowflake image with various grid positions.

Table 3.1 shows the error in the D calculated using the method proposed above compared with the actual D for the standard fractal patterns. For the first fractal image, its actual D is 1.893, while that calculated using the proposed method is 1.8642, giving an error of 1.52 %. In all of these standard cases, the error in the D estimation using the proposed method is less than 6.6 % when compared with the actual D, and this error is accepted because the D calculated is within the respective sets and did not overlap with the rest of the images. The proposed method gives improved estimates of the D as the D increases. This investigation demonstrates that the box counting method provides accurate D calculations. The proposed method has been used to calculate the D values for different laminates as shown in Figure 3.19 for some laminates by taking single image.

Table 3-1: The error between the fractal dimension values found using the proposed method compared with the actual D values for the standard patterns.

Fractal image	D (the proposed method)	D (the actual)	Error (%)
Sierpinksi carpet	**1.8642**	**1.893**	**1.52**
An area	**2.0112**	**2**	**0.56**
Kock island	**1.599**	**1.5**	**6.6**
Sierpinski gasket	**1.6285**	**1.585**	**2.7**
Koch snowflake	**1.3025**	**1.262**	**3.2**

D=1.84 for T4wt **D=1.88 for T5wt** **D=1.91 for T6wt**
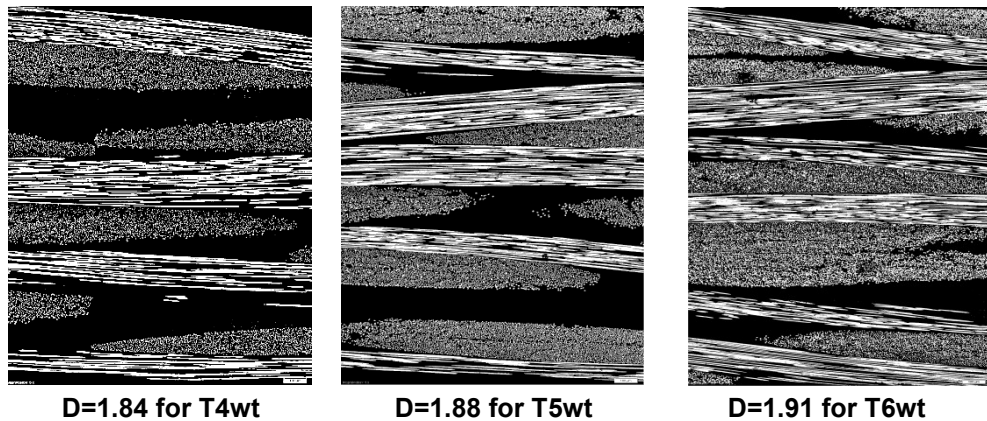
Figure 3-19: Different D values for some different laminates

3.8 Static and dynamic mechanical properties, and fractography.

3.8.1 Interlaminar shear strength (ILSS)

Fibre reinforced plastic composite materials show excellent strength and stiffness properties when loaded along the fibre direction. Structures under in-plane loading usually outperform their metallic counterparts, especially when subjected to fatigue loading, as the fatigue limit in composite materials is a high percentage of the tensile strength. However, the ability of the composite to withstand out-of-plane loading is governed predominantly by the properties of the matrix, which has a much lower static strength and is much more sensitive to fatigue. This is of particular importance with thick components. The

interlaminar shear strength is a measure of the ability of the laminate to resist delamination and was assessed in this work using the ISO 14130:1998 short-beam method (Figure 3.20) which essentially measures the adhesive force between fibre and resin. It should be noted that the short beam shear method, whilst widely used, has a number of problems associated with it in terms of assessing a 'true' interlaminar shear strength [134]. These include the dependence of the ILSS on support span-to-laminate thickness ratio and the fact that the stress state is not pure shear.   However, when making a comparison between the thin laminates used in this work, these influences are minimised. Five rectangular samples with dimensions 20x10x2 mm (length L, width W and thickness T) were cut with their L-direction parallel with the warp fibres, from each glass fibre laminate panel (manufactured by the infusion process), giving 15 ILSS test samples for each level of consolidation and hence 45 samples in total. Five samples of the same dimensions were cut with their L-direction in either the warp or weft directions from each of the six carbon fibre RTM laminate plates (comprising plain or twill weave with 4, 5 or 6 fabric layers (giving 60 samples in total)).   Tests were conducted using an Instron 5582 universal testing machine (serial number: 5582J7466) with a ±100 kN static range load cell (serial number: UK195) and a test speed of 1 mm/min and a constant span of 10 mm. The ILSS was calculated from Equation 3.3.

$$\tau = 0.75 \; \frac{Fmax}{bh} \tag{3.3}$$

Where τ is the ILSS (Pa), F_{max} is the maximum load (N), b is the width of the samples (m) and h is the thickness of the samples (m).
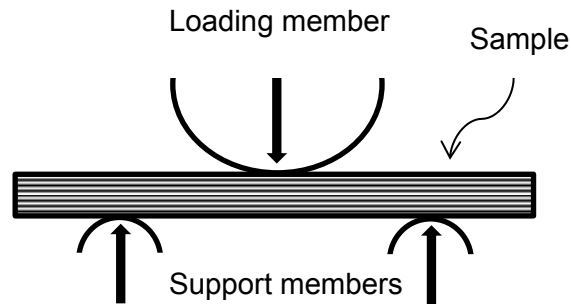
Figure 3- 20: short-beam method for ILSS test.

3.8.2 Tensile strength

The tensile strength is one of the most important mechanical parameters used to design composite structures in terms of the uniaxial stiffness and strength. Tensile tests were performed according to the British Standard BS EN ISO 527-4 for isotropic and orthotropic fibre-reinforced plastic composites. The tests were carried out in the 0° direction (warp direction), of the infused glass fibre laminates. The specimen dimensions were 250x25x2 mm with a 150 mm gauge length between the grips. Testing used an Instron 5582 universal testing machine (serial number: 5582J7466) with a ±100 kN static range load cell (serial number: UK195) and a crosshead speed = 2 mm/min. Strain was measured by an extensometer with a gauge length of 50 (mm), and the strain was held at a value of 0.02 (mm/mm), to permit removal of the extensometer before sample failure (to avoid any instrument damage during failure). The specimen was aligned with the load chain using a protractor. Five samples were cut in the warp direction from each panel of the glass fibre laminates, giving 15 samples for each level of consolidation and 45 samples in total.

3.8.3 Flexural (bending) modulus E$_b$ and ultimate flexural strength UFS

Four-point bend tests were conducted according to the British Standard EN ISO 14125:1998 for fibre-reinforced plastic composites as shown in Figure (3.21). An Instron Electropuls E300 (serial number: 5527-103) with a ±5 kN dynamic load cell (serial number: 107190) and test speed 1 mm/min was used. Tests were carried out in both the warp and the weft directions, of the RTM carbon fibre laminates, using specimens with dimensions of 100x15x2 mm (LxWxT). Five samples were cut from each direction of 3 different plates for each weave style (giving 60 samples in total). In bend the maximum tensile and compressive stresses act on the load-bearing faces of the sample and can be calculated using Equation 3.4.

$$\sigma = \frac{3Fa}{bh^2}$$

(3.4)

Where, σ is the stress (Pa) and F is the applied force (N).
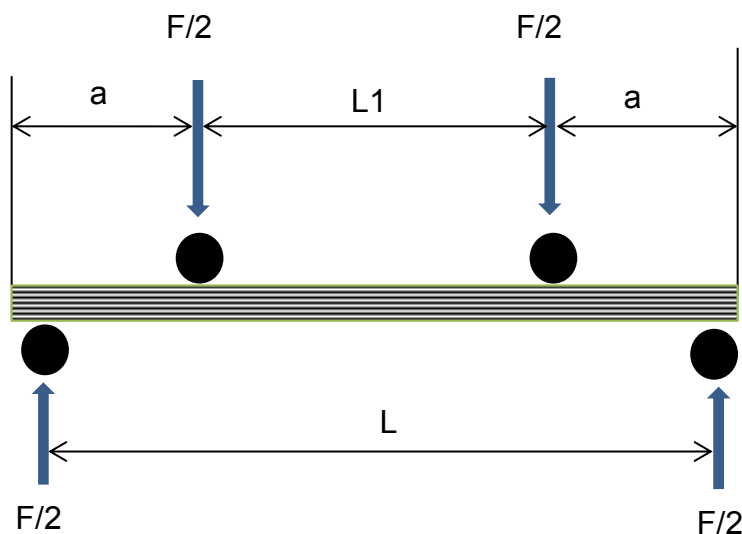
Figure 3- 21: The four-point bending test.

[72]

The flexural (bending) modulus of elasticity was calculated using Equation 3.5.

$$E_b = 0.21 \frac{\Delta F}{\Delta d} \frac{L^3}{bh^3} \tag{3.5}$$

Where E_b is the flexural modulus of elasticity (MPa), d is the beam mid-point deflection (m) and L is the span (m).

In calculating the flexural modulus, the displacement at mid-span should be used, although many researchers do not respect this requirement. A travelling microscope was used to measure the mid-point deflection (d) under flexural loading. The ultimate flexural stress (UFS), σ' (Pa) was then calculated using Equation 3.6.

$$\sigma' = \frac{3F'a}{bh^2} \tag{3.6}$$

Where F' is the maximum applied force (N) and a is the displacement between the point of application of the force and the support point.

3.8.4 Volume fraction V$_f$

Laminate thickness is an important parameter in work on composite materials, because one can use the thickness to estimate the quantity of resin used and hence predict the local mechanical properties [37] to assist in creating an optimum design. Furthermore, after manufacturing the laminates, their thickness[7] may have changed in the manufacturing process.

The total fibre volume fraction for specimens made with different fabrics and various numbers of layers was found from Equation 3.7, by substituting the

---

[7] The thickness values are squared in the denominator of Equations 3.4 & 3.6 and cubed in the denominator of Equation 3.5.

[73]

thickness values of the samples from the warp and the weft direction of each plate and each weave style (10 samples/plate) [135].

$$\text{Total } V_f = n \, A_F \, / \, \rho_f \, t \qquad\qquad\qquad (3.7)$$

Where V_f is the fibre volume fraction, n is the number of layers, A_F is the areal weight of fabric (kg/m^2), ρ_f is the density of the fibre (kg/m^3) (ρ_f equals 1800 kg/m^3 for woven carbon used in the RTM laminates and 2540 kg/m^3 for woven glass used in the infusion laminates) and t is the laminate thickness (m).

The stressed fibre volume fraction for the same specimens (those machined parallel to the beam's principal axis) is found using Equation 3.8, i.e. multiplying the total V_f (Equation 3.6) by the fibre orientation distribution factor ηo (equation 3.9).

$$\text{Stressed } V_f = \eta_O \, (n \, A_F \, / \, \rho_f \, t) \qquad\qquad (3.8)$$

Where, in-plane for woven reinforcement

$$\eta_O = \frac{\text{warp or weft yarn number}}{\text{Total yarn number}} \qquad\qquad (3.9)$$

For woven carbon fabric, areal weight, determined by weighing 1 m^2 fabric samples, was found to be 300.8 g/m^2 for plain weave and 320 g/m^2 for twill weave (confirming the values from the manufacturer). The tow counts were also measured, and yarn counts were 380 tows/m for both warp and weft in the plain weave and for warp in the twill weave, while the yarn count for the twill weft was 420 tows/m.

Therefore;

$$\eta_O = 380/760 = 0.5 \text{ for both warp and weft in the plain weave.}$$

[74]

$\eta_O = 380/800 = 0.475$ for warp in the twill weave.

$\eta_O = 420/800 = 0.525$ for weft in the twill weave.

3.8.5 Four-point bending fatigue test

In real service situations, composite laminates are not only subjected to static load, but also subjected to fatigue and impact loads. In addition, fatigue life is affected by fibre distribution which also has an effect on their static mechanical properties. Fatigue testing in tension was undertaken for the carbon fibre laminates. Initial work considered tensile fatigue on five samples (similar to the samples used in Section 3.7.2), but all failures occurred at the grips. Subsequently, therefore, constant amplitude four-point bend fatigue testing was chosen to investigate the fatigue properties of the carbon fibre laminates. Tensile fatigue testing has the advantage of testing the complete section thickness and generally gives a lower fatigue limit than bending, but flexure is representative of many service loading situations and enhances the possibility of delamination, which is an important factor in failure of composite materials. In addition, in four-point bending, the region of the specimen between the inner load points will be in pure bending, which is advantageous in terms of analysis.

In order to achieve relatively long fatigue lives and to test a large number of specimens, a high test frequency is desirable [136]. Furthermore, the higher thermal conductivity of carbon-fibre-based systems permits the use of higher test frequencies compared with glass-fibre-based or aramid-fibre-based systems [137]. Some researchers have found that there is no effect of frequency on the fatigue life [138], while others have observed a determined effect of higher frequency on fatigue life [11, 139-141]. Such observations are

likely to be a result of the localised heating at the crack tip arising from hysteretic energy input during strain cycling. This study compares different fibre distributions in otherwise very similar composite laminates with a constant frequency chosen for all laminate testing.

Fatigue cyclic loading frequency 10 Hz was chosen as a compromise between reducing test time, avoiding crack tip heating, and reducing specimen resonance. Although most other fatigue studies do not appear to have considered this issue, the present study does consider resonance because it could lead to failures other than the fatigue failure. The resonant frequency is calculated by Equation 3.11 [142, 143] for clamped-clamped boundary between middle rollers.

$$\omega_n = \frac{22.4}{L^2} \sqrt{EIL/m} \tag{3.10}$$

Therefore, $f = \frac{3.56}{L^2} \sqrt{EIL/m}$ (3.11)

Where, ω_n is the natural frequency (rad/s), f is the frequency (Hz), L is the distance between the middle rollers (m), E is the flexural modulus (Table 4.2), I is the second moment of inertia (m^4) and m is the mass of the sample (kg). The distance between the middle rollers was 27 mm and the width of the sample was 15 mm with values for the flexural modulus, mass and thickness of specimens given in Table 3.2. The 10 Hz test frequency is well below the fundamental resonant frequency (given in table 3.2) for all samples.

Table 3-2: Input data for calculating the resonant frequency of all samples.

Laminate	E (GPa)	Mass (g)	Thickness (mm)	Frequency (Hz)
P4wp	38.9	4.2	1.902	**226**
P4wt	31.2	4.04	1.84	**197**
T4wp	30.9	4.38	2.072	**225**
T4wt	34.6	4.23	2.03	**235**
P5wp	40.8	4.52	1.964	**235**
P5wt	39.2	4.34	2.022	**245**
T5wp	36.8	4.89	2.27	**266**
T5wt	42.4	4.83	2.268	**287**
P6wp	45.6	4.85	2.152	**274**
P6wt	41.4	4.85	2.136	**259**
T6wp	40.6	5.58	2.406	**286**
T6wt	42.4	5.25	2.362	**293**

The four-point bending fatigue tests were performed at room temperature under load control, in accordance with British Standard EN ISO 14125:1998 for fibre-reinforced plastic composites as shown in Figure 3.19. An Instron Electropuls E300 testing machine (serial number: 5527-103) with a ±5 kN dynamic load cell (serial number: 107190) was used. The tests were carried out on specimens machined with their longitudinal axis parallel with either the warp or the weft directions the laminate plates. Specimen dimensions were 100x15x2 mm (length x width x thickness) and the span L was 81 mm. Maxima in tensile and compressive stresses occur on the lower and upper surfaces of the sample respectively, and are calculated using Equation 3.4. The load cycling amplitudes were chosen on the basis of using a percentage of the ultimate flexural strength (UFS).

Fatigue properties in composite laminates depend on test parameters such as cyclic load wave form, the amplitude of the applied stress, the mean stress during cycling, frequency and stress ratio (R). The latter is the ratio of minimum applied stress (σ_{min}) divided by the maximum applied stress (σ_{max}). Hence in tension-tension fatigue 0< R <1, for fully reversed cycles R = -1, and for compression-compression fatigue R >1.

In the case of four-point bend testing, R=0.1, the upper surface experiences compression, while the lower surface experiences tension. Most fatigue studies on composite laminates use a frequency 10 Hz and R 0.1. Although it would be preferable to use R = 0, contact is lost on the specimen faces at minimum load and specimens move during the test, which is undesirable [11, 144].

In order to obtain S-N curves for the laminates, samples were loaded under constant amplitude sinusoidal loading until failure occurred. The number of cycles to failure, maximum and minimum applied loads, and maximum and minimum displacement under the load points were monitored during the tests in order to provide information on the decrease in stiffness (modulus) of the specimen during the test. The testing machine was tuned for each sample to account for changes in sample stiffness that might affect the test accuracy. Trial tests were used to confirm the range of the load levels to be used. Fatigue data were then generated at six load levels of 95% to 82.5% step 2.5% of the UFS. To reduce the time spent on generating the fatigue test matrix , a single set of repeat tests was performed for each laminate condition (giving 12 fatigue samples in total for each condition) which should be sufficient [137] to establish a basic S-N curve. The complete test matrix encompasses two fibre architectures (twill and plain weave) two directions in the laminate (warp and

weft) and 4, 5 or 6 fabric layers. 144 fatigue specimens were therefore tested in order to obtain S-N curves for all composite laminate conditions.

A bi-linear relationship between the maximum flexural stress S and log N, the number of load cycles to fatigue failure, is widely used to fit experimental fatigue data [89], as shown in Figure 3.22. The fatigue life data can then be described by Equation 3.12.

$$S = -A \log N + B \tag{3.12}$$

Where; A is the fatigue strength exponent and B is the fatigue strength coefficient.
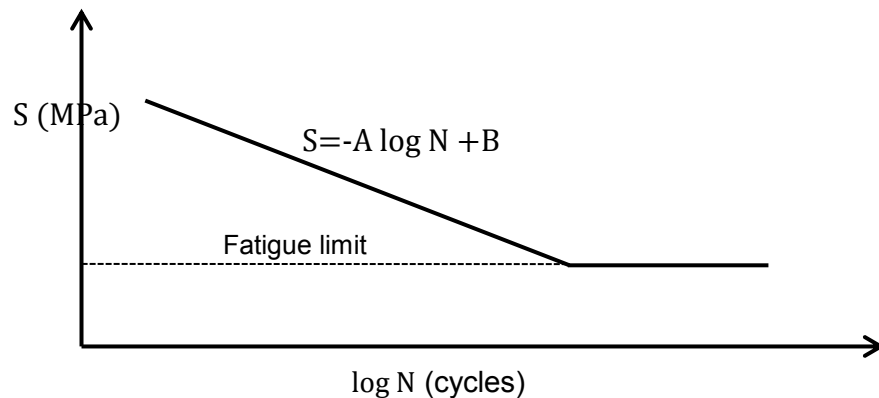
Figure 3-22: Typical S-N curve.

3.8.6 Fatigue damage index (FDI) and failure analysis

The cumulative fatigue damage index, FDI, was identified by Clark et al. [88]. It is derived from stiffness degradation for composite sandwich materials. In common with other materials, composite laminates are expected to fail when the accumulated damage exceeds a critical value. However, fatigue damage cannot be measured directly [89]. Therefore, the FDI has been defined in terms

of the flexural modulus decrease observed in composite materials as fatigue cycling progresses.

$$FDI = 1 - (E_b / E_o) \qquad\qquad (3.13)$$

Where, E_b is the current flexural modulus and E_o is the original flexural modulus.

In this study, the fatigue tests are performed under load control, and therefore increasing damage reduces the stiffness of the specimens (and hence reduces the modulus of elasticity) which leads to an increase in deflection that can be monitored. The flexural modulus of elasticity can be calculated using Equation 3.5. The fatigue loads (load and displacement of the loading points) are recorded on a cycle-by-cycle basis by the Electro-puls testing machine.

To calculate the flexural modulus, the displacement of the beam at the mid-span should be used. A traveling microscope was used to calibrate the beam mid-point deflection (d) as a function of displacement under the loading points as shown in Table 3.3. Hence, by plotting this data as shown in Figure 3.23, the relationship between mid-span and load point displacements can be determined, as indicated in Equation 3.14.

Table 3-3: The data from the traveling microscope and the Electropuls machine.

$d_{loading\ member}$ (mm)	$d_{mid\ span}$ (mm)
1	1.26
1.5	1.8
2	2.37
2.5	2.92
3	3.4
3.5	4.03
4	4.6
4.5	5.1
5	5.7
5.5	6.25
6	6.7
6.5	7.35
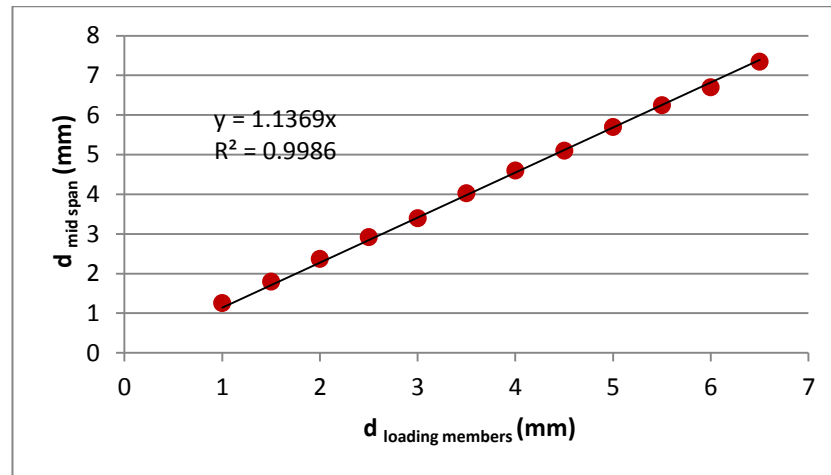
Figure 3-23: The calibration curve between the displacement under the loading points and the mid span of the laminate.

$$d \text{ mid span} = 1.1369 * d \text{ loading points} \qquad (3.14)$$

3.9 X-ray computed tomography

Once the S-N curves had been obtained for all laminates, an investigation into the relationship between fatigue life, crack initiation and the fatigue damage index was initiated. This involved, applying specific numbers of fatigue cycles to additional specimens at several load levels, with the cycle number being chosen as a proportion of the fatigue life calculated using Equation 3.12 at the particular load level. The tests were stopped once the desired cyclic life was reached.

Fatigued samples were then examined using a micro-CT scanner (Skyscan 1174 X-ray microtomograph, serial no 021), to identify the onset of failure or a nascent damage zone. Success in this process relies on a high resolution in the CT images. In CT scanning, the X-ray beam passes through the composite laminate from different angles to create multiple images that can be reconstructed to yield a 3D image of the interior of the laminate, hence showing the size and distribution of any crack-like features. A high resolution involves

[81]

taking an image for every 0.5^{o} for a full rotation of the sample (giving 720 images in total for each sample). If the CT images contain features with low density, that is likely to signify the beginning of crack formation.

Chapter 4 RESULTS AND DISCUSSION

4.1 Introduction

In Chapter Four, results are presented for the material characterisation and mechanical property experiments described in Chapter Three.

4.2 Fractal dimension – mechanical property relationships for infused woven glass laminates

As described in Chapter 3, glass composite laminates were manufactured by the infusion process. Three plates were manufactured at each level of consolidation and five test samples were cut from each of the three plates (giving 15 samples at each level of consolidation) for determination of the ILSS, the UTS and the fractal dimension.

Olympus Stream image analysis software (5M04733) was used to analyse 90 images of the various microstructures at each level of consolidation with the region of interest (ROI) technique. Initial work demonstrated that the polishing technique used to prepare the specimens gave low quality images while the ROI did not adequately represent the whole image. The polishing process was modified and the final process used in this work is presented in Appendix A-3. This procedure was used to prepare the specimens and obtain 15 new images of the microstructure as demonstrated in Figure 4.1 (five images from each plate) for each level of consolidation were acquired (giving 45 images for analysis in total). These were used to investigate the correlation between either the D, or the fibre volume fraction, and the mechanical properties for each laminate plate.

(a)   (b)
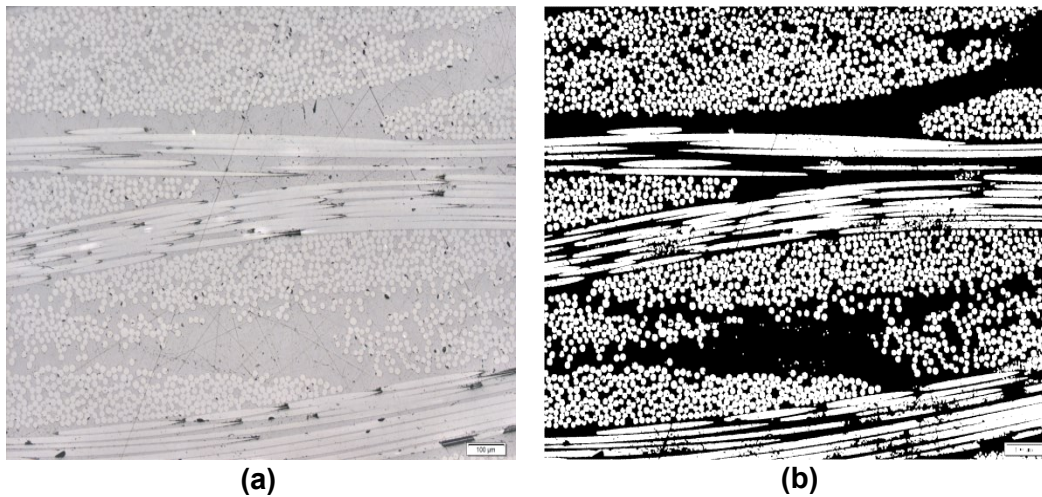
Figure 4-1: Typical micrographs of glass fibre – epoxy composite of 900 mbar, (a) Original and (b) In binary format.

The microstructures were characterised for each laminate using the box-counting method for calculating the D and the V_f. Interlaminar shear strength (ILSS) and quasi-static tensile tests were performed to measure the ILSS, elastic modulus (from the slope of the stress-strain curve) and ultimate tensile stress (UTS). Table 4.1 presents the mean mechanical properties and image analysis data, for the woven glass fabric laminates at different levels of consolidation.

Table 4-1: The mean mechanical properties and image analysis data.

Level of consolidation	UTS (MPa)	Elastic modulus (GPa)	ILSS (MPa)	D	V_f (%)
Hand Lay-up	265	12.1	18.4	1.712	23.5
Infusion 600 (mbar)	385	17.2	24.7	1.797	30.3
Infusion 900 (mbar)	398	17.4	31.3	1.866	52.1

Due to the different numbers of the specimens used in the mechanical testing and microstructural characterisation, the value of the standard error is used to check the variation in the data, where larger specimen numbers give a smaller standard deviation. The standard error is calculated using Equation 4.1. [145]

$$\text{Standard error} = \frac{STDEV}{\sqrt{n}} \qquad\qquad (4.1)$$

Where, $STDEV$ is the standard deviation and n is the sample size.

Figure 4.2 illustrates the increase observed in UTS with increase in the level of consolidation. The laminates that were infused under 900 mbar had the highest value of UTS. The elastic modulus also increased with increase in the consolidation level as shown in Figure 4.3. Furthermore, the results show that the ILSS increased with increasing level of consolidation as shown in Figure 4.4. In all cases, the increase in all mechanical properties as a function of increase in the level of consolidation due to an increase in the fibre volume fraction, V_f, (Figure 4.5). Therefore, consolidation of the laminate under 900 mbar gave significant improvement in mechanical properties compared with the other levels of consolidation. A further useful outcome is that laminates with high level of consolidation have fewer RRV as shown in Figure 3.9, where the RRV is inversely proportional to the fibre volume fraction, V_f.
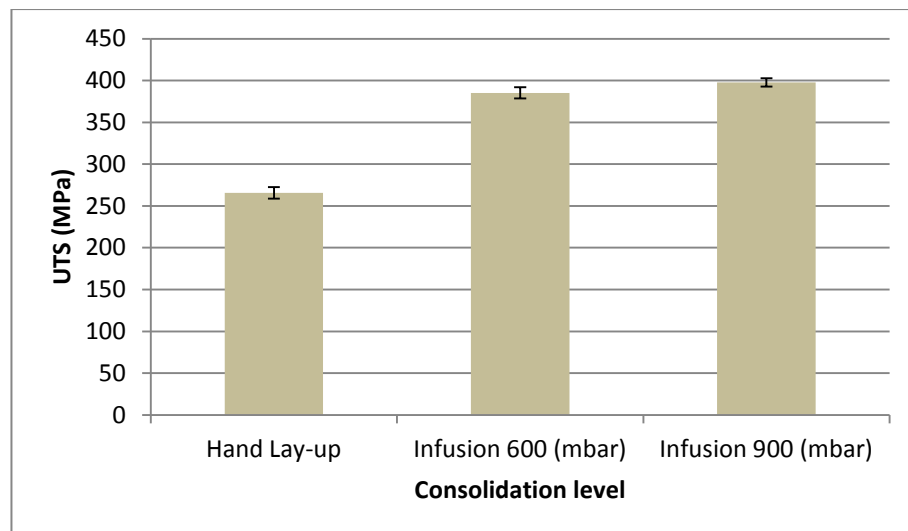
Figure 4-2: The Ultimate tensile strength UTS with standard error as a function of the level of consolidation.
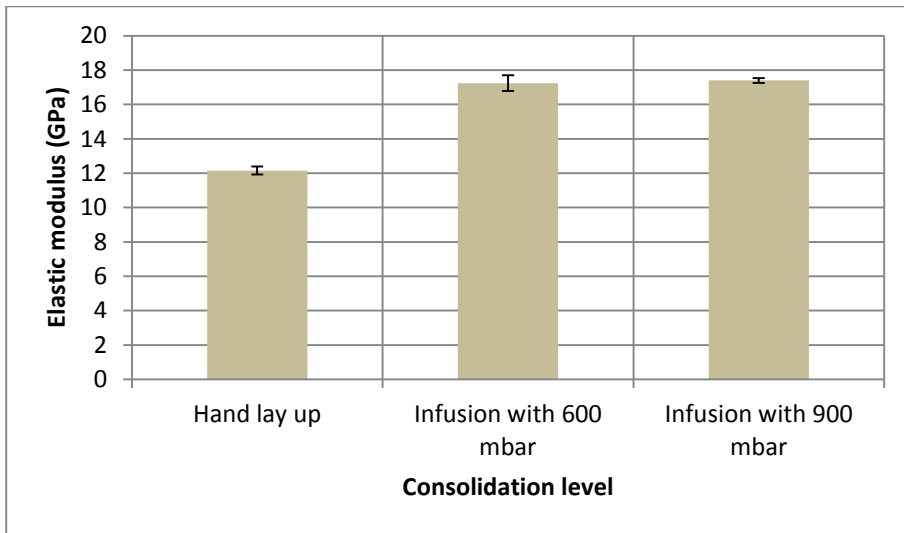
Figure 4-3: The elastic modulus with standard error as a function of the consolidation level.
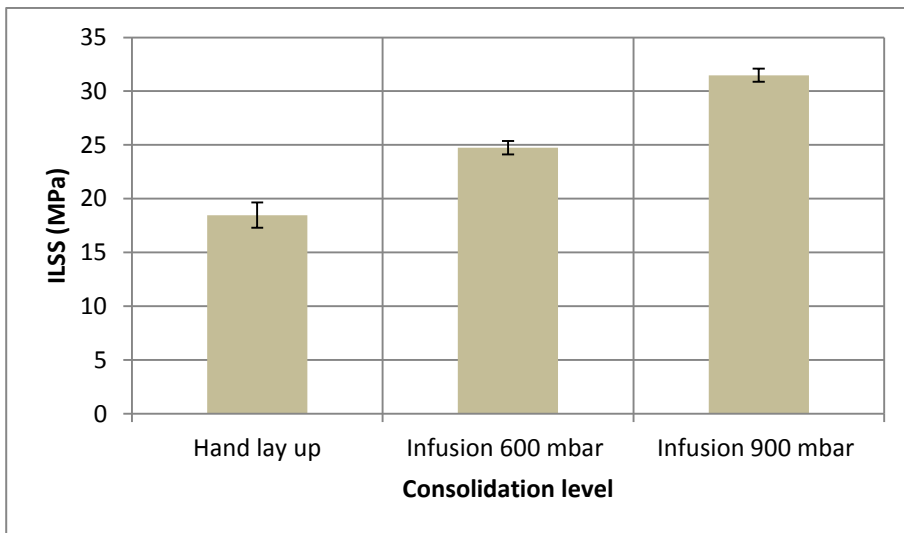
Figure 4-4: The interlaminar shear strength ILSS with standard error as a function of the consolidation level.
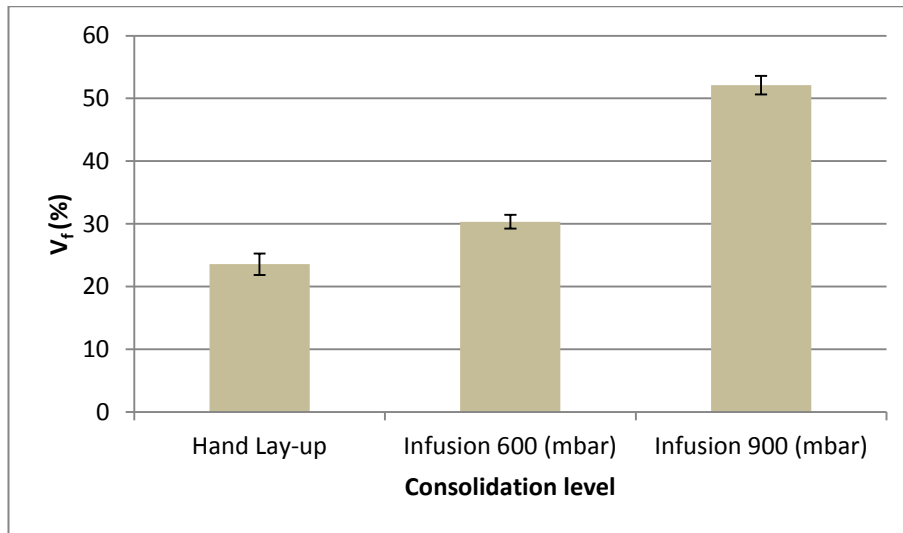
Figure 4-5: The fibre volume fraction V_f with standard error as a function of the consolidation level.

Figure 4.6 illustrates the observed increase in fractal dimension with increase in level of consolidation. A higher level of consolidation increases the fibre volume fraction V_f of the laminate and the uniformity of the fibre distribution, and hence a higher fractal dimension as seen in Figure 4.7. Furthermore, a higher infusion pressure can sometimes increase the uniformity of the fibre distribution within the laminate, and hence reduce the clustering of the fibres which, in turn, reduces the RRV content. This situation is in keeping with that shown by Pearce et al. [48] to increase the mechanical properties of the laminate. Figure 4.8 further shows that a strong link exists between fractal dimension and interlaminar shear strength (ILSS), while, Figure 4.9 illustrates the increase observed in the elastic modulus with increase in level of consolidation and with the fractal dimension. A similar trend is observed in UTS as shown in (Figure 4.10).

These results indicate that mechanical properties are strongly influenced by volume fraction, with an increase in V_f directly correlating with an increase in properties. Similar trends exist between fractal dimension D and mechanical

properties and hence these key performance indicators can be predicted for a particular manufacturing process and level of consolidation, from characterisation of the D using image analysis. A high D value implies a high V_f and/ or a uniform fibre distribution and leads to good mechanical properties. It should be noted that these observations and relationships are true when analysis of the D is performed with the resin as background. However, if we determined the D with the fibre as background, this will be reversed which means that all these trends would then be a function of a decrease in D.
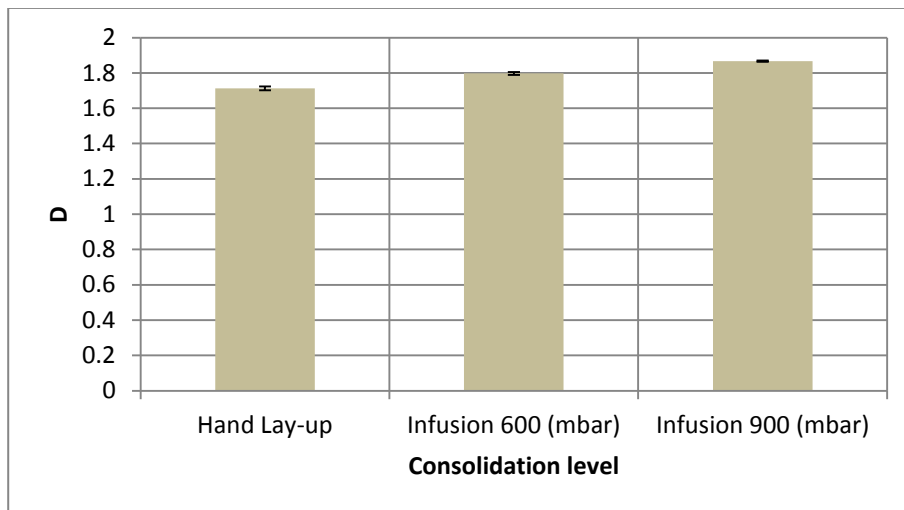
Figure 4-6: The D with standard error as a function of the level of consolidation.
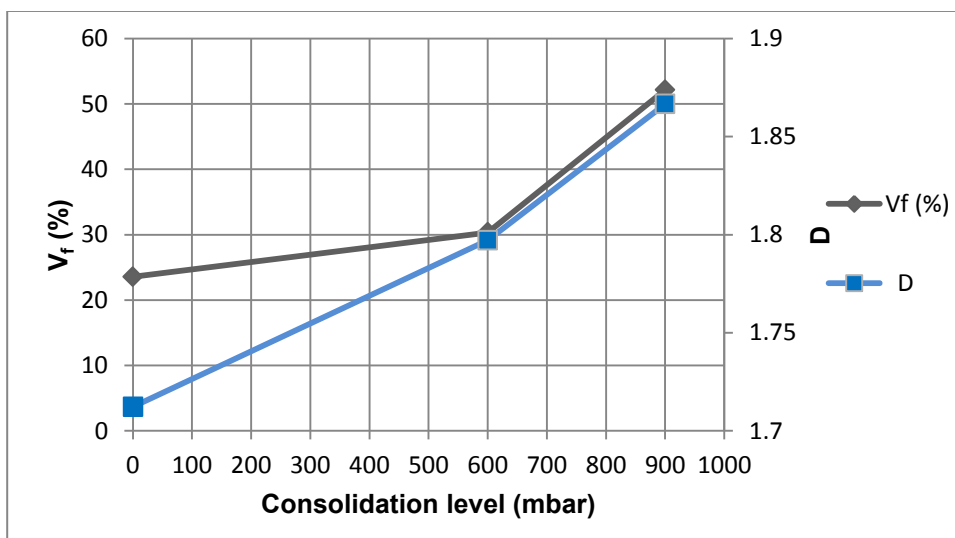
Figure 4-7: The fibre volume fraction and the fractal dimension as a function of the level of consolidation.

[90]
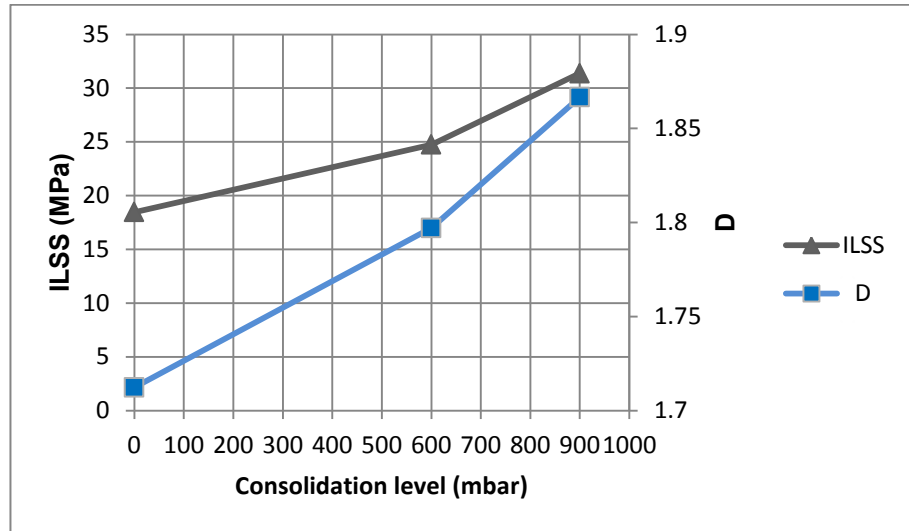
Figure 4-8: The interlaminar shear strength and the fractal dimension as a function of the level of consolidation.
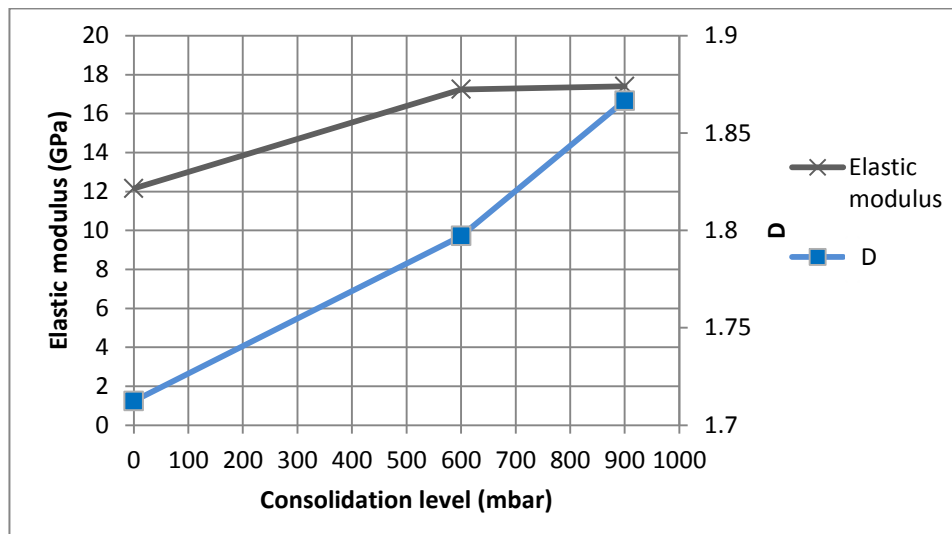
Figure 4-9: The elastic modulus and the fractal dimension as a function of the level of consolidation.
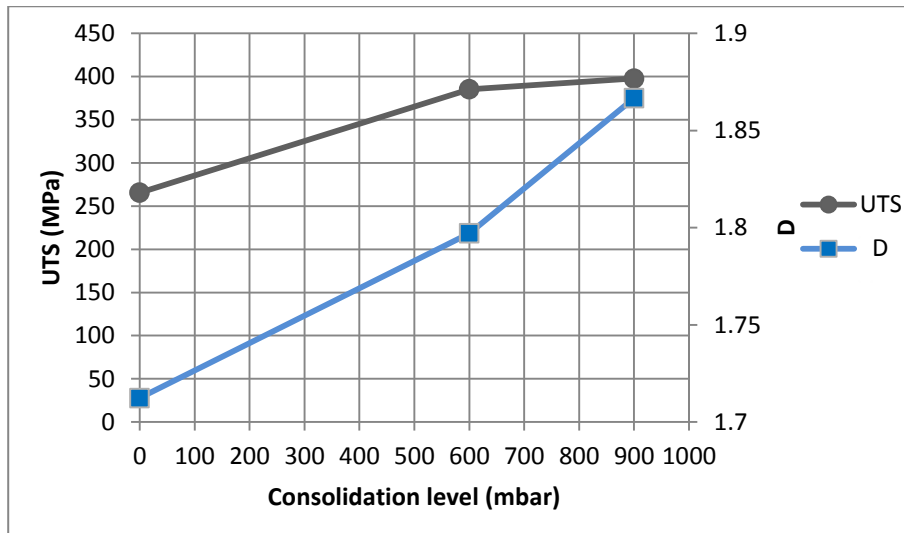
Figure 4-10: The Ultimate tensile stress and the fractal dimension as a function of the level of consolidation.

The underlying hypothesis presented in this thesis is that either D or V_f or both, will correlate with mechanical properties and therefore be able to act as a predictor of mechanical performance of the composite laminate. A point of considerable interest is then, which of these two parameters is better and why? To explore this further, the mechanical properties are plotted against the D and V_f respectively in Figures 4.11 and 4.12. Fitting linear relationships between UTS and both D and V_f, the correlation between the UTS and the D (R^2 = 0.8633 Figure 4.11a) is better than the correlation between the UTS and the V_f (R^2 = 0.5537 Figure 4.11b). Similar trends are found for the cases of ILSS and elastic modulus (Figure 4.12 and Figure 4.13 respectively).
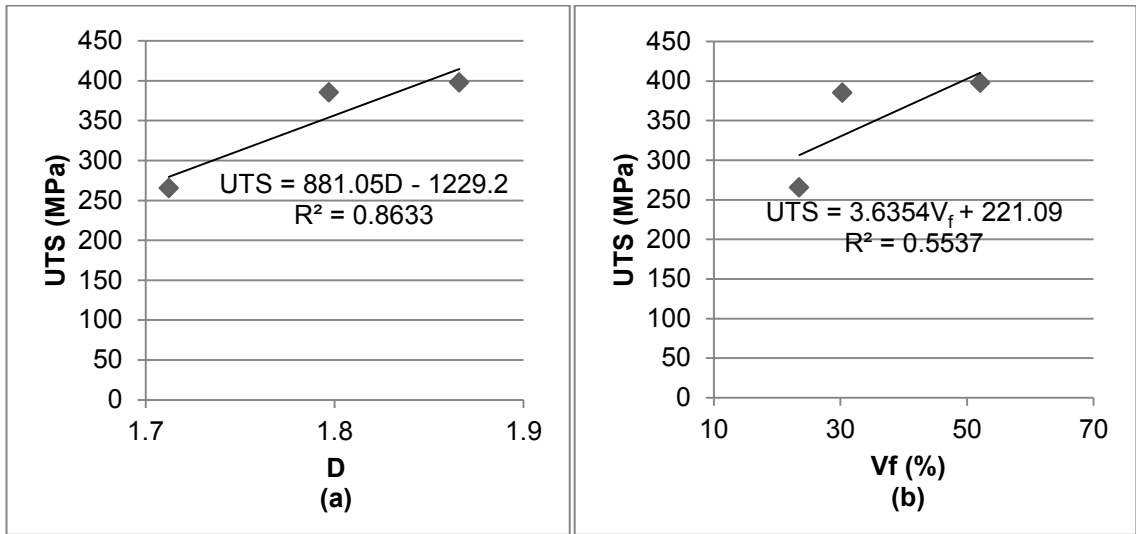
Figure 4-11: Woven glass laminates: a) Ultimate tensile strength UTS versus fractal dimension D and b) UTS versus the fibre volume fraction V_f.
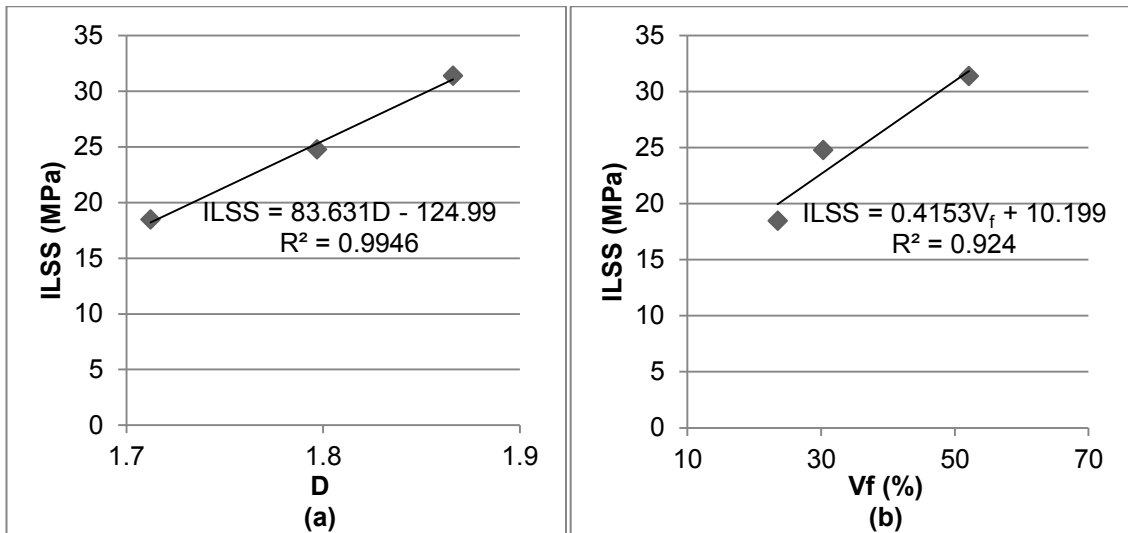
Figure 4-12: Woven glass laminates: a) ILSS versus fractal dimension D and b) ILSS versus the fibre volume fraction V_f.
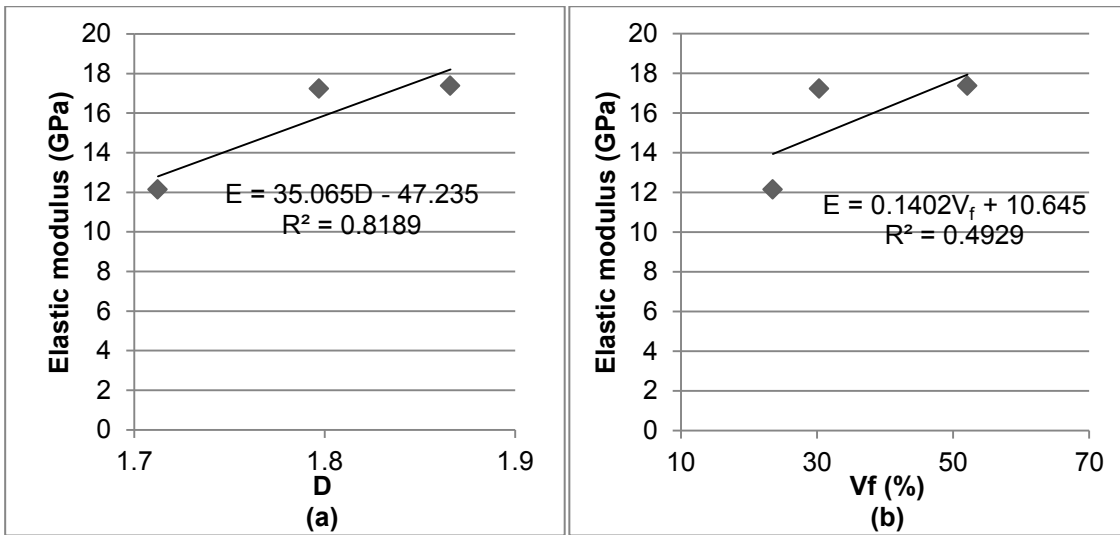
Figure 4-13: Woven glass laminates: a) The elastic modulus versus fractal dimension D and b) The elastic modulus versus the fibre volume fraction V_f.

All these results indicate that the D is proportional to the level of consolidation, and that V_f, ILSS, elastic modulus and UTS generally increase with increase in D. Performing the correlation using a linear relationship suggests that the fractal dimension may be a better parameter to characterise the mechanical properties of fibre reinforced composites than V_f, and indicates that the fractal dimension could be used to compare mechanical properties, for different fibre reinforced composite laminates, with a high D implying a high level of mechanical properties. The analysis reported in this section was the first step in the investigation of the effect of fibre distribution on mechanical properties, as mentioned in the objective of the work and illustrated schematically in Figure 1.2. The next step in the work is analysing the performance of different woven fabric laminates manufactured to possess similar V_f, but with different fibre distribution. The RTM process was used in this part of the work.

4.3 Fractal dimension – mechanical property relationships for RTM laminates

This section discusses the relationship between D and mechanical properties for the carbon fibre composite laminates that were manufactured using the RTM process. In a similar fashion to the results discussed in Section 4.2, microstructures were quantified for each laminate, in both the warp and weft directions, using the box-counting method to characterise the D, the stressed V_f (defined in equation 3.8)[8] and the total V_f. Interlaminar shear strength, ILSS, and four-point bending tests have been undertaken to obtain values for the flexural bending modulus (E_b) and the ultimate flexural stress (UFS). Table 4.2 presents the mean mechanical property and image analysis data for the woven carbon fibre fabric laminates, with the two different fibre architectures (plain and twill weave) and 4, 5 of 6 layers of fabric.

Figure 4.14 presents the UFS data for all the RTM specimens and demonstrates that the UFS of the twill fabric laminates is higher than that of the plain fabric laminates in the weft direction and that this trend is reversed in the warp direction, although the UFS for both fabrics increases with increasing number of fabric layers (as would be expected from the rule-of-mixtures). In the case of the ILSS data (Figure 4.15) the twill fabric has higher strengths in both the warp and the weft directions. Data for the flexural modulus E_b (see equation 3.5 for the definition) indicates that the plain fabric is stiffer than the twill fabric in the warp direction and less stiff than the twill in the weft direction as shown in Figure 4.16, because the flexural modulus data are consistent with the fibre volume fraction data (Figure 4.17), except the flexural modulus of the twill in the

---

[8] (i.e. V_f weighted to account for only the fibres in the stressed direction)

weft direction, where the yarn count was higher than others (420 tows/m) and the crimp[9] of the twill fabric could be less than the crimp of the plain fabric. Data for V_f indicates that the plain weave fabric has better performance than the twill weave fabric in both warp and weft directions (Figure 4.17). There is a general trend observed in all four mechanical property parameters to increase with increasing number of fabric layers.

Table 4-2: The mean mechanical property and image analysis data for woven carbon fibre laminates.

Laminate	Direction	Symbol	D	Stressed V_f (%)	Total V_f (%)	UFS (MPa)	ILSS (MPa)	E_b (GPa)
4 layers (Plain)	Warp	P4wp	1.835	18.2	36.4	561	43.8	38.9
	Weft	P4wt	1.809	17.5	35.1	463	40.5	31.2
4 layers (Twill)	Warp	T4wp	1.826	16.5	34.9	548	46.8	30.9
	Weft	T4wt	1.862	18.3	34.8	608	45.9	34.6
5 layers (Plain)	Warp	P5wp	1.859	20.9	41.9	670	47	40.8
	Weft	P5wt	1.841	20.6	41.2	567	44.1	39.2
5 layers (Twill)	Warp	T5wp	1.844	18.3	38.6	642	51.3	36.8
	Weft	T5wt	1.893	20.6	39.2	719	49.3	42.4
6 layers (Plain)	Warp	P6wp	1.892	23.8	47.6	725	48.9	45.6
	Weft	P6wt	1.850	23.3	46.6	623	44.9	41.4
6 layers (Twill)	Warp	T6wp	1.863	20.6	43.4	711	50.1	40.6
	Weft	T6wt	1.912	23.2	44.2	743	51.7	42.4

[9] Crimp: The waviness of the fibre in a fabric, expressed numerically as the crimp ratio, being the yarn length divided by the cloth length.
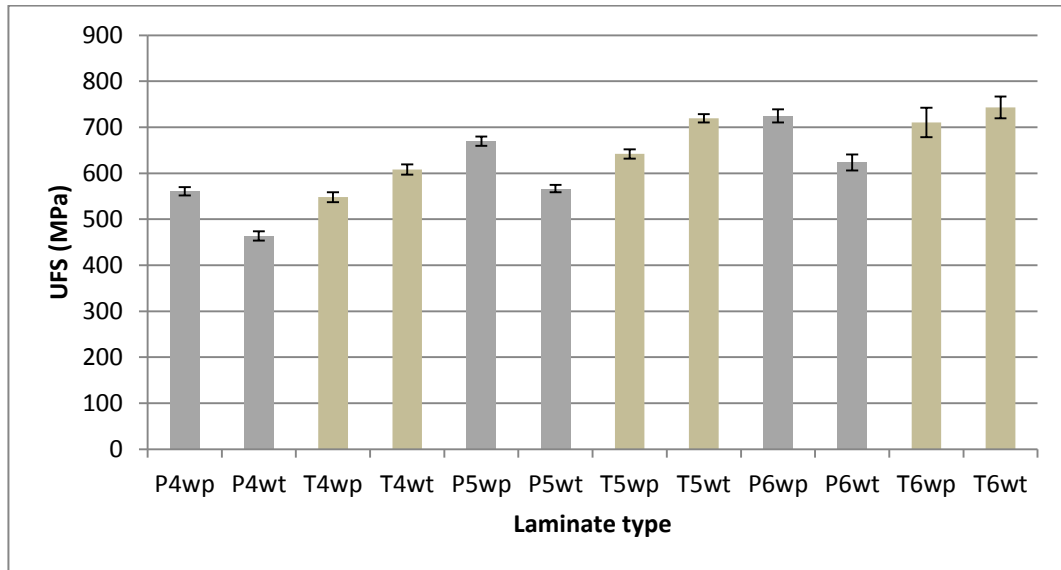
Figure 4-14: UFS with standard error for the various woven carbon laminates in warp (wp) and weft (wt) directions.
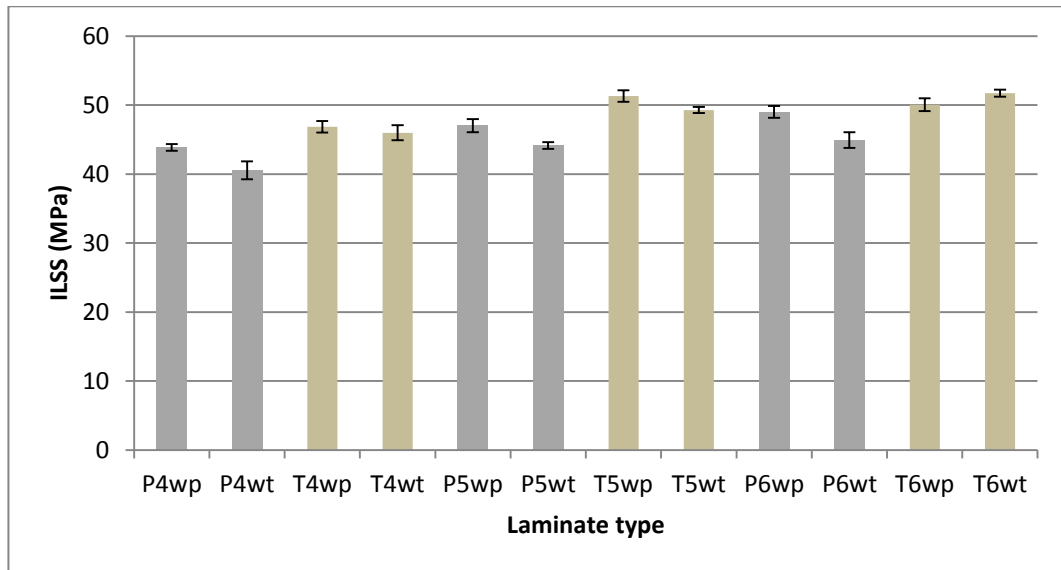
Figure 4-15: ILSS with standard error for the various woven carbon laminates in both warp and weft directions.
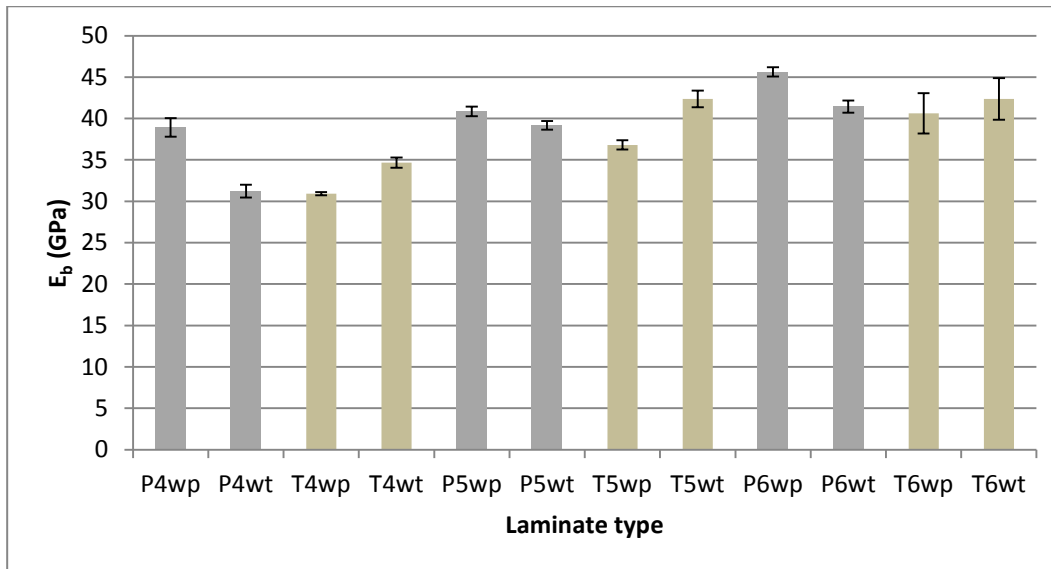
Figure 4-16: E_b with standard error for the various woven carbon laminates in both warp and weft directions.
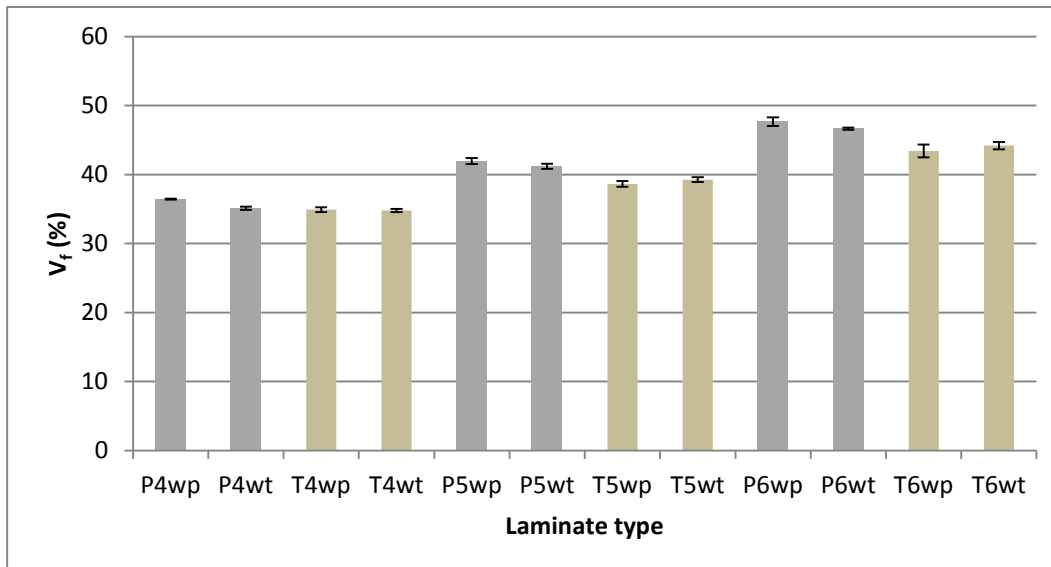
Figure 4-17: V_f with standard error for the various woven carbon laminates in both warp and weft directions.

For each of the six RTM composite laminates considered in this work, the microstructures were characterised in terms of the fractal dimension (D). To minimise the error in determination of fractal dimension, it was necessary to analyse a number of images and obtain an averaged value for the D. This will be illustrated here for the cases of the plain weave 4-layer weft direction (P4wt) and the twill weave 6-layer weft direction (T6wt) laminates (see column 7 of Table 4.2 for notation) which have, respectively, the lowest and highest values

of UFS. Figure 4.18 illustrates that the error in the fractal dimension (Equation 4.2) is reduced to a very low value once 20 images from different sections are used to obtain D values (as was done in this study).

$$Error\ in\ D\ (\%) = \frac{ABS(D_{mean} - D_{ni})}{D_{mean}} \times 100 \qquad (4.2)$$

Where, *ni* is the number of images.
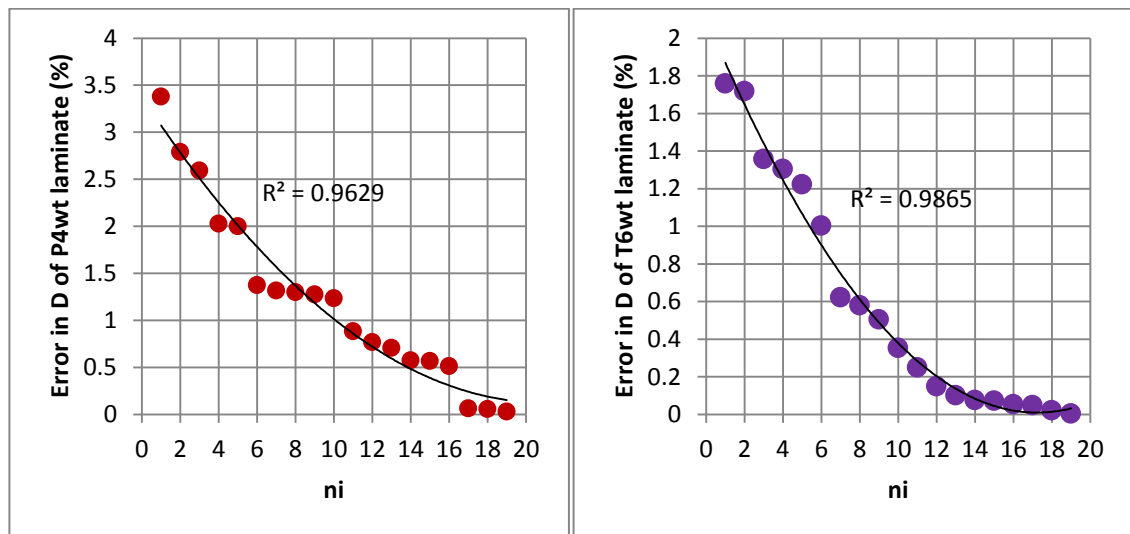
Figure 4-18: The error value of the fractal dimension against the number of images used in its determination.

Figure 4.19 shows values of the D, obtained from analysis of 20 images from five different sections, for each laminate type in both the warp and the weft direction. Figure 4.19 illustrates that the D of the twill fabric laminates is higher than the D of the plain fabric laminates in the weft direction, but that this trend is reversed in the warp direction. The D in both cases increases with increasing number of fabric layers.

[99]
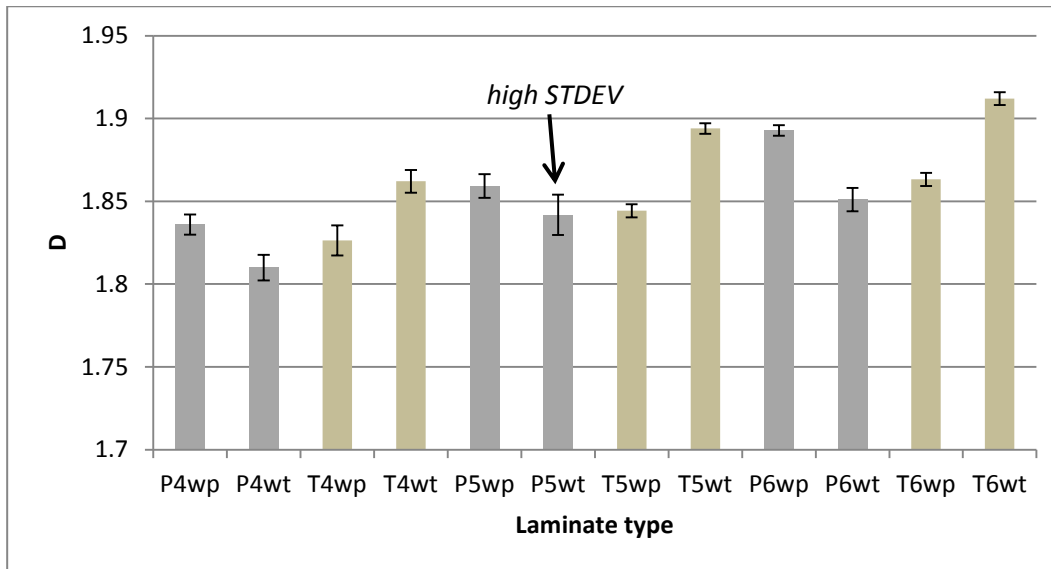
Figure 4-19: D with standard error for the various woven carbon laminates in both directions.

The laminate P5wt had an increase in the standard error as shown in Figure 4.19, due to longitudinal voids present in some microscopic images of this laminate as shown in Figure 4.20.

Longitudinal voids
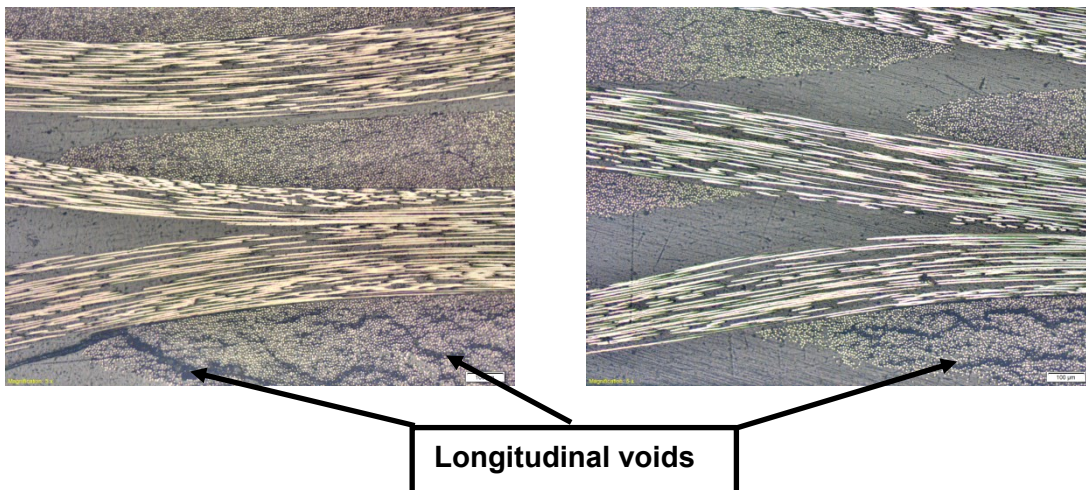
Figure 4-20: Longitudinal voids observed in the P5wt laminate.

Figure 4.21 plots the increase in D as a function of number of fabric layers in the laminate in both the warp and weft directions, and the general trend observed in the fibre volume fraction is to increase with increasing number of fabric layers (Figure 4.17), which therefore correlates with the observed trends

in the fibre volume fraction and the fractal dimension. This supports the results (see Figure 4.7) of the glass woven laminates that were manufactured by the infusion process. Again the laminate P5wt showed a slightly different behaviour compared with the data for other laminates as shown in Figure 4.21 (lowest R^2=0.9061), due to the features observed in Figure 4.20 for this laminate.
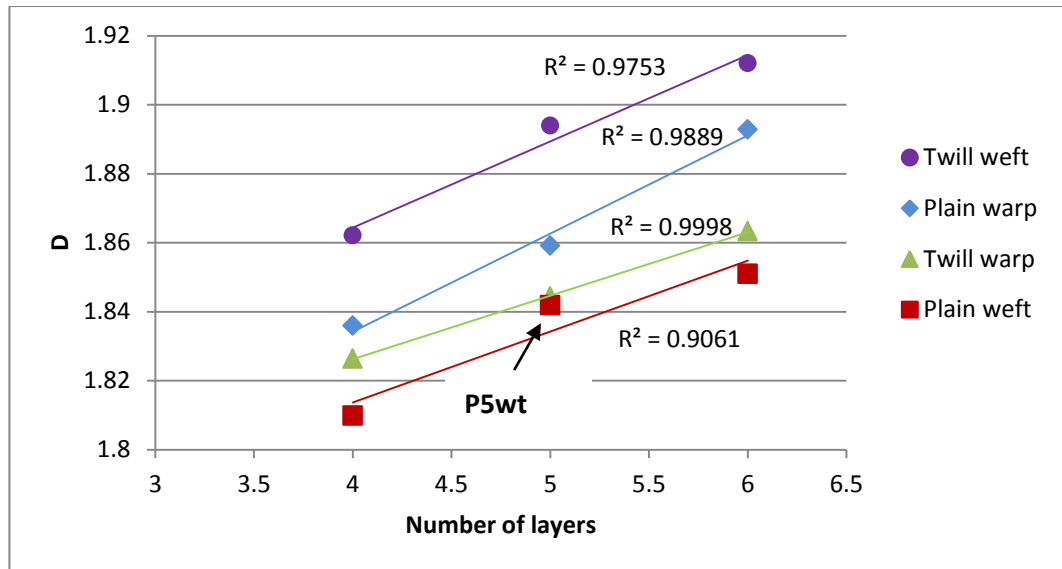
Figure 4-21: Fractal dimension versus number of layers; for a constant laminate thickness as used here, D is therefore proportional to V_f.

The UFS in twill warp and plain weave warp directions are very similar for the same n, while the UFS in the twill weave weft direction is significantly higher than any of the others and the UFS in the plain weave weft direction is lower. To a first approximation, the strength of the plain weave n-layer weft laminate is similar to that of the n-1 layer twill weave warp or plain weave warp and the UFS of the n-layer plain weave warp and n-layer twill weave warp directions is similar to that of the n-1 twill weave weft (Figure 4.22).
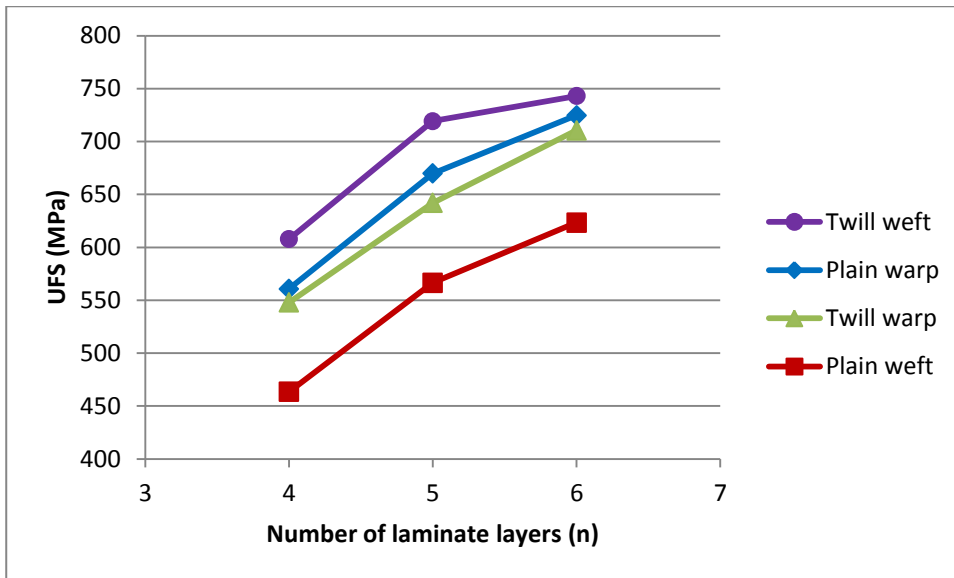
Figure 4-22: UFS versus number of layers for the various woven carbon laminates.

In a plain weave fabric each warp fibre passes alternately under and over each weft fibre, but in twill fabric two (or more) warp fibres alternately weave over and under two (or more) weft fibres in a regular repeated manner (Figure 4.23). Therefore, the plain fabric has a higher crimp than the twill fabric.

(a)   (b)
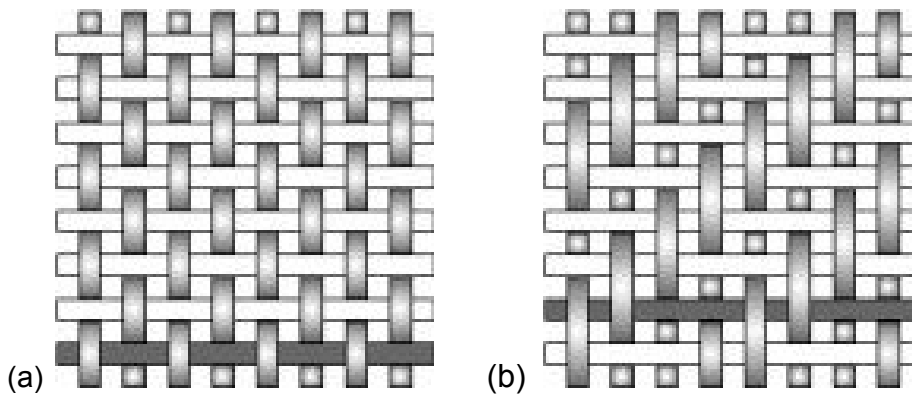
Figure 4-23: (a) Plain weave and (b) 2/2 twill weave.

The measurement of crimp from microstructure images of composites is not trivial as it is necessary to follow fibres which often disappear from the plane of the image.   The crimp increases the out-of-plane distortion of the tows and therefore reduces the UFS. Table 4.3 presents rule-of-mixtures prediction for

the elastic tensile modulus E_t (Equation 4.3)[10]. The out-of-plane η_O (E_b / E_t) is essentially $\cos^4\theta$. The angle θ was calculated by using Equation (4.4) and found to be in the range $14.9^o - 22.7^o$ for all laminates which is lower than the maximum crimp angle measured from typical micrographs (Figure 4.24), and is consistent with this angle varying along the length of the fabric (down to a minimum of zero degree).

$$E_t = \eta_O \; V_f \; E_f + V_m \; E_m \qquad\qquad (4.3)$$

$$\theta = \cos^{-1} (E_b / E_t)^{0.25} \qquad\qquad (4.4)$$

Table 4.4 presents the ranking of fractal dimension and UFS data for the various types of laminate tested in this work, and it is clear that the value of these two parameters varies in a consistent and linked way for all four fabric types tested. The microstructural images shown in Figure 4.24 were generated by merging 30 contiguous (10 horizontal by 3 vertical) microstructural images from sections of the respective laminates. The shape and distribution of the RRV differ between the plain and twill fabrics with continuity of RRV around tows occurring in the plain weave fabric, but not in the twill weave fabric. The distribution of fibres within the composite has been quantified using a fractal dimension (D) box counting method for 20 non-overlapped contiguous vertical strips taken from different sections from each laminate.

---

[10] Where E_f = 235 GPa and E_m = 2.85 GPa.

Table 4-3: The prediction for the elastic modulus Et and the out-of plane η_O from the rule-of-mixtures.

Laminate	V_f~warp	V_f~weft	V_m	E_b(GPa)	E_t(GPa)	E_b/E_t	$\eta_O = (E_b/E_t)^{0.25}$	Angle θ
P4wp	0.182		0.64	38.9	44.6	0.87	0.966	14.9
P4wt		0.175	0.64	31.2	43.1	0.72	0.923	22.7
T4wp	0.165		0.65	30.9	40.8	0.76	0.933	21.1
T4wt		0.183	0.65	34.6	44.8	0.77	0.937	20.4
P5wp	0.209		0.58	40.8	50.9	0.80	0.946	18.9
P5wt		0.206	0.58	39.2	50.1	0.78	0.941	19.8
T5wp	0.183		0.61	36.8	44.8	0.82	0.952	17.8
T5wt		0.206	0.61	42.4	50.1	0.85	0.959	16.4
P6wp	0.238		0.53	45.6	57.4	0.79	0.944	19.3
P6wt		0.233	0.53	41.4	56.3	0.74	0.926	22.2
T6wp	0.206		0.56	40.6	50.0	0.81	0.949	18.4
T6wt		0.232	0.56	42.4	56.1	0.76	0.932	21.2

Figure 4.24 supports the premise that strength increases with fractal dimension. If the tow acts as a crack-arrester for the RRV in the twill fabric (as indicated by the lack of continuity of the RRV around a tow), then one might expect smaller defects, and hence higher strengths, in fabrics with a twill weave, compared with plain weave fabrics.

Table 4-4: UFS & D from highest to lowest value.

No. of layers (n)	UFS rank order from highest to lowest for n layers.	D rank order from highest to lowest for n layers.
4,5 &6	Twt (Twill weft direction)	Twt (Twill weft direction)
4,5 &6	Pwp (Plain warp direction)	Pwp (Plain warp direction)
4,5 &6	Twp (Twill warp direction)	Twp (Twill warp direction)
4,5 &6	Pwt (Plain weft direction)	Pwt (Plain weft direction)

P5wt with D=1.841 & UFS=567 MPa

T5wt with D=1.893 & UFS=719 MPa

P6wt with D=1.85 & UFS=623 MPa

T6wt with D=1.912 & UFS=743 MPa
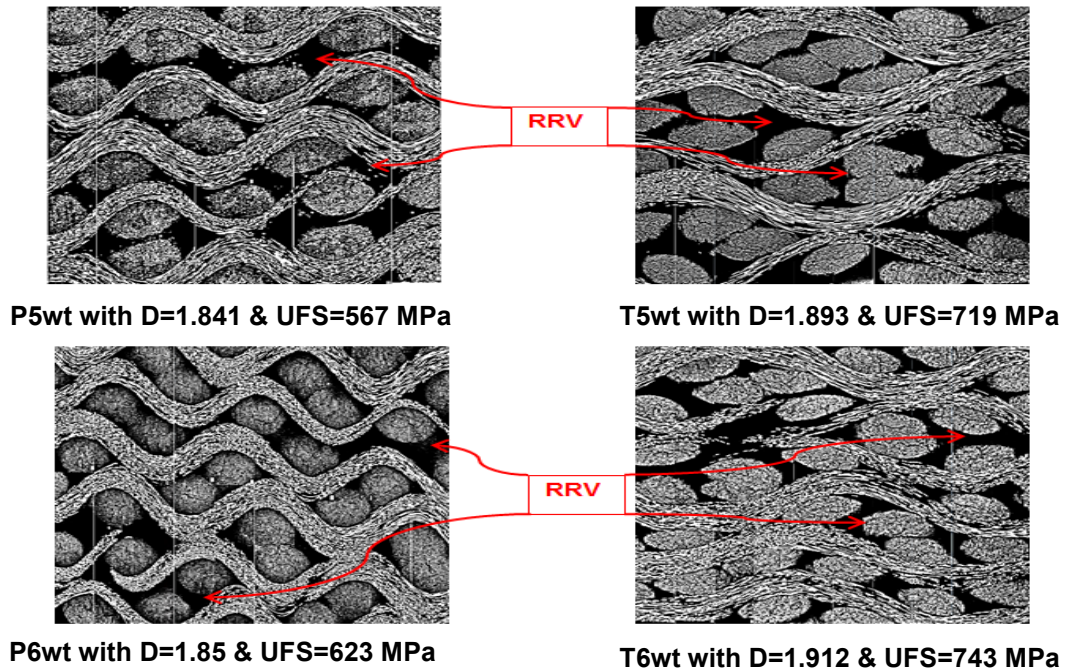
Figure 4-24: Merged contiguous microstructural images from five (upper) or six (lower) ply laminates of plain (left) or twill (right) weave fabrics showing the continuous horizontal RRV around the tows that occurs in plain, but not twill, composites fabrics.

In this study, second order polynomial regression has been chosen for all data, as it has a high value of R^2 compared with other regressions for all static properties such as UFS, ILSS and E_b, where R^2 is a statistical measure of how close the data are to the fitted regression line. It is also known as the coefficient of determination [146]. However, R^2 does not indicate whether a regression model is adequate. Sometimes a low R^2 value gives a good model, or a high R^2 value for a model that does not fit the data [147]. For checking the goodness-of-fit, Figures (4.25-4.27) illustrate the actual values for all static properties such as UFS, ILSS and E_b versus the predicted values of them using the linear and the second order polynomial regression. For all static properties, the R^2 in the second order polynomial was higher than the R^2 of the linear model. Therefore, the second order polynomial regression seems to provide a better fit than the linear regression. Furthermore, increasing the uniformity of the fibre distribution could reduce the RRV, and that is likely to lead to a higher strength level in the

composite laminate. Furthermore, the behaviour of the composite laminates under flexural loading is a direct consequence of multiple damage events, which are governed by different factors. All of these factors could lead to the observed non-linear behaviour of composite laminates as a function of fibre distribution.
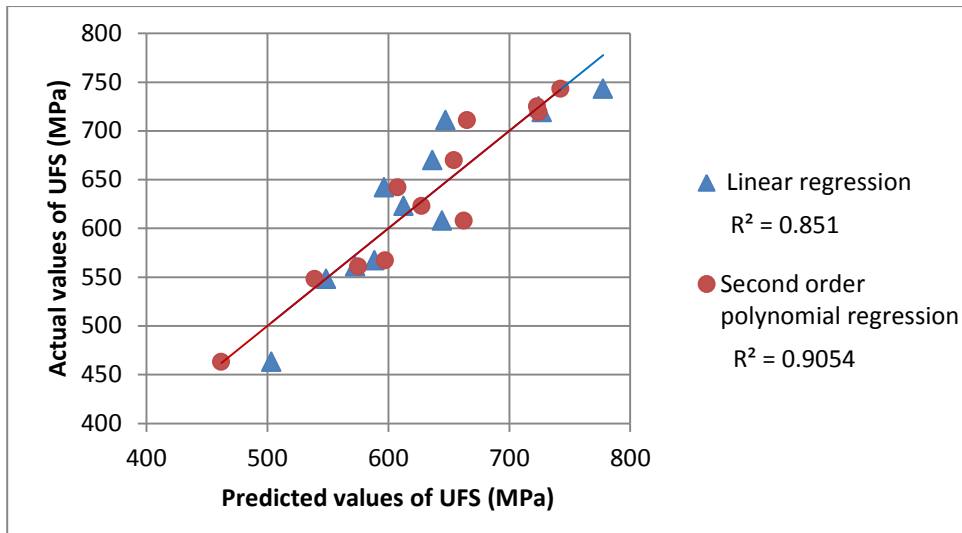
Figure 4-25: Actual values versus the predicted values of UFS.
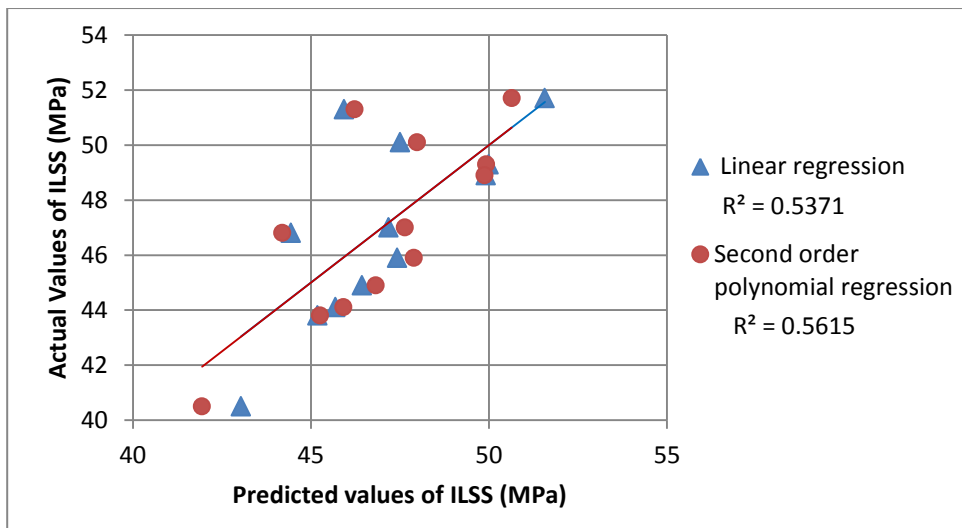
Figure 4-26: Actual values versus the predicted values of ILSS.
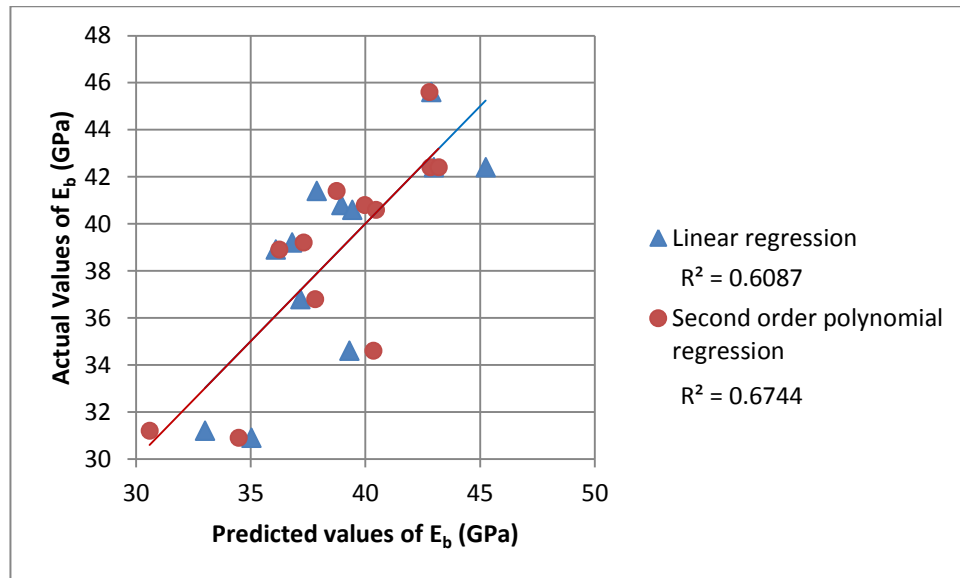
Figure 4-27: Actual values versus the predicted values of E_b.

The rule-of-thumb [148] and analysis of variance (ANOVA) techniques have been used to confirm the results statistically, in order to check the existence and the significance of the correlations. According to the rule of thumb,

If ABS R ≥ 2/($\sqrt{nd}$)

then a correlation exists [149], where nd is the number of data points for each correlation, and R is the Pearson coefficient (the Pearson Correlation Coefficient which is used to measure the strength of a correlation association between two variables, where the value R = 1 means a perfect positive correlation and the value R = -1 means a perfect negative correlation). In this data set, nd=12 for all laminates. That means,

If ABS R $\geqslant$ 0. 577   (for all laminates)

then the correlation exists. Furthermore, in ANOVA, [148, 150] the p-value is used in the context of null hypothesis testing in order to quantify the idea of statistical significance of evidence. When p < 0.05 it means that the correlations are significant with *moderate* evidence against the null hypothesis in favour of

[107]

the alternative, if $0.001 < p < 0.01$ means that the correlations are significant with *strong evidence* against the null hypothesis in favour of the alternative, and if $p< 0.001$ means that the correlations are significant with *very strong evidence* against the null hypothesis in favour of the alternative. In this study, most laminates have ABS R$\geqslant$ 0. 577, and $p < 0.05$, with some correlations having p-values in the range $0.001 < p < 0.01$ and even $p < 0.001$, which implies that most correlation curves obtained with second order polynomial trend/regression lines were significant and that correlations exist for all laminates, with just two exceptions: (i) the ILSS versus the stressed V_f and (ii) the ILSS versus the total V_f as shown in Table 4.5.

Table 4-5: ANOVA for second order polynomial trend/regression type.NB: Rule-of-thumb If ABS R≥0.577, gives TRUE for ALL correlations and p < 5% means ALL data set correlations are significant.

Correlation	R (Pearson coefficient)	p-value	The significant status
UFS vs D	0.950	0.000027	Significant with very strong evidence
UFS vs Stressed V_f	0.740	0.028	Significant with moderate evidence
UFS vs Total V_f	0.728	0.033	Significant with moderate evidence
ILSS vs D	0.746	0.025	Significant with moderate evidence
ILSS vs Stressed V_f	0.386<0.577	0.4864	No correlation and not significant
ILSS vs Total V_f	0.518<0.577	0.2437	No correlation and not significant
E_b vs D	0.825	0.005	Significant with strong evidence
E_b vs Streesed V_f	0.922	0.000184	Significant with very strong evidence
E_b vs Total V_f	0.876	0.00137	Significant with strong evidence

Figure 4.28 illustrates the correlations plotted for UFS versus D, the stressed V_f and the total V_f for all laminates. The UFS is clearly related to the D, with a

weaker relationship with the stressed V_f and a low correlation with the total V_f. The correlation between UFS and D is significant with very strong evidence (R^2 = 0.9034 and p=0.000027) as shown in Figure 4.28a, which is better than the correlation between UFS and the stressed V_f (R^2 = 0.5487 and p=0.028) or the total V_f (R^2 = 0.5307 and p=0.033) as shown in Figures (4.26b and 4.26c) due to the much lower R^2 and high p-values in the last two cases.

Figure 4.29 illustrates the trend in the ILSS as a function of the three parameters of D, stressed V_f and total V_f respectively. It is clear that the ILSS correlates reasonably well with D (R^2 = 0.5579 and p=0.025) , but it does not correlate well with the stressed V_f (R = 0.386 and p=0.4864) or with total V_f (R = 0.518 and p=0.2437). However the correlation between ILSS and D is statistically significant with moderate evidence (p< 0.05) due to the ILSS being dominated by resin properties and interface adhesion rather than the fibre distribution.

Figure 4.30 illustrates the trend in the E_b as a function of the D, the stressed V_f and the total V_f for all laminates respectively. For all laminates, there is a correlation between the parameters plotted because R>0.577, and it is clear that the E_b correlates better with the stressed V_f (R^2 = 0.8505 and p= 0.000184) as shown in Figure 4.30b, or the total V_f (R^2 = 0.7688 and p=0.00137) as shown in Figure 4.30c, than it does with D (R^2 = 0.6822 and p=0.005) as shown in Figure 4.30a. This is expected from the rule-of-mixtures estimation for elastic properties, where the flexural modulus is proportional with the V_f.
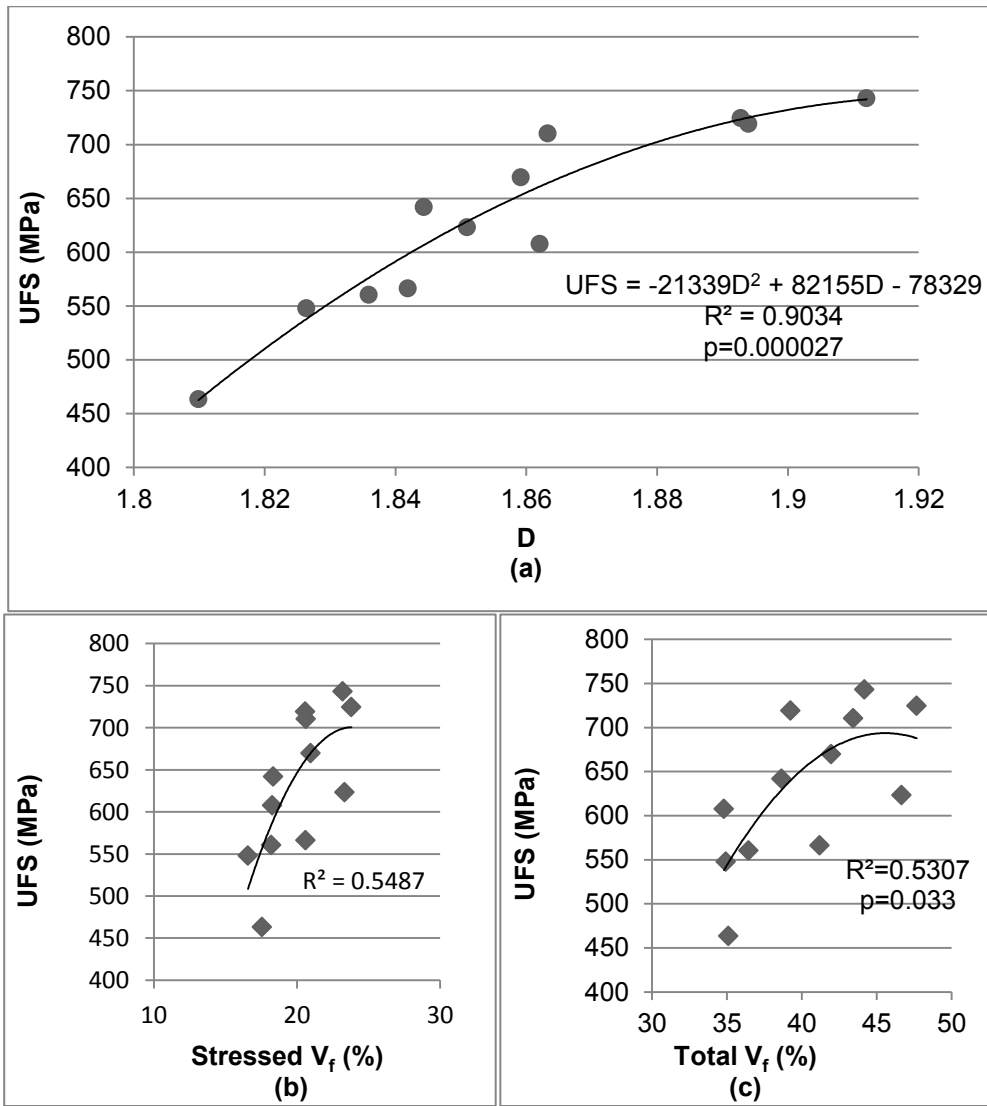
Figure 4-28: All laminates: a) Ultimate flexural strength UFS versus fractal dimension D, b) UFS versus stressed fibre volume fraction V_f and c) UFS versus total fibre volume fraction V_f.
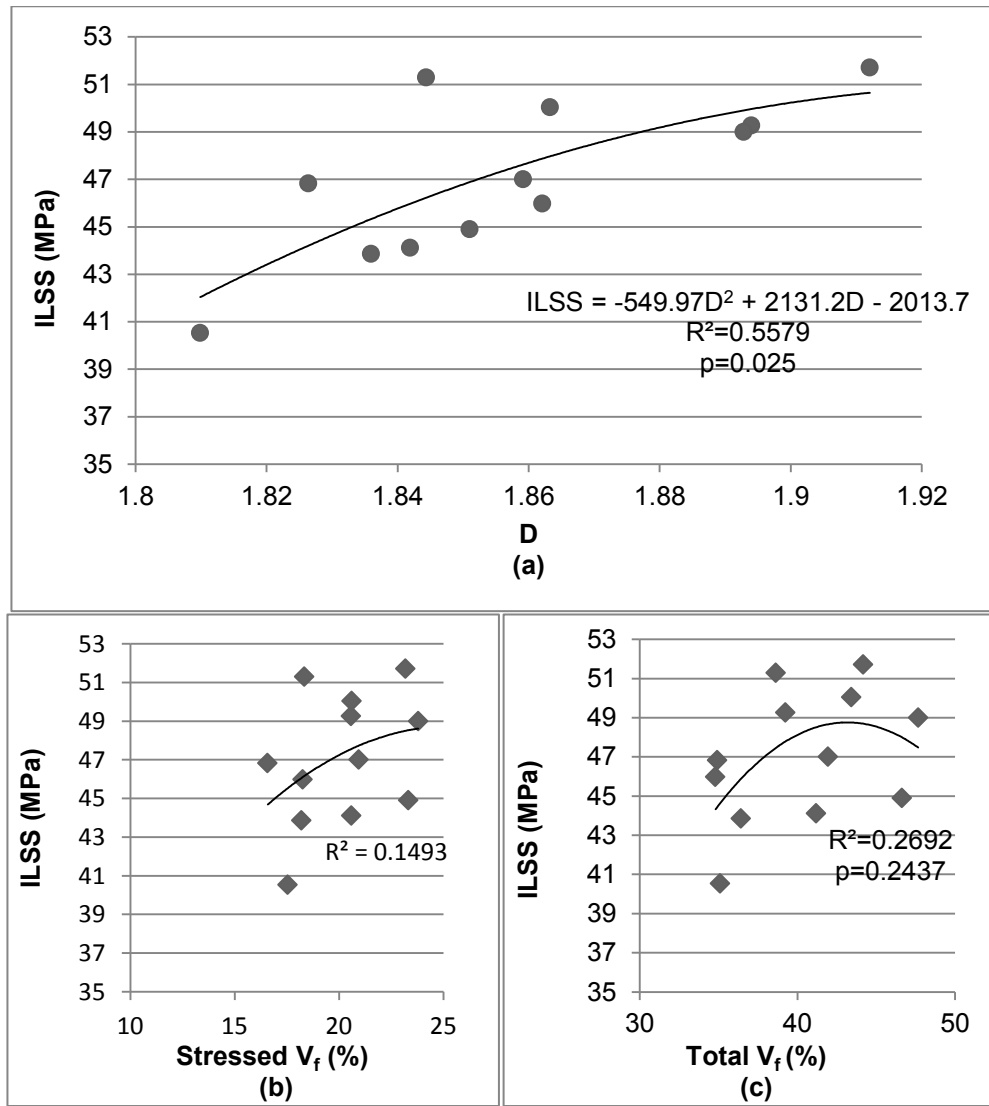
Figure 4-29: All laminates: a) Interlaminar shear strength ILSS versus fractal dimension D, b) ILSS versus stressed fibre volume fraction V_f and C) ILSS versus total fibre volume fraction V_f.

The equation shown in chart (a):

$$E_b = -1278.4D^2 + 4881.4D - 4616.6$$
$$R^2 = 0.6822$$
$$p = 0.005$$

Chart (b): $R^2 = 0.8505$, x-axis: Stressed V_f (%)

Chart (c): $R^2 = 0.7688$, $p = 0.00137$, x-axis: Total V_f (%)
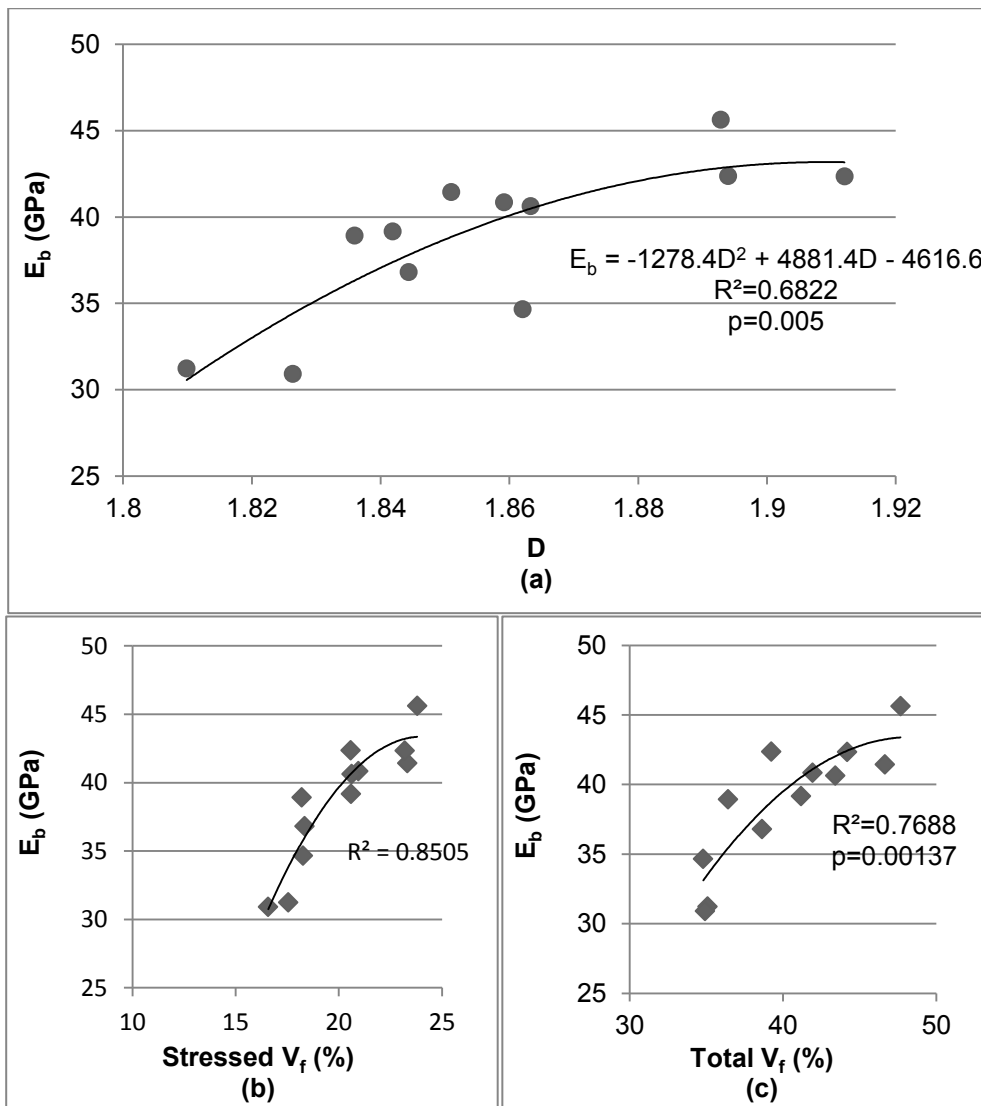
Figure 4-30: All laminates: a) flexural modulus of elasticity E_b versus fractal dimension D, b) E_b versus stressed fibre volume fraction V_f and c) E_b versus total fibre volume fraction V_f.

Less uniformity (equivalent to greater clustering) in the fibre distribution leads to more or larger RRV, and the mechanical properties are inversely proportional to increase in the RRV. Increasing the RRV increases local stress concentrations at tows and increases the crack growth, hence leading to reduced static and dynamic properties of the composite laminate as mentioned in Figure 2.7. In contrast, increased uniformity in fibre distribution will reduce the stress concentration and crack growth within the laminate and should thus lead to improved mechanical properties in the composite laminates. Furthermore, as

[112]

stated earlier for clustered fibres, the tow centres will be some distance from the surface of the material, whereas for uniformly distributed fibres there will be more reinforcements adjacent to the sample surface (further from the neutral axis in bending) with an expectation of a higher flexural modulus in the latter case.

This supports the hypothesis that the mechanical properties of the composite laminates depend on the fibre distribution, which is measured by the D, more strongly than by the fibre volume fraction.

For the full data set and from Figures 4.28a, 4.29a and 4.30a the equations linking mechanical properties with the D were found to be:

$$\text{UFS (MPa)} = -21339D^2 + 82155D - 78329 \quad (R^2{=}0.9034) \quad (4.5)$$

$$\text{ILSS (MPa)} = -550D^2 + 2131D - 2014 \quad\quad (R^2{=}0.5679) \quad (4.6)$$

$$E_b \text{ (GPa)} = -1278D^2 + 4881D - 4616 \quad\quad (R^2{=}0.6822) \quad (4.7)$$

The boxes that were used to calculate the D were defined parallel with the distribution of bending and shear stresses as shown in Figure 4.31. The correlation between the boxes and the stress directions within the laminate cross-sections makes the D a useful parameter in exploring relationships between mechanical properties and manufacturing processes and fabrics in the laminates as mentioned earlier. Correlations between these parameters either do not exist or are less apparent for the case of the total V_f. Furthermore, the correlation between D and the UFS is higher than the correlation between D and the ILSS, as discussed in the previous sections. In addition to the reasons mentioned previously, another contributory factor in these observations is the bending stress which has a linear relationship across the thickness (boxes) of

the laminate, while the shear stress does not follow a linear relationship as shown in Figure 4.31.
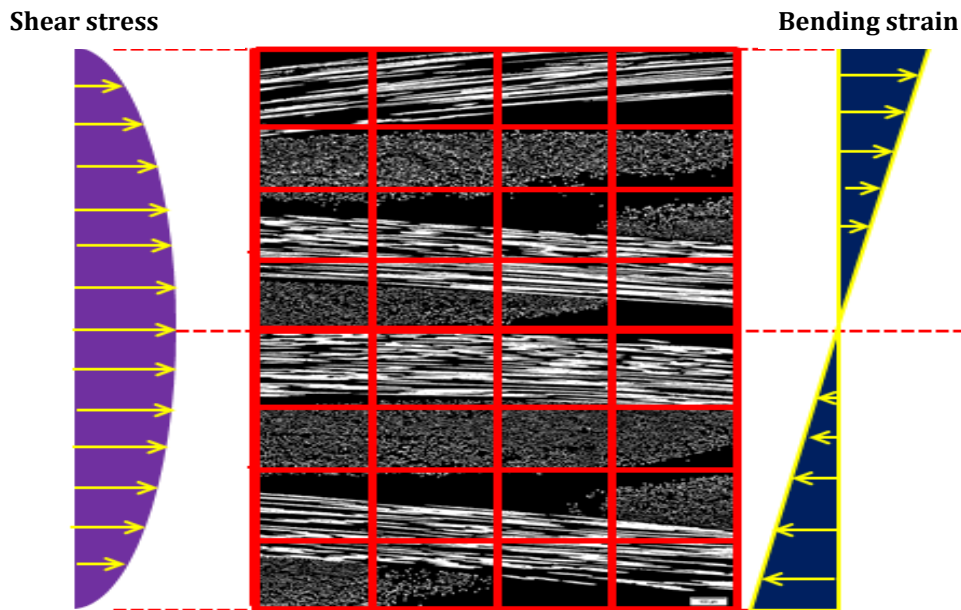
Figure 4-31: The correlation between the distribution of the bending strain and shear stresse to the box counting method.

In summary:

- The strength of the composite laminates shows a clear dependence on the fibre distribution as well as the fibre volume fraction, and the UFS is proportional to the D according to Equation 4.5.

- The ILSS is proportional with a second order polynomial to the D but the relationship is less significant than the relation between the UFS and the D. Here, the relationship is Equation 4.6.

- The flexural modulus E_b is proportional with a second order polynomial to the stressed V_f, the total V_f and D for different laminates, and it correlates with V_f better than the D, which is expected from the rule-of-mixtures. The corresponding relationship is Equation 4.7.

[114]

These results obtained with the laminates manufactured using RTM confirm the results obtained from the laminates made under resin infusion, i.e. that the fractal dimension can be a measure of the fibre distribution and can therefore be correlated with the (quasi-static) mechanical properties (E_b, UFS and ILSS) of fibre reinforced composites. These observations provide confidence that investigating the effect of fibre distribution on the fatigue properties of the fibre-reinforced composites will provide useful insights into the process-property-performance relationships.

4.4 The fatigue properties of carbon laminates manufactured by the RTM process

4.4.1 The S-N Curves

In this study, a logarithmic regression (Equation 3.12) has been chosen to characterise the fatigue data. This is due to the high value of R^2 compared with that found for other forms of regression relationships for the S-N curve data, where R^2 is 'best fit indicator' [146]. Figures 4.32, 4.33 and 4.34 present the S-N fatigue data obtained in four-point bending, in both the warp and weft directions, for plain and twill weave laminates with 4, 5 and 6 layers of fabric. The UFS data are also plotted on the same curves, taking the flexural failure to coincide with one-half cycle of loading [137]. Figure 4.32 demonstrates that the T4wt laminate shows a high fatigue performance due to the high UFS and high D, while the P4wt laminate shows a low fatigue performance due to the low UFS and low D as shown in Table 4.2. Fatigue performance ranks in the sequence T4wt >P4wp >T4wp > P4wt, i.e. when the laminates are subjected to the same flexural stress, it is expected that, on average, the fatigue life would rank from high to low in the same sequence. This observation is related to the

static properties, where $UFS_{T4wt} > UFS_{P4wp} > UFS_{T4wp} > UFS_{P4wt}$. Furthermore, the ranking is the same for the fibre distribution, which is measured by the D, where $D_{T4wt} > D_{P4wp} > D_{T4wp} > D_{P4wt}$ as shown in Table 4.2. Similar behaviour occurs for the same reasons, with the five and six layer laminates as shown in Figure 4.33 and 4.34 respectively. The conclusion drawn from these observations is that the fatigue life of the composite laminates depends on the fibre distribution (as measured by the D) and that the laminates with high flexural strength will show high fatigue life, as has been observed by other workers [66, 86]. This leads to general hypothesis that fatigue life is proportional to the D and to the UFS as will be discussed later.
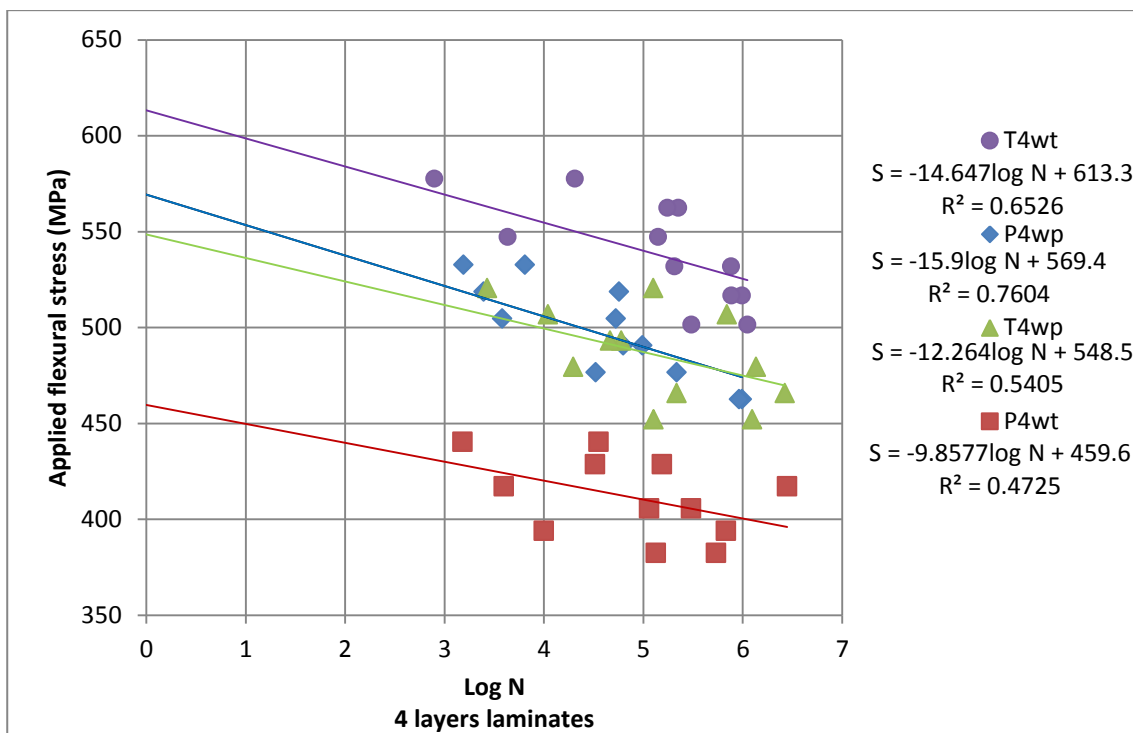
Figure 4-32: S-N curves for 4 layer plain and twill weave laminates in both the warp and weft directions.

As shown in Figures 4.32-4.34, there was significant scatter in the S-N data, which relates to the different mechanisms of failure that can occur in composite laminates. Another contributory factor is the high amount of samples and different areas (between the RTM mould edges and the mould centre) from

where the samples are cut. Furthermore, the anisotropic materials (e.g. fibre reinforced composites) are very sensitive to the loading path, and that could happen when the cut of the samples is not parallel to the warp and weft direction. Therefore, it is expected that the scatter of the composites is higher than that of the isotropic materials.
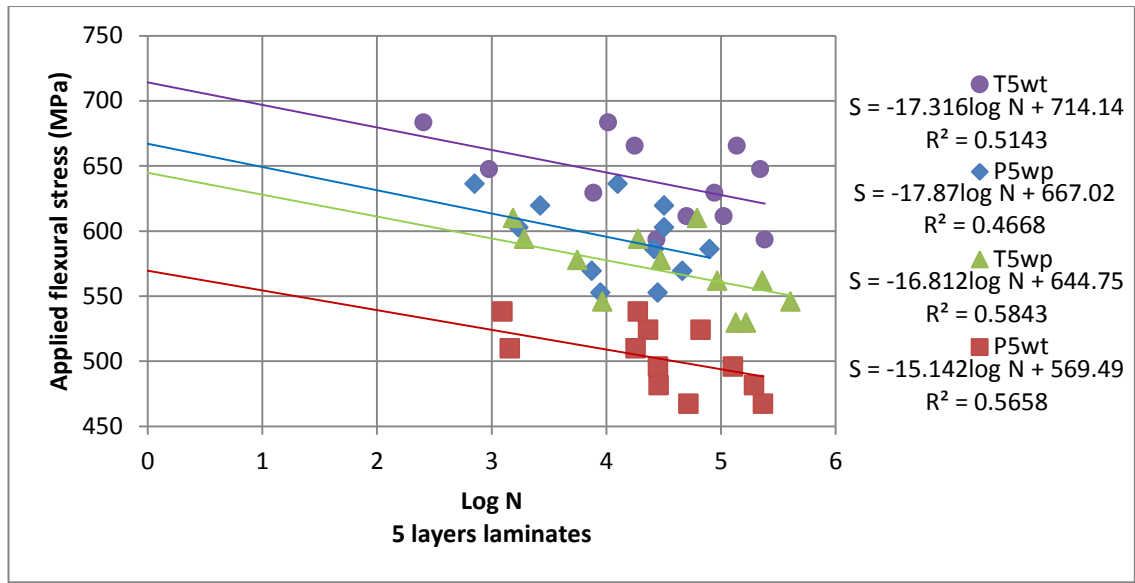
Figure 4-33: S-N curves for 5 layer plain and twill weave laminates in both the warp and weft directions.
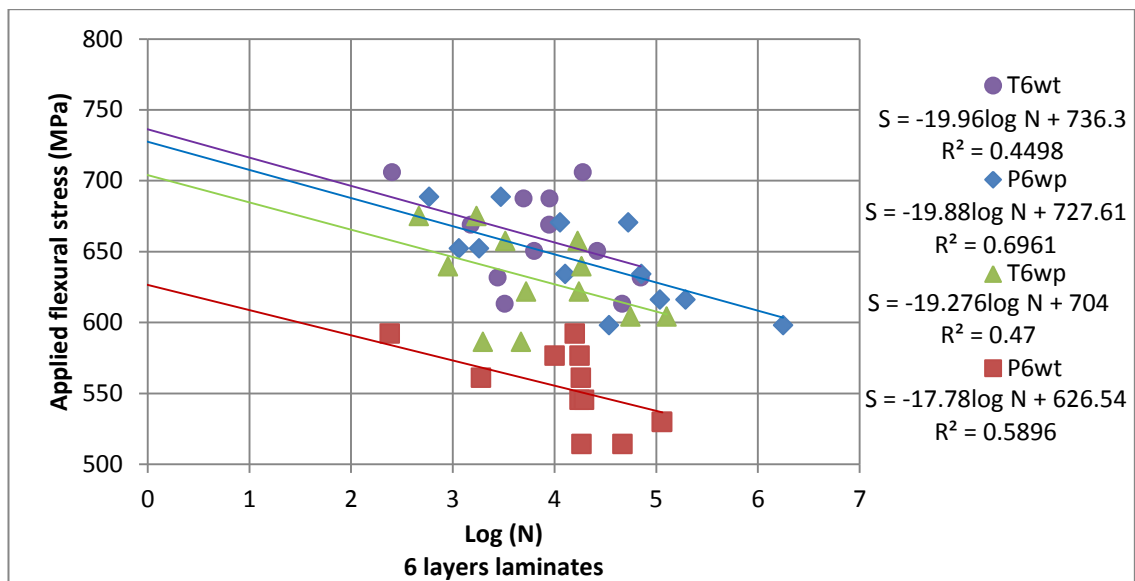
Figure 4-34: S-N curves for 6 layer plain and twill weave laminates in both the warp and weft directions.

[117]

Again, the rule-of-thumb and analysis of variance (ANOVA) statistical techniques [148] will be used to discuss the scatter observed in the fatigue data, in order to check the significance of the correlations between applied flexural stress and fatigue life. In this data set, nd=13 for all laminates, so if **ABS R$\geqslant$ 0.554**, then the correlation exists. In this data set, all laminates have ABS R$\geqslant$ 0.554 and $0.001 < p < 0.01$ with some correlations having $p < 0.001$. The interpretation is that the S-N curves characterised with a logarithmic regression are significant and that correlations exist between these parameters for all laminates as indicated in Table 4.6.

Table 4-6: ANOVA for the S-N curves fitted with logarithmic regression lines. NB: Rule-of-thumb states that if ABS R ≥ 0.554 gives TRUE for ALL correlations and p < 5% then ALL data set correlations are significant.

Laminate	R (Pearson coefficient)	p-value
P4wp	0.87	0.0001
P4wt	0.68	0.009
T4wp	0.73	0.004
T4wt	0.80	0.0008
P5wp	0.68	0.01
P5wt	0.75	0.003
T5wp	0.76	0.002
T5wt	0.71	0.005
P6wp	0.83	0.0003
P6wt	0.76	0.002
T6wp	0.68	0.009
T6wt	0.67	0.01

Figures 4.35-4.38 show that, for a constant specimen thickness of 2 mm, the fatigue life increases with an increase in the number of fabric layers for a particular type of laminate. This reflects the increasing fibre volume fraction in

the laminate (as the RTM mould cavity depth was fixed in all cases), and the associated increase in D and flexural strength that was observed in the laminates as the number of fabric layers increases (see Table 4.2). For all types of laminate used in this testing programme, the fatigue strength coefficient B and the fatigue strength exponent A (Equation 3.12) increased with increase in number of fabric layers, as can be seen in Figures 4.35-4.38. The resin type and fibre/matrix adhesion would be similar for all the laminates considered in this work and the fatigue behaviour of the composite laminates is mainly controlled by the fibre distribution which was different for all laminates.
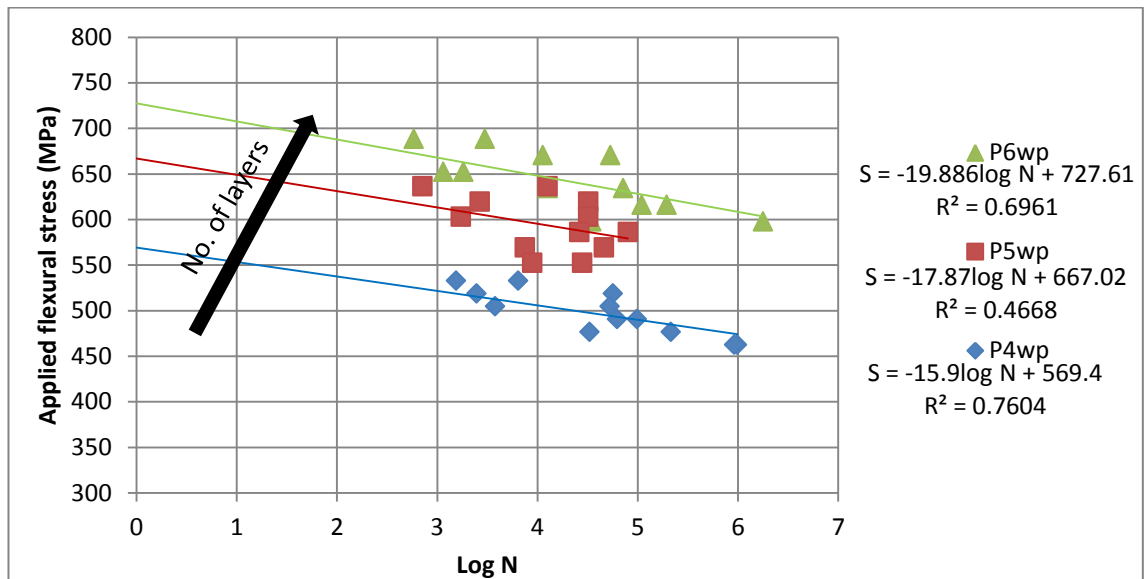
Figure 4-35: S-N curves for the plain weave laminates in the warp direction for 4, 5 and 6 fabric layers.
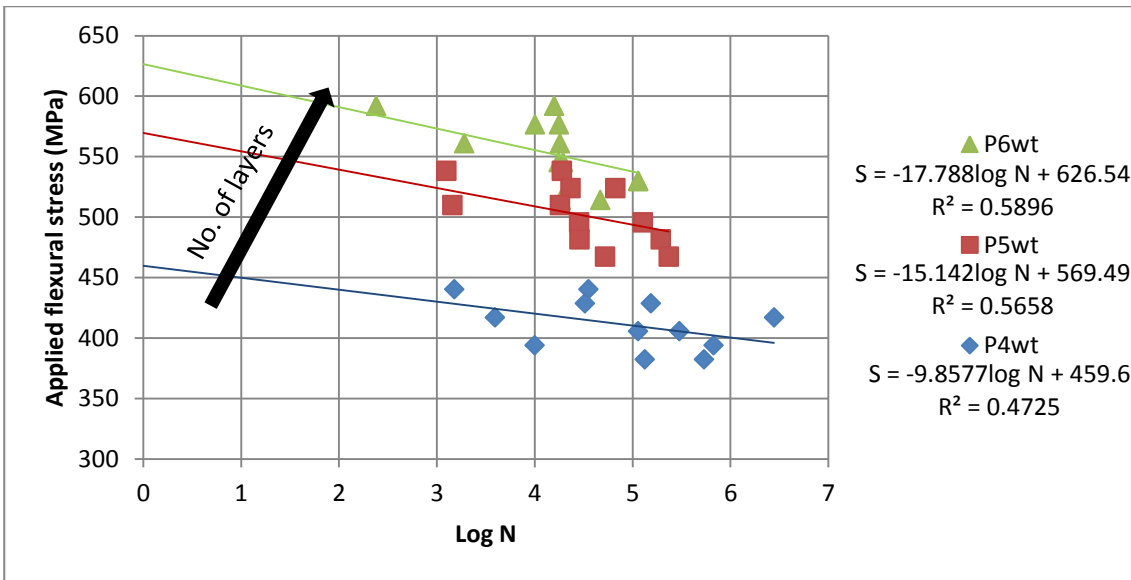
Figure 4-36: Semi-log S-N curves for the plain weave laminates in the weft direction for 4, 5 and 6 fabric layers.
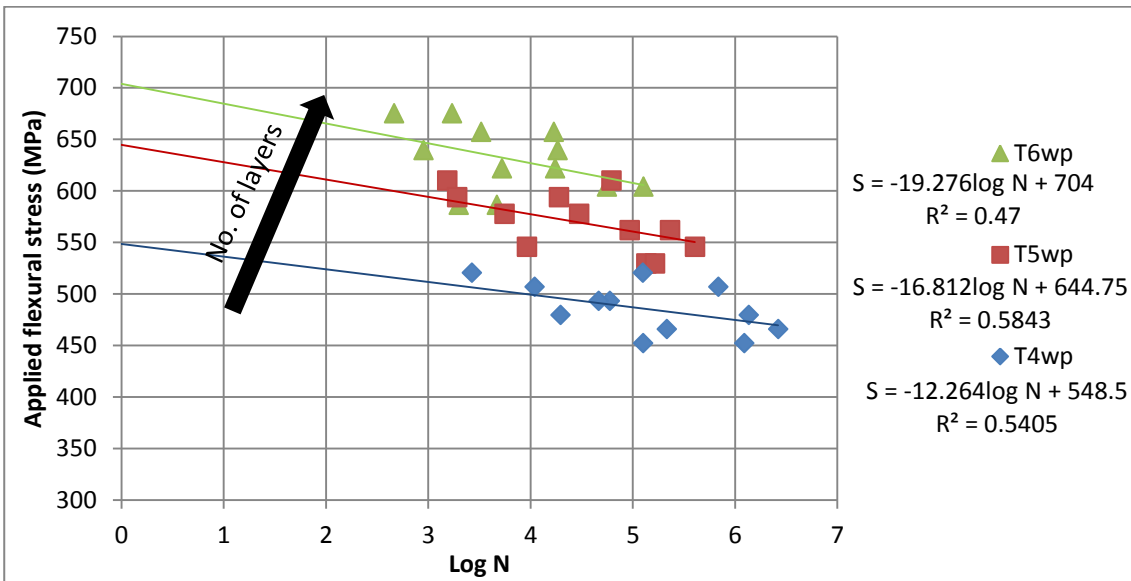
Figure 4-37: Semi-log S-N curves for the twill weave laminates in the warp direction for 4, 5 and 6 fabric layers.
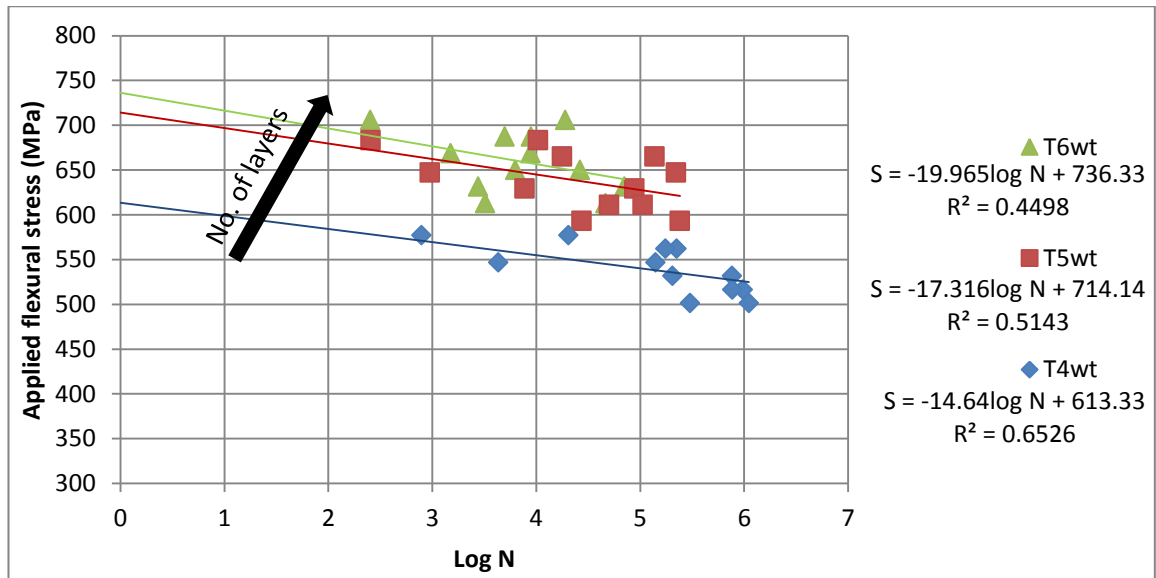
Figure 4-38: Semi-log S-N curves for the twill weave laminates in the weft direction for 4, 5 and 6 fabric layers.

Both the UFS and the D are proportional to the number of fabric layers, and an increase in number of fabric layers equates to an increase in fatigue life as mentioned before. Within a single fibre architecture (twill or plain weave), the reduction in the fatigue life was faster for those laminates with more layers as evidenced by the values of the parameter A given in Table 4.7. This is due to the visco-elastic behaviour of the matrix used in composite laminates which has a significant effect on the fatigue life of composite laminates [11].

Table 4-7: Fatigue constants based on the laminate type.

Laminate	A	B (MPa)
P4wp	-15.9	569.4
P4wt	-9.86	459.6
T4wp	-12.26	548.5
T4wt	-14.65	613.3
P5wp	-17.87	667
P5wt	-15.14	569.5
T5wp	-16.81	644.7
T5wt	-17.32	714.1
P6wp	-19.89	727.6
P6wt	-17.79	626.5
T6wp	-19.28	704
T6wt	-19.97	736.3

4.4.2 Maximum displacement and modulus of elasticity

In order to calculate the flexural modulus during the bending fatigue tests, the maximum displacement at the midspan was calculated using Equation 3.14. Figure 4.39 illustrates a typical deflection response observed at midspan, for the 5 layer laminates with either plain or twill fabric (level load=85%UFS), as a function of the life fraction consumed (i.e. number of cycles (N) divided by the number of cycles at failure (N_f). In Figure 4.39, the rate of change in deflection divides into three regions as follows;

• The initial region 1 with a rapid increase in deflection as the applied load is ramped up to reach the required level. This period is 1-2 % of the failure time.

• An intermediate region 2, in which a steady-state slow increase in deflection occurs as fatigue damage accumulates; this region continues to around 90% of the total life, N_f.

• Region 3, in which the rate of deflection increases rapidly in an exponential manner until failure occurs. This region is associated with a sudden loss of strength and stiffness and is accompanied by cracking sounds (audible acoustic emission) for all the specimens in this test programme. This indicates the onset of failure.

From Figure 4.39, one can observe that the value of the steady-state deflection depends primarily on the fabric architecture (plain or twill weave) and whether the specimen has its longitudinal axis in the warp or the weft direction.

[122]
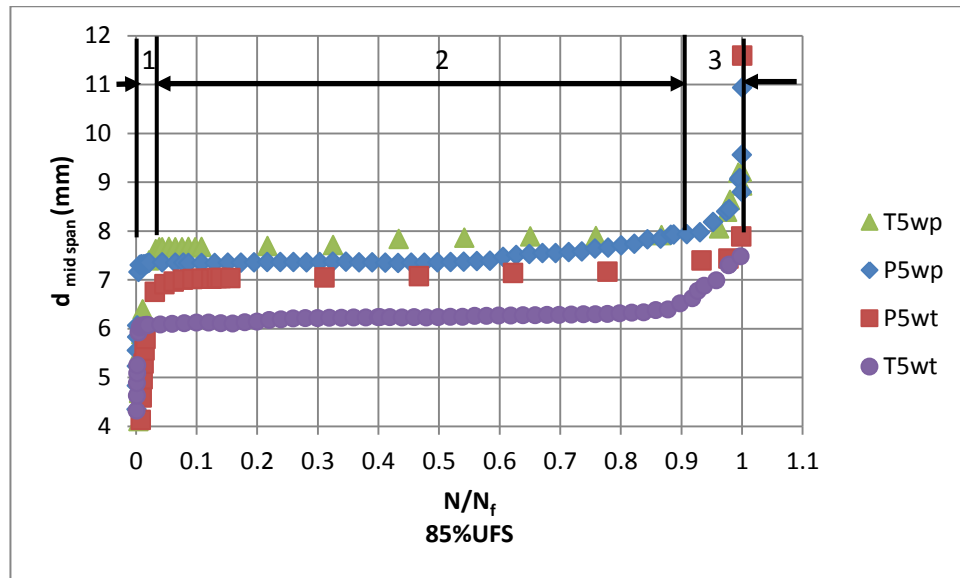
Figure 4-39: A typical deflection response observed at the midspan in the five layer laminates with either plain or twill weave fabrics.

Figure 4.39 relates to a specific stress equal to 85% of the UFS, and the deflection reflects the value of applied load. For the particular case of 85% of the UFS and the 5 layer fabrics, it is clear that the laminates in either plain or twill weave fabrics are stiffest when the specimen axis is parallel with the weft direction, and that the twill weave laminates are stiffer than the plain weave laminates.

In this study the fatigue tests were conducted under load control, therefore the change in deflection reflects a change in stiffness or modulus of elasticity of the samples, arising from the development of damage zones in the laminates. The flexural modulus of elasticity can be calculated using Equation 3.5. The applied fatigue loads were recorded automatically from the Electropuls test machine, allowing the actual flexural modulus to be calculated at any point in the fatigue test. Figure 4.40 illustrates the change in the flexural modulus under fatigue test, E_{ff} as a function of the normalised life fraction (N/N_f) at an applied load of 85%UFS. It is clear from Figure 4.40 that the laminate T5wt has a high flexural modulus and this can be correlated with the high fatigue life seen in Figure 4.33.

[123]

Figure 4.41 presents normalised flexural modulus data, i.e. the ratio of E_{ff} to the original flexural modulus E_o, as a function of life fraction N/Nf for all five layer laminates at an applied load of 85%UFS. As expected, Figure 4.41 demonstrates that the change in flexural modulus can be divided into three similar regions to those observed for deflection, as shown in Figure 4.39:

• The initial stage which occurs within the first 10% of life, and where there is a marked reduction in flexural modulus degradation to ~96% of the original flexural modulus. This reduction could be related to development of matrix cracks at this period.

• An intermediate stage, where there is a gradual linear reduction in modulus degradation as a function of life fraction which continues to around 90% of N_f.

• A final stage, in which the modulus decreases rapidly and which culminates in sample failure due to local damage development.
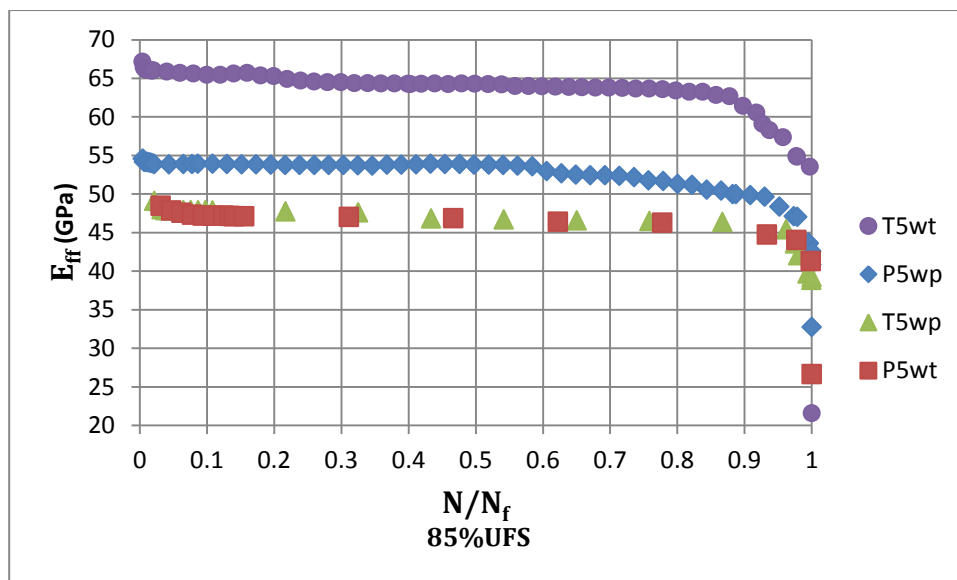
Figure 4-40: Flexural modulus as a function of fatigue life fraction for the 5-layer laminates.
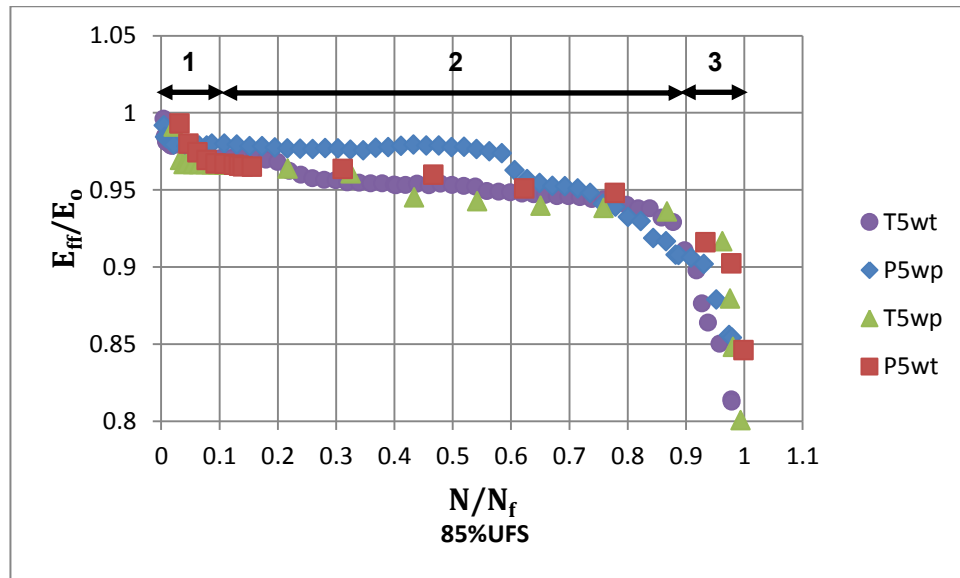
Figure 4-41: Normalised flexural modulus as a function of fatigue life fraction for the 5-layer laminates.

It is also clear that when considering normalised flexural modulus, all the specimens of 5-layer laminates show similar behaviour, with the exception of the plain weave fabric in the warp direction. This particular case has a higher value of E_{ff}/E_o for approximately the first 60% of the fatigue life, where after it shows similar behaviour to the other laminate specimens.

Similar behaviour occurs for the normalised flexural modulus as a function of fatigue life fraction at different levels of applied fatigue load (e.g. 95%UFS and 85%UFS) as shown in Figure 4.42.

In the specimens tested in this programme of work, a 5-6% decrease in the flexural modulus indicates the beginning of the region of final failure in the composite laminates under fatigue loading. This decrease could be related to the rise of temperature that usually accompanies fatigue testing [84]. Fatigue failure mechanisms in composite laminates are more complex than those which occur in metals, and failure in composite laminates under fatigue loading can occur through matrix cracking, interfacial debonding, delamination, fibre pull-out and fibre breakage. Furthermore, in flexural fatigue testing, one face of the

[125]

sample is in tension and the other one is in compression. The observed mechanisms of failure change between these two types of load.

4.4.3 Fatigue damage index (FDI)

The fatigue damage index (FDI) has been defined in Equation 3.13 in terms of the flexural modulus decrease observed in composite materials as fatigue cycling progress. Figure 4.43 shows the value of FDI as a function of the normalised life fraction N/N_f for typical laminates fatigued at 85%UFS. Defining a fatigue damage index in terms of the decrease observed in flexural modulus means that failure does not correspond with a value of FDI = 1.0. A value of FDI = 0.1 corresponds with a value of N/N_f > 90% of fatigue life, while FDI = 0.2 would indicate imminent failure.
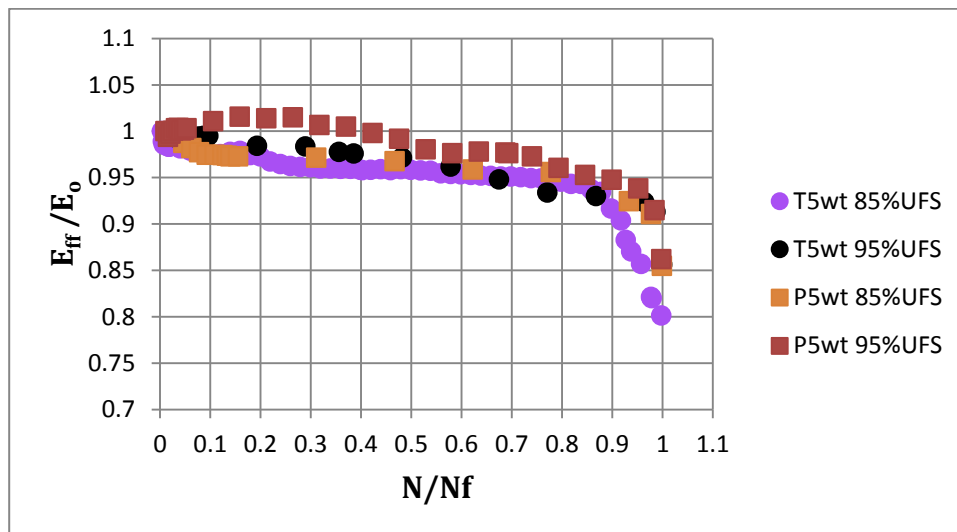
Figure 4-42: Normalised flexural modulus as a function of fatigue life fraction for two different applied load levels.
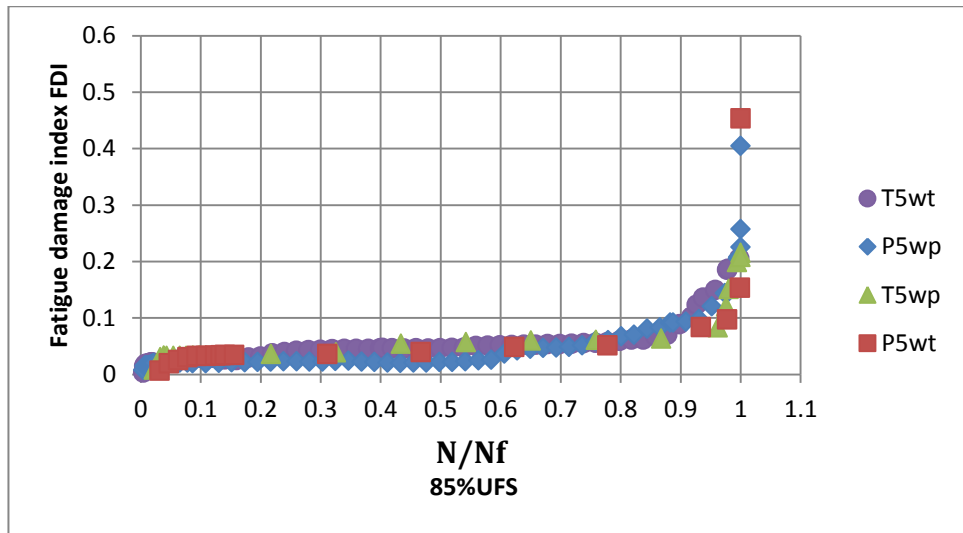
Figure 4-43: Fatigue damage index as a function of life fraction for different laminates.

The FDI as defined above increases only slightly over the range life fraction $0 < N/N_f < 0.9$ (Figure 4.43) but increases exponentially in the range $0.9 < N/Nf < 1.0$. Similar behaviour is observed when considering other load cases (95%UFS and 85%UFS) as shown in Figure 4.44. It is interesting to note that the twill weave 5-layer weft direction specimen (T5wt – which has high fatigue strength) displays a different behaviour in the final 10% of life compared with the lower fatigue strength laminate P5wt.
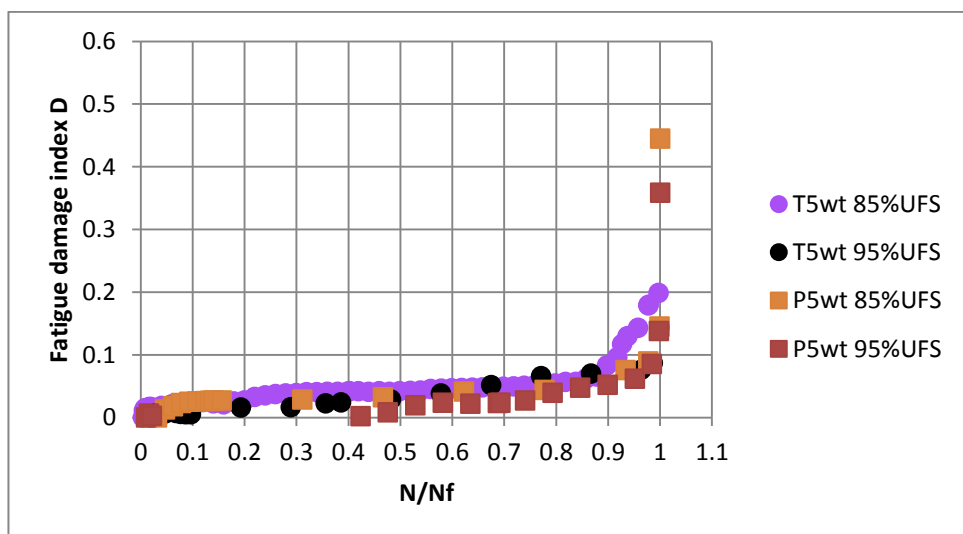
Figure 4-44: Fatigue damage index as a function of life fraction for two different load levels.

[127]

It was observed that most of the fatigue specimens failed in the expected central region (middle of the lower loading roller span). However, some specimens failed near to one of the loading points, particularly at higher applied load levels, i.e. 90-95% UFS as shown in Figure 4.45. In these cases cracking did not begin exactly below the loading point, but rather in close proximity to it. This could be due to the local stress concentration becoming more important at higher applied loads, as a result of the compression stresses induced at the loading point (leading to a localised multiaxial stress state) as well as a potential thermal influence from friction and fretting between the loading point and the specimen.
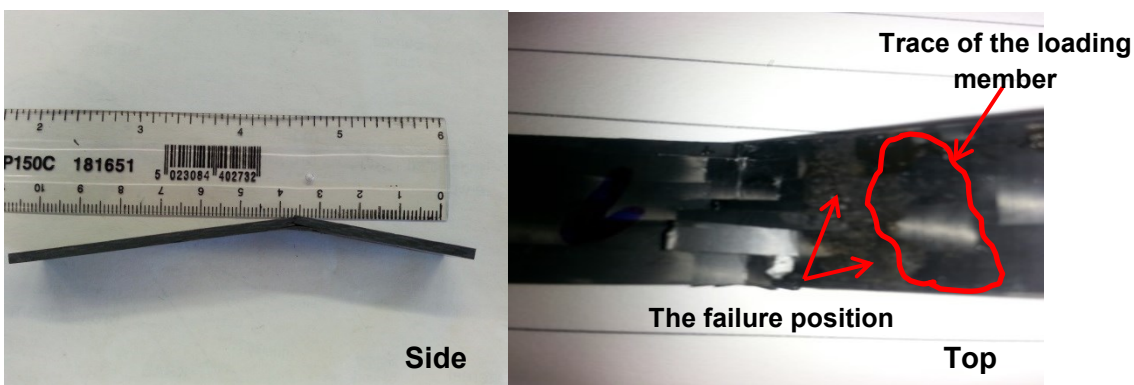
Figure 4-45: Examples of specimens where failure occurred close to the loading points.

The fatigue damage index can be used to identify the onset of cracking in fatigue specimens. Figures 4.43 and 4.44 illustrate that the fatigue damage index starts to increase above $N/N_f \approx 0.85$. In an attempt to explore the ability of the FDI to predict the onset of cracking irrespective of the level of applied fatigue load, four fatigue specimens were tested under several different load levels (R=0.1 and f=10 Hz) and with a sequence of life fraction, as illustrated below;

- A T5wp specimen was subjected to fatigue testing at 95%UFS for a number of cycles $N = 0.6N_f$.

- A P5wp specimen was subjected to fatigue testing at 92.5%UFS for a number of cycles $N = 0.7N_f$.

- A P5wt specimen was subjected to fatigue testing at 90%UFS for a number of cycles $N = 0.8N_f$.

- A T5wt specimen was subjected to fatigue testing at 87.5%UFS for a number of cycles $N = 0.9N_f$.

N_f is calculated from Equation 4.8, which is a rearrangement of Equation 3.12, taking the A and B values from Table 4.7 for each laminate type.

$$N = \log^{-1}\left(\frac{B-S}{A}\right) \qquad (4.8)$$

The Electropuls testing machine was set to stop the test when it reached the required number of cycles for each specimen. The fatigued specimen was then examined using a Skyscan micro-CT scanner to see if any indications could be found of incipient cracking. No trace of cracking was apparent in the X-ray scans for the specimens tested to life fractions of $0.6N_f$, $0.7N_f$ or $0.8N_f$, as shown in Figure 4.46 which illustrates the cross-sections from the three samples.
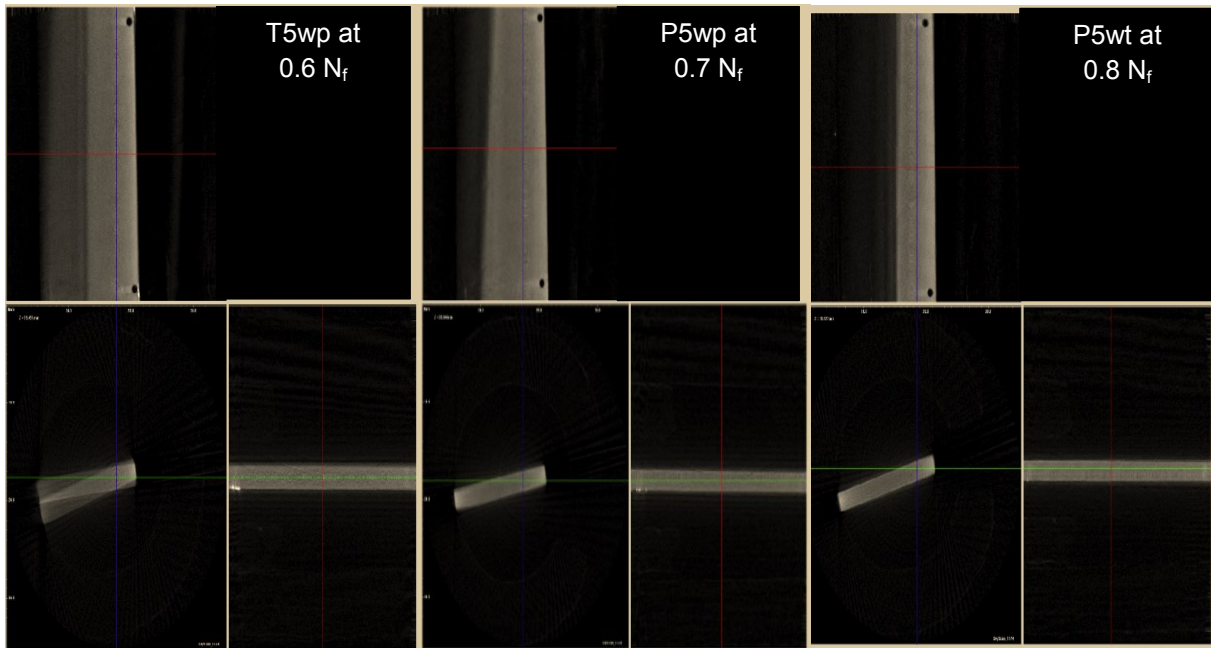
Figure 4-46: Computed tomography (CT) images for three different laminates tested to various life fractions at different load values.

The CT images do, however, contain low density features in the specimen tested to 90%N_f which are likely to reflect damage zones in the composite (Figure 4.47). This life fraction corresponds to the onset of the region where there is a fast reduction in flexural modulus and an equivalent rapid increase in the fatigue damage index, FDI. It is also the case that these low density regions coincide with the positions where failure is observed to have occurred in other specimens tested to failure, as shown in Figure 4.48. These positions reflect the maximum tensile and compressive stresses that act on the contact faces of the specimens, and the RRV in some laminates allow cracks to both cross from one ply to another and to change their direction of propagation as shown in Figure 4.49. This can occur because of the low strength of the RRV.
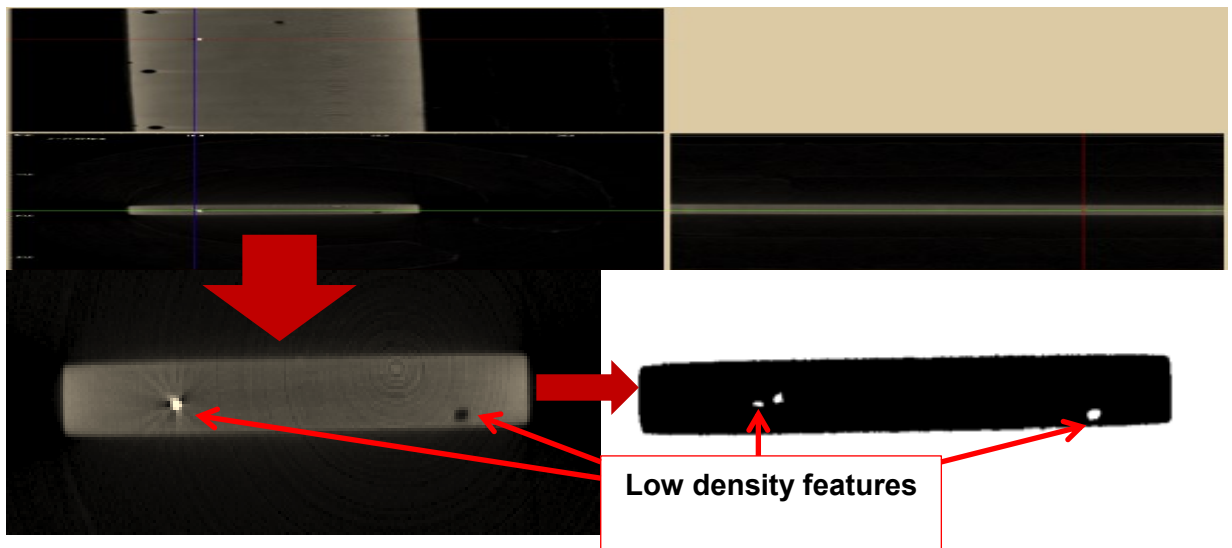
Figure 4-47: CT scan images for a laminate T5wt at N=0.9N_f.

4.4.4 The correlation between fatigue and static mechanical strength

In the fatigue data presented in Figures 4.32 to 4.34, the UFS data are plotted on the same curve with the flexural test being taken as equivalent to failure in 0.5 cycles of loading [137]. The flexural fatigue stress at 0.5 fatigue cycles will be very close to the flexural fatigue stress at 1 fatigue cycle and the difference between them can be neglected. Therefore, one can assume that at $N=1$ cycles, $S = UFS$; substituting that into Equation 3.12, i.e. S = -A log(N)+B, gives $B=UFS$.

Therefore,

$$S = \text{-A} \log(N) + UFS \tag{4.9}$$

Where, UFS and A are different for each laminate.
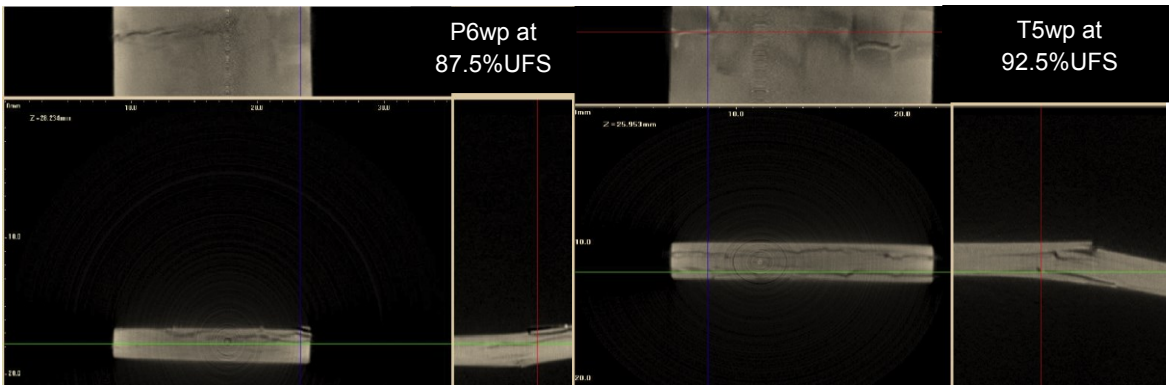
Figure 4-48: CT images showing the failure positions for various laminates and load levels.
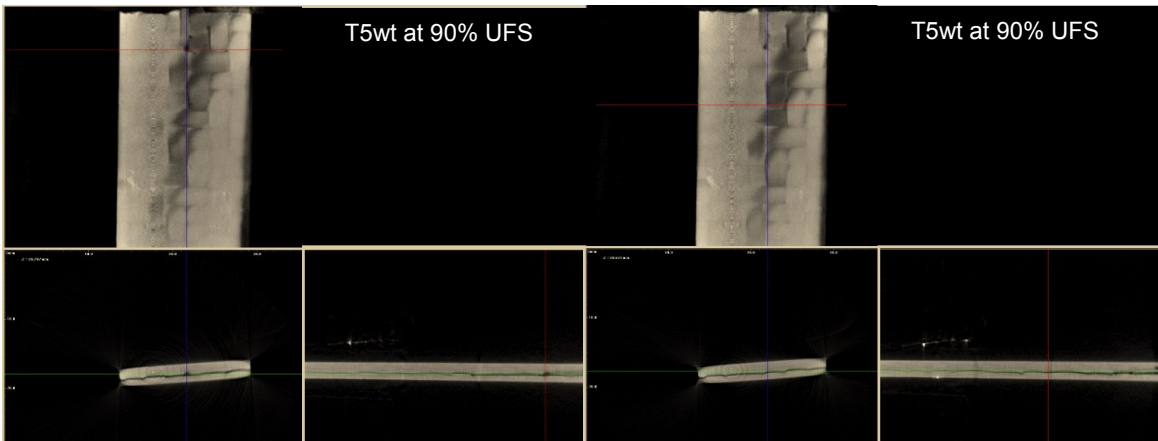
Figure 4-49: CT images showing crack propagation in various laminates and load levels.

Hence the RRV and the fibre distribution are constants for each type of laminate, energy that cause failure at fatigue load could be related to the energy that cause failure at static load. Therefore, the fatigue properties could be related to the static properties. Figure 4.50a plots absolute value of A as a function of UFS for all laminates. The constant A in the SN relationship is proportional to the

UFS and a second order polynomial can be used to fit this correlation (polynomial because the R^2 value for the second order polynomial fit is higher than the R^2 value for a linear fit) while the p-value of 0.000082 indicates a significant correlation between |A| and the UFS. Furthermore, the predicted |A| values using the second order polynomial regression was better than that of the linear regression (Figure 4.50b), and |A| is proportional to the UFS according to the relationship

$$|A| = -0.00006UFS^2 + 0.1075UFS - 26.901 \hspace{2cm} (4.10)$$

$A = -6E-05UFS^2 + 0.1075UFS - 26.901$

$R^2 = 0.8769$

$p = 0.00008$

(a)

2nd order polynomial regression $R^2 = 0.8769$

Linear regression $R^2 = 0.8559$

(b)
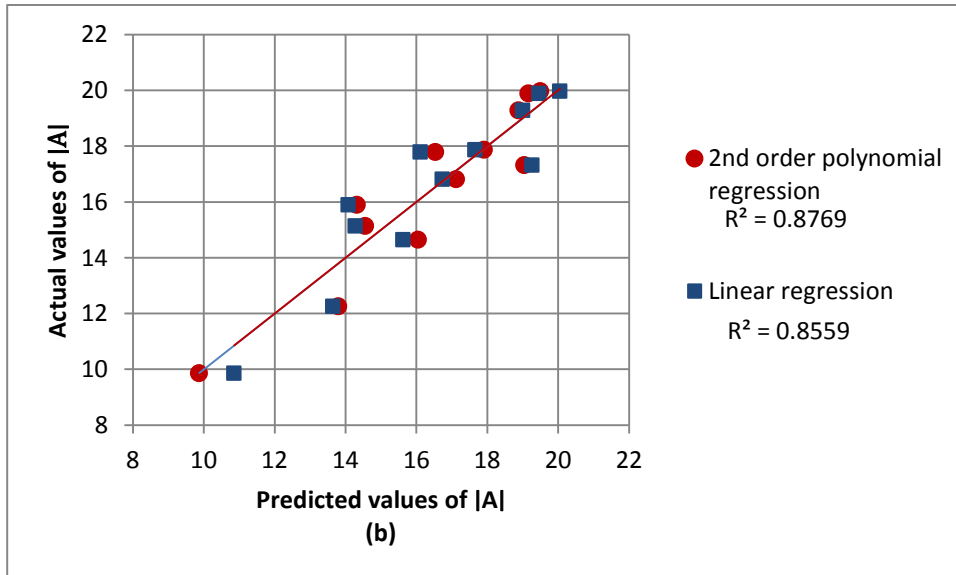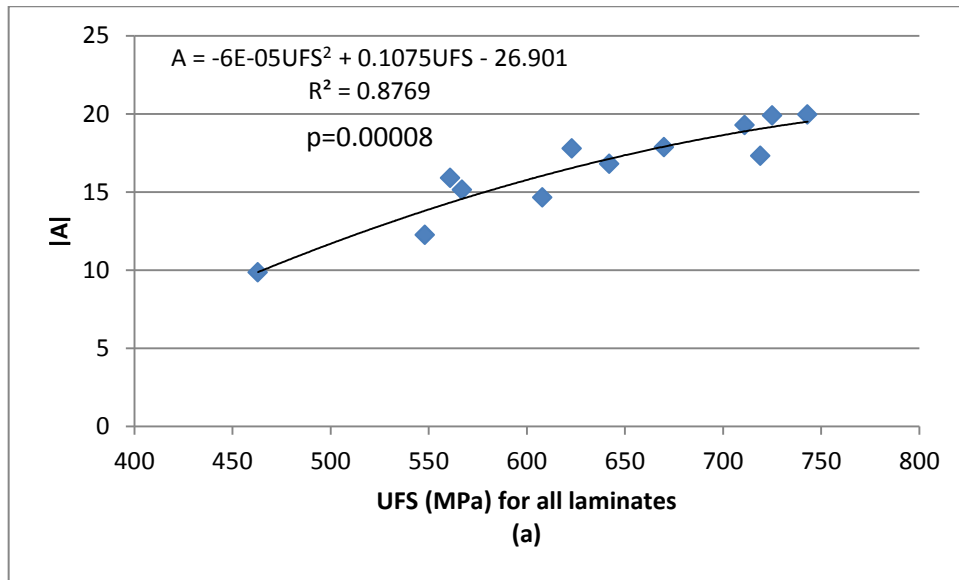
Figure 4-50: (a) The correlation between A and the UFS for all laminates and (b) The actual values versus the predicted values of A.

4.4.4.1 Extrapolation of Equation 4.10

The following theoretically indications need to be confirmed by additional tests.

In practice, need safety factor and recognise limit and their fatigue. From typical

S-N curve at A=0, we might be expect that the laminate will not fail for an infinite

number of cycles at that stress (endurance limit) as shown in Figure 3.21.

Substituting A=0 in Equation 4.9, gives,

[134]

$$S_{endurance} =- (0) \log(N) + UFS$$

and by applying that in Equation 4.10 to find the two roots of this equation.

$$0 = -0.00006\ S^2_{endurance} + 0.1075\ S_{endurance} - 26.901$$

Therefore, $S_{endurance} = 1491$ MPa is rejected as it is greater than UFS for all laminates where as $S_{endurance} = 301$ MPa is sensibly below UFS for all laminates and might be accepted. The endurance limit, obtained from the correlation between the slope of the S-N curve A and the UFS, is shown in Table 4.8 for all composite laminates in this study.

Table 4-8: The endurance limit for all laminates obtained from the experimental correlation between A and the UFS.

Laminate	Endurance limit (%)= $(\dfrac{301}{UFS}*100)$
P4wp	53.7
P4wt	64.9
T4wp	54.9
T4wt	49.5
P5wp	44.9
P5wt	53.1
T5wp	46.9
T5wt	41.8
P6wp	41.5
P6wt	48.3
T6wp	42.4
T6wt	40.5

As noted earlier, the fibre distribution plays a critical role in determining fatigue performance and it is therefore useful to separate the data into plain weave fabric and twill fabric results as shown in Figure 4.51, which again demonstrates

that A is proportional to the UFS and that the relationship between them is not linear for either the plain or the twill weave laminates.
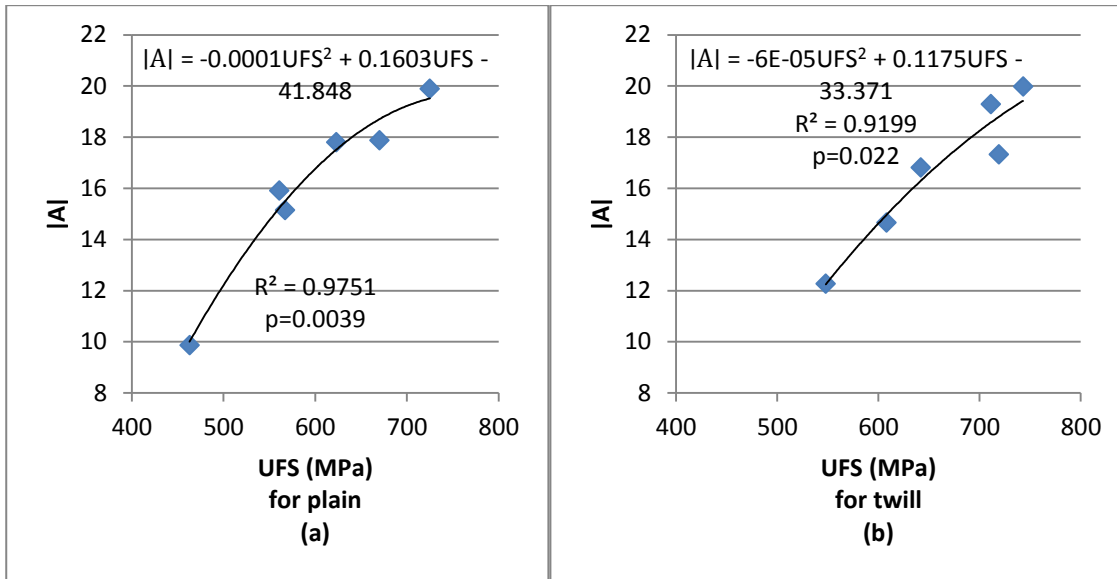
Figure 4-51: A versus UFS for a) plain fabric and b) for twill fabric.

The p-value of plain laminates in Figure 4.51 is 0.0039 and the p-value for the twill laminates is 0.022. They are both < 0.05 which indicates a significant correlation between |A| and the UFS for both types of fabric.

From Figure 4.51a,

$$|A|_{plain} = -0.0001UFS^2 + 0.1603UFS - 41.848 \qquad (4.11)$$

As mentioned before at A=0, $S_{endurance}$ = UFS, and by applying that in Equation 4.11 to find the two roots of this equation;

$S_{endurance} = 1274$ MPa > UFS_{static} for all plain laminates which is not accepted.

or $S_{endurance} = 328$ MPa < UFS_{static} for all plain laminates which is accepted.

From Figure 4.52b,

$$|A|_{twill} = -0.00006UFS^2 + 0.1175UFS - 33.371 \qquad (4.12)$$

[136]

Again at $A=0$, $S_{endurance} = UFS$ and by applying that in Equation 4.12 to find the two roots of this equation;

$S_{endurance} = 1614$ MPa $>$ UFS for all twill laminates which is not accepted or

$S_{endurance} = 345$ MPa which is sensibly $<$ UFS for all twill laminates and is therefore accepted.

Therefore the endurance limit stress for twill laminates (345 MPa) is higher than the endurance limit stress of plain laminates (328 MPa), and this is expected because the crimp ratio in plain fabric laminates is higher than that in the twill fabric laminates. The endurance limit based on the type of fabric is given in Table 4.9.

Table 4-9: The endurance limit of the plain and twill laminates based on the correlation between A and the UFS.

Laminate	Endurance limit (%UFS)	Laminate	Endurance limit (%UFS)
P4wp	58.5	T4wp	63
P5wp	49	T5wp	53.7
P6wp	45.3	T6wp	48.6
P4wt	70.8	T4wt	56.8
P5wt	57.9	T5wt	48
P6wt	52.6	T6wt	46.4

The fatigue life (N) corresponding to a particular value of UFS under any applied flexural fatigue load S can be calculated from Equation 4.13, which is a rearrangement of Equation 4.8,

$$N = \log^{-1}\left(\frac{UFS-S}{A}\right) \tag{4.13}$$

Where,

$A_{all\ laminates} = -0.00006UFS^2 + 0.1075UFS - 26.9$

$A_{plain} = -0.0001UFS^2 + 0.1603UFS - 41.848$

And $A_{twill} = -0.00006UFS^2 + 0.1175UFS - 33.371$

Equation 4.14 represents an equation that can predict fatigue life as a function of the UFS for any value of applied flexural fatigue stress S, where S and UFS have units of MPa.

4.4.5 The correlation between the fatigue life and the fibre distribution

In this study as mentioned earlier, second order polynomial regression has been chosen for the correlation between the fatigue parameter |A| and the fibre distribution, as it has a higher value of R^2 compared with other regressions. Furthermore, the predicted values using the second order polynomial regression was better than that of the linear regression (Figure 4.52).
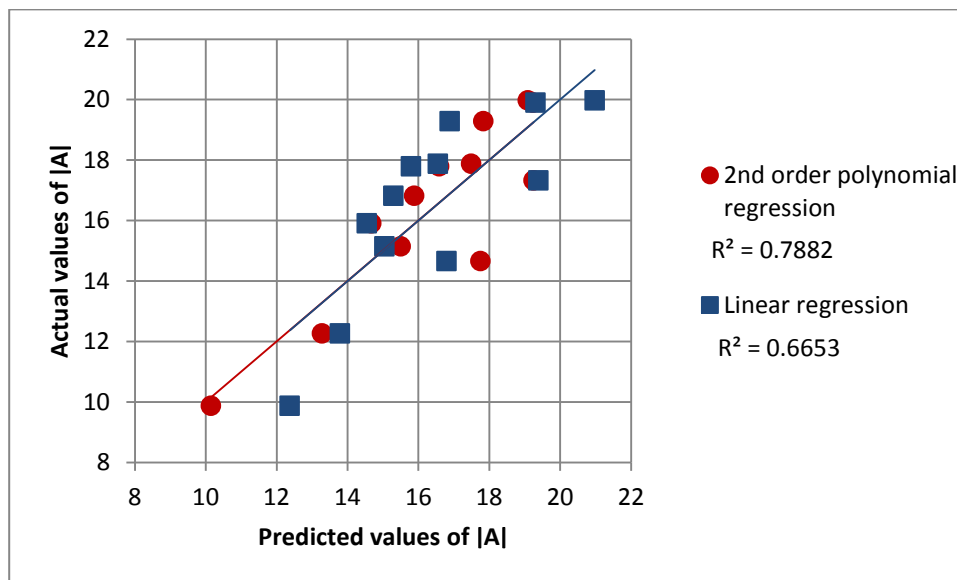
Figure 4-52: The actual values versus the predicted values of |A|.

By plotting the absolute value of the fatigue parameter A against the complete set of D data in these laminates, together with the data for stressed fibre volume

fraction and the total fibre volume fraction as shown in Figure 4.53, it is clear that there is a correlation between the fibre distribution measured by the D and the fatigue properties represented by the slope of the S-N curves A. The correlation between |A| and the D (R^2= 0.7915 and p=0.00086) is better than the correlation between |A| and the stressed V_f (R^2= 0.6979 and p=0.0045) or the total V_f (R^2= 0.723 and p=0.003).

The correlation found between the fatigue life and the UFS (Figure 4.50) is more significant than the correlation between the fatigue life and the fibre distribution (Figure 4.53a), as evidenced by the R^2 and p-values for the correlations. However, both correlations were significant.
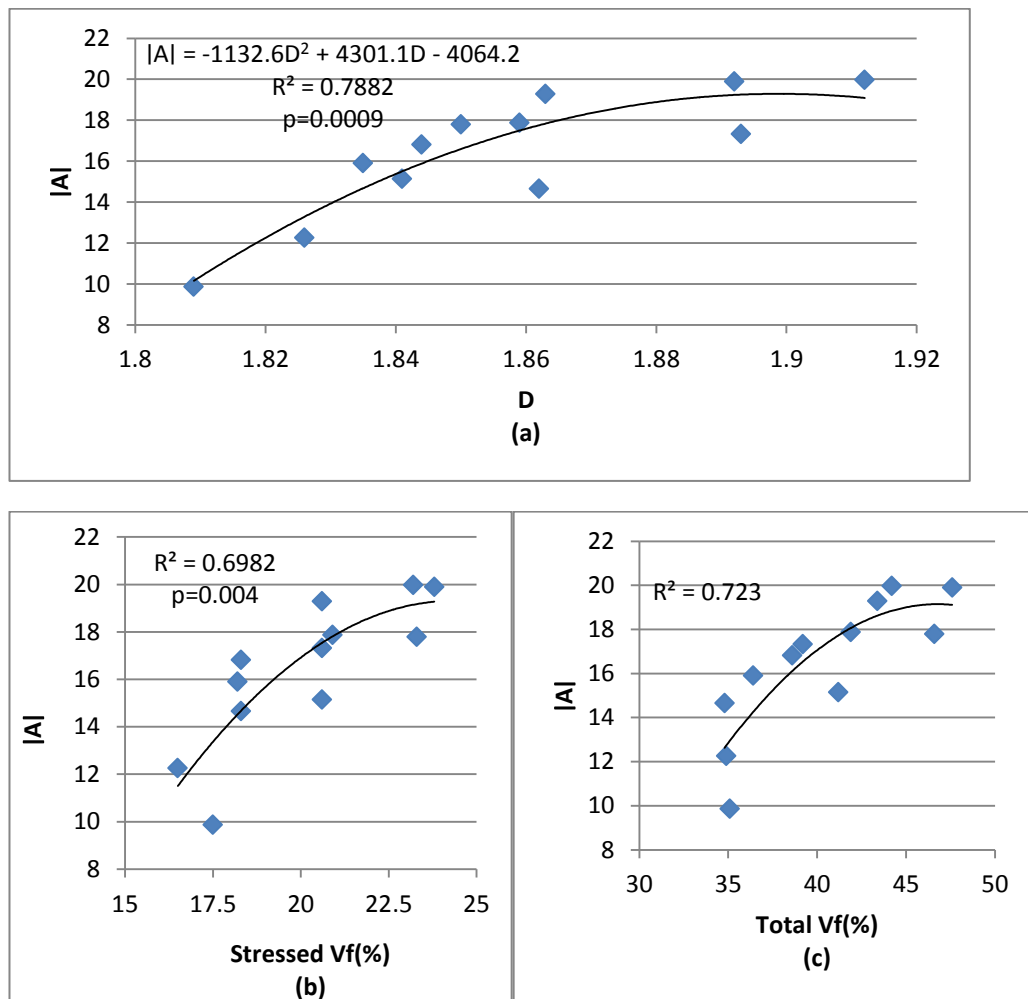
Figure 4-53: Data for all laminates: a) Fatigue parameter |A| versus D, b) |A| versus stressed V_f and c) |A| versus total V_f.

The correlation between fatigue life and the fibre distribution as shown in Figure 4.53a is

$$A = -1132.6D^2 + 4301D - 4064.2 \qquad (4.14)$$

Again by using the same assumption that at A=0 the laminate will not fail for an infinite number of cycles at that stress.

$$0 = -1132.6D^2 + 4301D - 4064.2$$

Gives $D_1 = 2.027 > 2$ (not accepted) or $D_2 = 1.77$ (accepted)

At A=0, $S_{endurance} = $ UFS, and by substituting $D=1.77$ in Equation 4.5,

$S_{endurance} = 232.4$ MPa.

Hence the endurance limit for all composite laminates found from the correlation between fatigue life and the fibre distribution is given in Table 4.10.

Table 4-10: The endurance limit of all laminates based on the correlation between A and the D.

Laminate	Endurance limit (%UFS)
P4wp	41.4
P4wt	34.7
T4wp	32.1
T4wt	50.2
P5wp	41
P5wt	37.3
T5wp	42.4
T5wt	36.2
P6wp	32.7
P6wt	38.2
T6wp	32.3
T6wt	31.3

The endurance limit based on the fibre distribution is likely to be safer to use in design than the endurance limit found using the UFS, as laminates could be manufactured with similar UFS values and different D values. Therefore, it is safer to take the lower endurance limit as first indicator, or the one that fitted the design conditions.

Finally, to find the life of the composite laminates, as mentioned above (Equation 4.13);

$$N= \log^{-1}(\frac{UFS-S}{A})$$

Using the values of UFS from Equation 4.5 and A from Equation 4.13, the relationship between fatigue life and D is:

$$N=\log^{-1}\left(\frac{-21339D^2+82155D-78329-S}{-1132.6D^2 + 4301D - 4064.2}\right) \qquad (4.15)$$

Equation 4.15 represents an equation to predict the fatigue life of the composite laminate based on the fibre distribution, which can be characterised by the D, at any value of the flexural fatigue stress S in MPa.

The fatigue life relationships found in this project for the twill and plain weave fabrics can be summarised as follows:

- The fatigue life of all the composite laminate specimens considered in this work shows a clear dependence on the static strength (UFS) as well as on the fibre distribution, characterised by the D.

- The correlation observed between fatigue life and the static UFS was better than the correlation observed between fatigue life and the fibre distribution, although both of them are statistically significant.

- The endurance limit (found using either the UFS or the D data) was inversely proportional to the UFS for all specimens and the endurance limit of twill weave fabric laminates was better than the endurance limit of the plain fabric laminates at similar values of UFS.

- The decrease in stiffness observed during fatigue cycling shows a clear trend with increase in the number of applied fatigue cycles.

- A decrease of *5-6%* in the flexural modulus of composite laminates was found to indicate the onset of crack initiation in the composite laminates under fatigue loading.

- The CT images demonstrate the presence of low density features at 90% of N_f.

- RRV in the composite laminates allow cracks to both cross from one ply to another and to change their direction of propagation.

- The D can be used to characterise the fatigue life and hence make life predictions for fibre-reinforced composites.

As a further validation of the relationships discussed in this chapter, another laminate was manufactured using the RTM process but with a different fabric architecture (basket weave) whilst keeping other processing parameters constant. The mechanical tests (static and fatigue) and the image analysis performed on this laminate are discussed in the next chapter.

Chapter 5 FURTHER EVALUATION OF THE OBSERVED CORRELATIONS USING A BASKET WEAVE LAMINATE

5.1 Introduction

This chapter seeks to further evaluate the applicability of the various correlations discussed in Chapter 4 for the original twill and plain weave fabrics using a third basket weave fabric laminate.

5.2 Materials and manufacturing laminate

6K carbon fibre architectures were woven by Carr Reinforcements using the same batches of fibre for both warp and weft directions of the fabric. The modulus of elasticity of the carbon fibres was 235 GPa. The areal density of the basket weave fabric was 470 g/m^2. Yarn counts were 380 tows/m for warp and 810 tows/m for the weft yarn count. The resin was Sicomin SR8100 epoxy with Sicomin SD8824 hardener in a weight mix ratio of 100:22. The RTM process was used to manufacture laminates for the experimental work, with the same cavity and vacuum closing of the mould as used for the twill and plain weave fabrics. The injection pressure was again +500 mbar

The plate was then cured under vacuum for 24 hours at ambient temperature. Full peripheral clamping vacuum (1000 mbar absolute) was maintained whilst the resin was cured. The plate was post-cured in an oven for 8 hours at 60 $^{\circ}$C according to the resin manufacturer's guidelines (Appendix A-3.2).

A single basket weave fabric laminate plate was manufactured with 4 layers of fabric. Five samples were cut from each of the warp and weft directions for each of the static mechanical tests (UFS and ILSS) and for the image analysis. However, nine samples were cut from each of the warp and weft directions for

the flexural fatigue tests. Then same sequence of mechanical tests (static and fatigue) and image analysis as described in Chapter 4 was conducted.

5.3 Static properties of the basket weave laminate

The basket weave microstructures were quantified, in both the warp and weft directions, using the box-counting method to determine the D and the total V_f. Interlaminar shear strength, ILSS, and the four-point bending tests were undertaken and provide values for the flexural bending modulus (E_b), the ultimate flexural stress (UFS) and ILSS. Table 5.1 illustrates the mean mechanical properties and image analysis data, for the basket weave laminate.

Table 5-1: The mean mechanical properties and image analysis data of basket weave laminate.

Laminate	Direction	Symbol	D	Total V_f (%)	UFS (MPa)	ILSS (MPa)	E_b (GPa)
4 layers (Basket weave)	Warp	BWwp	1.853	40	475	42	25
	Weft	BWwt	1.913	43	747	49	57

Figure 5.1 presents the UFS data and illustrates that the UFS in the weft direction is higher than the UFS in the warp direction, because the weft direction has a higher number of fibre tows (as would be predicted by the rule-of-mixtures). Similar behaviour was observed with the ILSS and the flexural modulus as shown in Figure 5.2 and Figure 5.3. Even though the number of tows in the weft direction (810/m) is higher than the number of tows in warp direction (380/m), there was not a big difference between the ILSS in the two directions because it depends primarily on the resin properties rather than the fibres properties. Figure 5.4 illustrates that the total V_f in the weft direction was higher than the warp direction. Similar behaviour was observed for the D as shown in Figure 5.5 for the warp and weft direction.
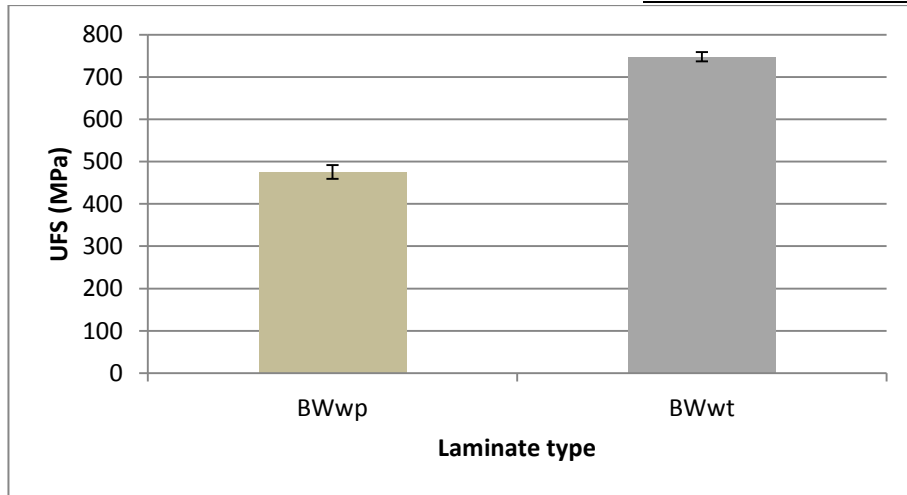
Figure 5-1: UFS with standard error for the basket weave laminate in both directions.
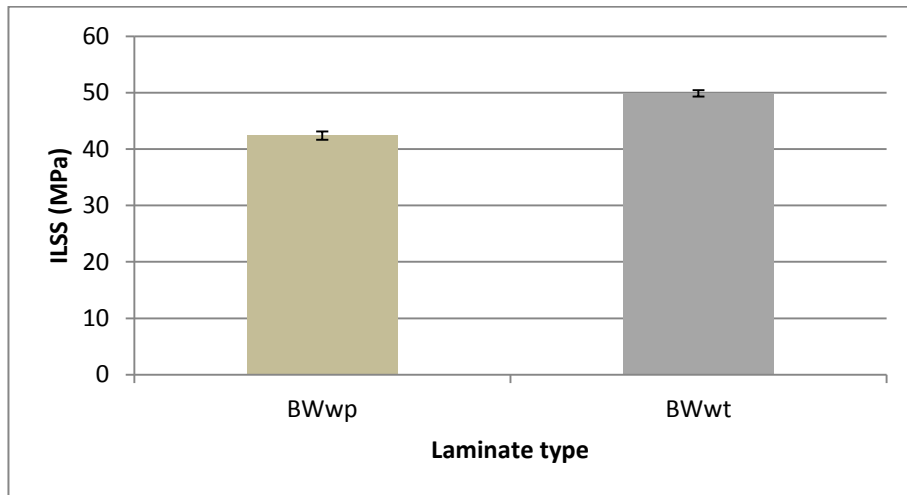
Figure 5-2: ILSS with standard error for the basket weave laminate in both directions.
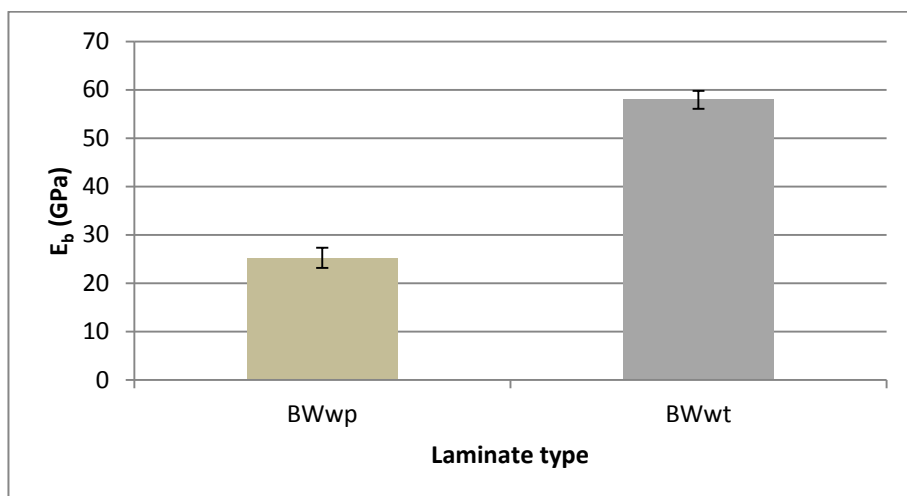
Figure 5-3: E_b with standard error for the basket weave laminate in both directions.

[147]
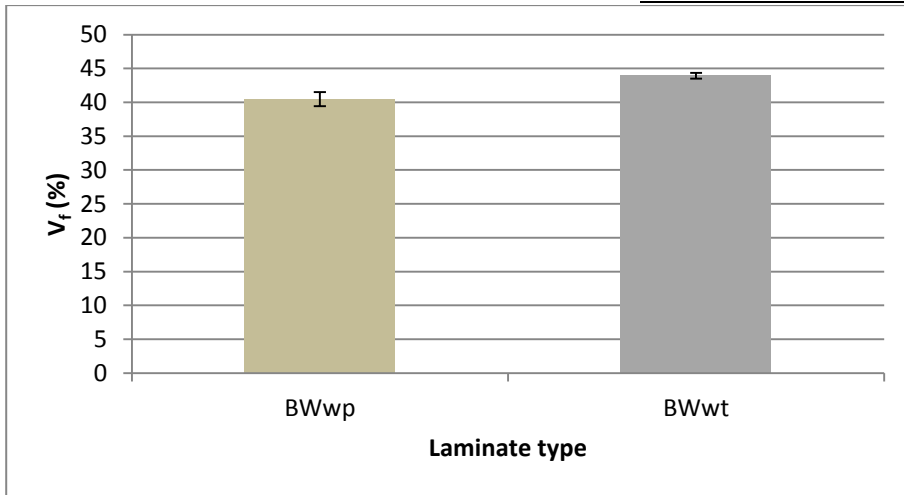
Figure 5-4: V$_f$ with standard error for the basket weave laminate in both directions.
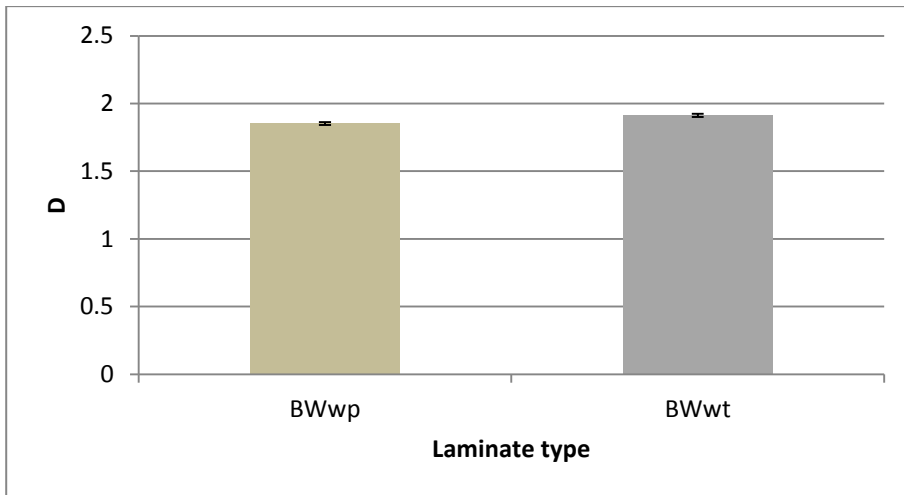
Figure 5-5: D with standard error for the basket weave laminate in both directions.

To validate the applicability of the correlations discussed in Chapter 4 for the static UFS, based on the fibre distribution, it is useful to use the D data for the basket weave laminate (column 4 in Table 5.1) to predict the values of the UFS, ILSS and E$_b$ by using Equations 4.5, 4.6 and 4.7 respectively as follows;

$$UFS \text{ (MPa)} = -21339D^2 + 82155D - 78329$$

$$ILSS \text{ (MPa)} = -549.97D^2 + 2131.2D - 2013.7$$

$$E_b \text{ (GPa)} = -1278.4D^2 + 4881.4D - 4616.6$$

[148]

Then, the error can be determined between the predicted values, found
according to the D, and the experimental values as shown in Table 5.2.

**Table 5-2: The error between the predicted and the experimental values of the UFS, ILSS
and the E_b.**

Laminate	D	UFS_{exp} (MPa)	UFS_D (MPa)	Error (%)	$ILSS_{exp}$ (MPa)	$ILSS_D$ (MPa)	Error (%)	Eb_{exp} (MPa)	Eb_D (MPa)	Error (%)
BWwp	1.853	475	634	33	47	42	12	39	25	36
BWwt	1.913	747	742	0.7	50	49	2	43	57	33

Table 5.2 shows that the errors between the predicted and the experimental
values of the UFS and ILSS were very small in the weft directions (0.7 and 2%),
while the errors in warp direction were significantly higher (33 and 12%) due to
the crimp ratio in the warp direction being higher in direct proportion to the
number of tows in the warp and weft directions (380 vs 810). However, the
errors in the predicted values of E_b were high because this parameter correlates
better with the stressed V_f than with the D (as would be expected from the rule-
of-mixtures), as mentioned in the previous chapter. Furthermore, the error
between the predicted and the experimental values of ILSS arises from the
ILSS dependence on the fibre distribution in addition to the resin properties.

To sum up, the predictions of the UFS and the ILSS, based on the fibre
distribution, could be useful for predicting the static properties for woven fabric
laminates, with smaller differences between the number of tows in the warp and
weft direction.

5.4 Fatigue life of the basket weave laminate

The four-point bending fatigue tests were performed at room temperature under
direct load control, according to the British Standard EN ISO 14125:1998 for

fibre-reinforced plastic composites as shown in Figure 3.19. An Instron

Electropuls E300 (serial number: 5527-103) fatigue testing machine fitted with a

±5 kN dynamic load cell (serial number: 107190) was used. The tests were

carried out on specimens cut in the warp and the weft directions with

dimensions of 100x15x2 mm (length x width x thickness) and the loading span

between the inner loading rollers was 81 mm (as for plain and twill samples).

In order to obtain S-N curves for the laminates, samples were loaded at

constant stress amplitude (R=0.1 and f=10 Hz) until failure occurred. The

number of sine wave load cycles to failure for each specimen was monitored.

Tuning of the Instron testing machine was performed for all samples because of

the changes in sample stiffness between individual specimens that could affect

the test accuracy. Fatigue data were generated at load levels of 95%, 90% and

85% of the UFS. To reduce the time necessary for preliminary or experimental

studies, three repeats of these three fatigue stress levels were done to provide

the fatigue data shown in Table 5.3.

**Table 5-3: S-N curve data for the basket weave laminate for the warp and the weft
direction.**

Level	BWwp	BWwp	BWwt	BWwt
(%UFS)	S	N	S	N
	(MPa)	(cycles)	(MPa)	(cycles)
100	475	0.5	747	0.5
95	451	2580	710	290
95	451	6349	710	518
95	451	17112	710	2438
90	428	93125	672	35415
90	428	85513	672	94651
90	428	12039	672	30327
85	404	496725	635	901665
85	404	58270	635	996496
85	404	79006	635	1555759

As used for the analysis of the S-N curves for the plain and twill weave laminates (Chapter 4), a logarithmic regression (Equation 3.12) was used to characterise the fatigue data, and the UFS data points were also plotted on the same curve at 0.5 cycles. Figures 5.6 illustrates the S-N curve for both warp and weft directions in the basket weave laminate. Figure 5.6 demonstrates that the weft direction of the basket weave laminate has higher fatigue strength due to the high UFS and D, while the warp direction of the laminate shows low fatigue properties due to the low values of these parameters in the warp direction (see Table 5.1).
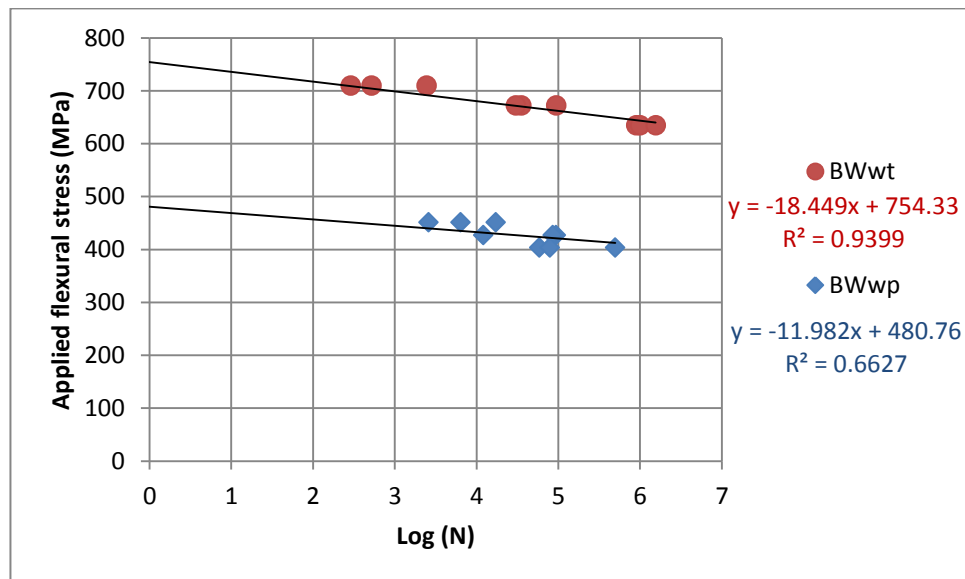
Figure 5-6: S-N curves for the warp and the weft directions in the basket weave laminate.

To explore the validity of the correlations discussed in Chapter 4 for the fatigue life in terms of UFS and fibre distribution, the data in Table 5.1 can be used to predict the values of |A| and B using Equations 4.5, 4.10 and 4.14 as follows;

$$\text{UFS (MPa)} = B_D = -21339D^2 + 82155D - 78329$$

$$|A|_{UFS} = -0.00006UFS^2 + 0.1075UFS - 26.901$$

[151]

$$|A|_D = 1132.6D^2 + 4301D - 4064.2$$

The errors between the predicted values, which are based on the fibre distribution and static properties, and the experimental values are shown in Table 5.4. Table 5.4 shows that in the weft direction the error between $|A|_D$ and $|A|_{S-N}$ values was very small (2%), while the error between $|A|_{UFS}$ and $|A|_{S-N}$ was higher (8%). However the errors in warp direction were significantly higher (38 and 11%) than the errors in the weft direction, due to the crimp ratio in the warp direction being higher, as reflected by the number of tows in the warp and weft directions (380vs810). Furthermore, Table 5.4 shows that the error between the B_D with B_{S-N} and B_{UFS} with B_{S-N} values were very small (2 and 1%) for the weft direction, and the error between the B_{UFS} and B_{S-N} for the warp direction was small (1%). However, the error between the B_D and B_{S-N} was higher (32%) for the warp direction.

Table 5-4: The errors between the predicted values and the experimental values the (the S-N curve shown in Figure 5.6) of the |A| and B based on the UFS and the D data.

Laminate	$|A|_D$	$|A|_{S-N}$	Error (%)	$|A|_{UFS}$	$|A|_{S-N}$	Error (%)
BWwp	16.64	11.98	38	10.62	11.98	11
BWwt	18.79	18.45	2	19.92	18.45	8
Laminate	B_D	B_{S-N}	Error (%)	B_{UFS}	B_{S-N}	Error (%)
BWwp	633	481	32	475	481	1
BWwt	742	754	2	747	754	1

Table 5.4 shows that the values of |A| and B based on a D analysis were higher than the experimental values taken from the S-N curves, but that the values of |A| and B based on an analysis of UFS were lower than the experimental values taken from the S-N curves. It is safer in design terms to take the higher value of |A| (which has a negative sign in the typical equation of S-N curve) and lower value of B as first indicators of fatigue performance. Therefore, it is recommended for this data set to predict |A| value based on the D (Equation 4.17), and to find a B value which is equal to the UFS.

To sum up, the relationships between the fatigue life parameters |A| and B, found using the fibre distribution and UFS data, could be useful in predicting the fatigue life for the woven fabric laminates, provided that only small variations between the crimp ratio exist in the warp and weft directions.

Chapter 6 CONCLUSIONS AND RECOMMENDATIONS FOR FUTURE WORK

6.1 Concluding comments

The study was carried out to investigate the effect of fibre distribution and resin-rich volumes, RRV, on the mechanical properties of fibre-reinforced composites. The study has also sought to explore whether the fibre distribution can affect the fatigue life of composites, particularly in woven carbon-epoxy laminates. In addition, the study has determined that using the fractal dimension with the box-counting method has the ability to describe the fibre distribution effects, and that the fractal dimension is suitable to distinguish the differences between various fibre architectures. The review of previous literature on this subject in the context of fibre-reinforced composites is inconclusive regarding several vital questions. These questions were centred on the relationships between mechanical properties and the microstructure of the composite laminates, and what the best method would be to measure the uniformity of the fibre distribution in a mesostructure analysis.

It has been found from the literature that the fibre distribution and the RRV can have a significant impact on the performance of composite laminates. Therefore the author cautions against reducing consolidation pressure or changing the fibre architecture for high performance composite structures, unless the consequences of such changes are fully understood for the reinforcement system in use. The literature review has also indicated that no one has focused on researching the effect of the fibre distribution on the fatigue properties of composite laminates. This study is believed to be the first systematic endeavour to correlate fibre distribution (measured as fractal dimension) with the fatigue life using sections of continuous woven reinforcement fabric laminates.

[157]

The study has shown that the variation in mechanical properties of composite laminates can be related to the various fibre distributions for laminates manufactured with similar processing parameters. The fibre distribution has been found to have a correlation with the mechanical properties (static and fatigue) of the fibre-reinforced composites, in addition to the correlation observed between fatigue life and static UFS. All correlations were statistically significant and exist for all the laminates tested in this study. Arising from these correlations, one can predict the fatigue life of the laminates used in this study or any laminate manufactured with similar processing parameters and a similar number of tows in the warp and weft directions.

6.2 Empirical correlations

The main empirical correlations are given in Chapter 4 of this thesis, and the following conclusions can be drawn from these correlations:

- The fractal dimension, D, can be used as a parameter to characterise the static and fatigue properties of fibre-reinforced composites.

- The strength of the composite laminates shows a clear dependence on the fibre distribution.

- Interlaminar shear strength, ILSS, correlates with the fibre distribution of the composite laminates.

- The fatigue properties of composite laminates have significant correlations with the fibre distribution and the static properties of the laminates.

- A reduction of 5-6 % in the flexural modulus of composite laminates indicates an increasing risk of failure of the composite laminates under fatigue loads.

- D can be used to predict the life of the fibre-reinforced composites.

- The endurance limits, based on either the static properties or the fibre distribution, appear to be inversely proportional to the strength for all laminates based on an extrapolation of a polynomial.

6.3 The implication of the correlations

The implications of the empirical correlations found in this study were checked for a different basket weave fabric in Chapter 5. The author has applied the various correlations to this different composite laminate, and from the percentage errors found between the predicted values and the experimental values, could conclude the following:

- The correlations between composite strength and the ILSS, based on the fibre distribution, could be useful to predict these properties for woven fabric laminates, but only with cases with small differences between the number of tows in the warp and weft direction.

- The correlations of the fatigue properties, based on the fibre distribution and static properties of the laminates could be useful for predicting the fatigue properties for the woven fabric laminates, but again only with cases with small variations between the crimp ratio in the warp and weft direction.

6.4 Recommendations for future work

In order to make the findings of this study more comprehensive the author recommends further study of the following factors and additional experimental data, which would facilitate attaining this goal:

- Future research should consider the measurement of the mean crimp angle for each weave style in both the warp and weft directions as a route to obtaining a fibre orientation distribution factor which could be used in the rule-of-mixtures for estimating and correcting, the mechanical properties. Such an analysis would require aggregation of the data sets.

- Study the effect of the crimp ratio in parallel with the fibre distribution, in order to create correlations that could explain the mechanical properties (static and fatigue) based on two different factors.

- Finding correlations between the fibre distribution and mechanical properties for other type of loads such as tensile, three-point bending, torsion and impact load.

- Addressing the relation between the stiffness degradation and increasing sample temperature.

- Using thermography to predict the final failure position under fatigue load according to the sample hot spots.

- Further research will concentrate on the description of damage accumulation, which hopefully will lead to a better understanding of failure mechanisms.

[160]

- Using CT scan images, with different equipment and a higher resolution, to measure the fractal dimension of the laminate; this could reduce the effort involved and the cost.

6.5 Limitations of the study

The study has investigated the effect of fibre distribution on the mechanical properties (static and fatigue) of the woven carbon-epoxy laminates, and the fibre distribution quantified by using the D (box counting method) in a mesostructural analysis. The correlations are based on flexural loading in the four-point bending test. As a direct consequence of this methodology, the study encountered a number of limitations, which should be considered in any future work:

- The correlations may not be suitable for other types of loading such as tensile, torsion, three-point bending, or impact loading.

- The correlations are not suitable for a macro or microstructural analysis.

- The fatigue cycles were sine wave type, therefore the correlations may not be suitable for other types of loading cycles.

- The correlations may not be suitable for other types of resin or fabric.

- The correlations may not be suitable for a test temperature different from the room temperature or lower or higher frequency of fatigue loads.

- To compare results for the fibre distribution with a fractal dimension analysis requires using the same box size and the grid position in the box counting method (ImageJ with FracLac add-in).

6.6 Postscript

In spite of what is often reported about the limited benefits of finding correlations between the mechanical properties (static and fatigue) and the fibre distribution from some microstructural images of the laminates, the author personally felt that there was some importance in finding these correlations, after spending a considerable amount of time in testing during this research.

Such limited applicability correlations could offer useful insights and contribute to resolving issues with improving the performance of the composite laminates, reducing the time of testing, reducing the cost of mechanical tests (static and fatigue) and reducing the risk of the failure of composite structures by predicting the life of the composite laminates. Equally, it can contribute to finding an explanation for the difference in the mechanical properties of laminates with similar fibre volume fraction and in improving the theoretical approaches for the static and the fatigue properties of composite laminates. All of this could lead to modified fibre architectures (without neglecting the permeability of the fabric employed), that could improve the performance of fibre-reinforced composites. Furthermore, the box counting method and fractal dimension can reduce an image of the key aspects of the microstructure to a single real number, and that could become a time-efficient way of data analysis.

Appendices

Appendix A-1: Mechanical properties of SR 8100 based laminates SR 8100 / SD 8734

Mechanical properties on cast resin :

Curing cycle		14 days @ AT*	SR 8100 / SD 8734		
			24 h AT* + 24 h @ 40 ℃	24 h AT* + 16 h @ 60 ℃	24 h AT* + 8 h @ 80 ℃
Tension					
Modulus of elasticity	N/mm²	3240	3000	2830	2864
Maximum resistance	N/mm²	59	72	74	75
Resistance at break	N/mm²	59	67	68	71
Elongation at max. load	%	2	3.5	4.3	4.7
Elongation at break	%	2	3.7	5.4	5.8
Flexion					
Modulus of elasticity	N/mm²	3320	3120	2880	2890
Maximum resistance	N/mm²	102	110	109	106
Elongation at max. load	%	3.7	4.7	5.5	5.7
Elongation at break	%	4.4	10	9.1	12.4
Charpy impact strength	KJ/m²	10	23	25	32
Glass Transition / DSC					
Tg1	℃	63	70	86	90
Tg1 max.	℃				90

*AT : Ambient Temperature.

Appendix A-2: Mechanical properties of Sicomin SR8100 epoxy with Sicomin SD8824

Mechanical properties on cast resin

Systems	Units	SR 8100 / SD 8822		SR 8100 / SD 8824	
Curing cycles		24 h @ AT + 24 h 40 °C	24 h @ AT + 16 h 60 °C	24 h @ AT + 24 h 40 °C	24 h @ AT + 8 h 60 °C
Tension					
Modulus of elasticity	N/mm^2	3000	2650	2700	2400
Maximum resistance	N/mm^2	70	66	60	59
Resistance at break	N/mm^2	63	61	50	50
Elongation at max.load	%	3.3	4.1	3.2	3.9
Elongation at break	%	3.8	5.5	3.8	5.9
Flexion					
Modulus of elasticity	N/mm^2	3390	3060	2970	2850
Maximum resistance	N/mm^2	115	120	108	106
Elongation at max.load	%	3.9	5.6	4.9	5.7
Elongation at break	%	5.8	9	11.8	12
Charpy impact strength	kJ/m^2	19	27	52	52
Water absorption 48 h / 70 °C	%	1.2	1.1	1.2	1.2
Glass Transition / DSC					
Tg1	°C	66	80	63	74
Tg1 max.	°C		90		81

*AT : Ambient Temperature.

Appendix A-3: The polishing process by using BUEHLER device

	Force (N)	Time(min.)	r.p.m
Grinding (SiC Grade)			
320	30	3	400
400	30	3	400
600	30	3	400
800	30	3	400
1200	20	3	400
Polishing Grade (µm)			
15	**By hand**	3	400
6	**By hand**	3	400
1	**By hand**	3	400

Appendix B1: Selective images taken during testing and production of laminates and the mechanical test samples.

Figure B1-1: Casting the samples (from the infusion and RTM laminates) for image analysis.

Figure B1-2: The travel microscope with the electro-pulse machine.
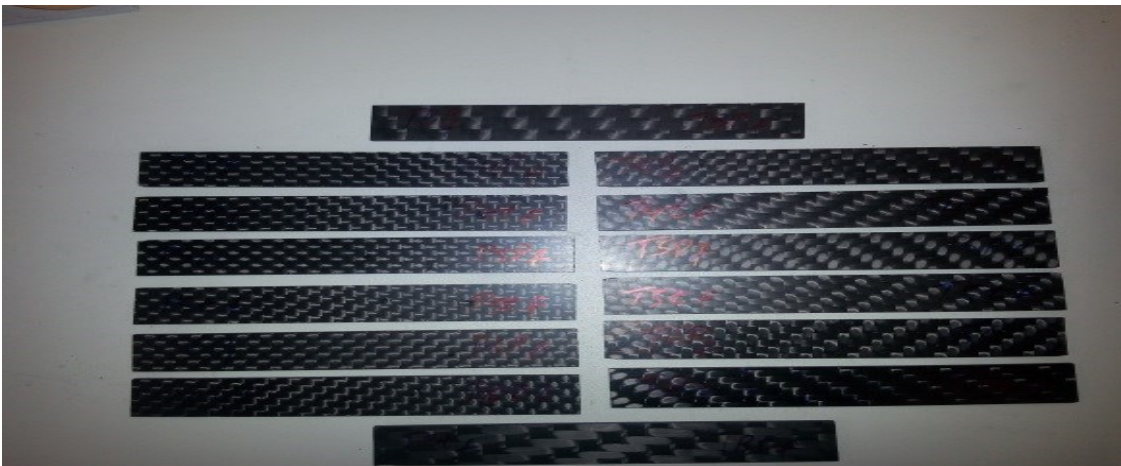
Figure B1-3: The RTM samples for the flexural loading.

Figure B1-4: The X-ray tomograph (Micro CT) scanner for nondestructive three-

dimensional microscopy.
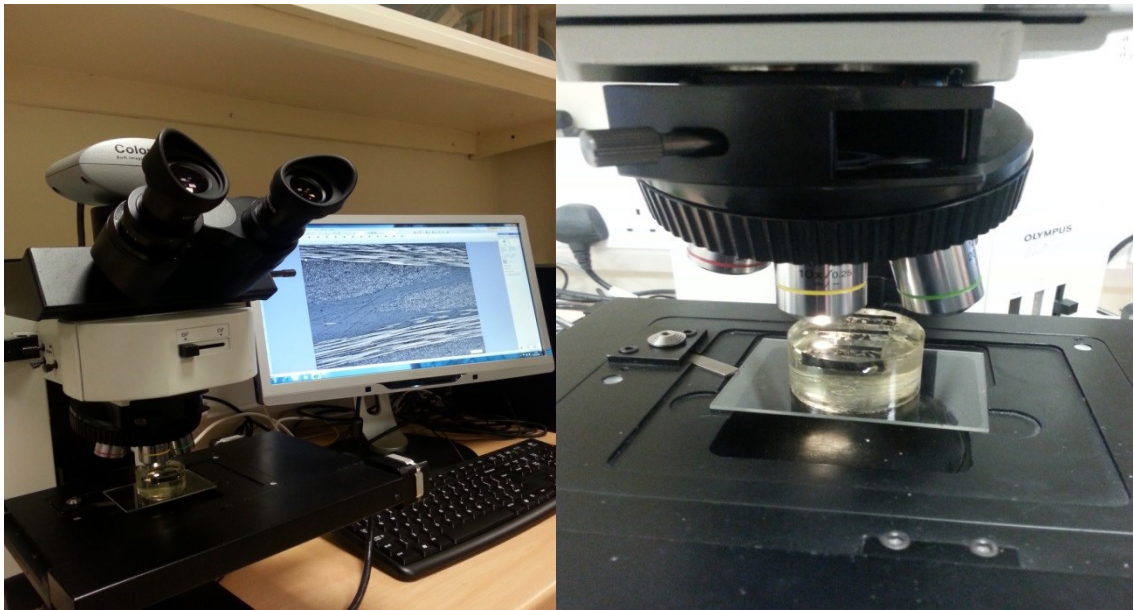
Figure B1-5: The capturing of the microstructure images by using the Olympus BX60 microscope with Olympus Stream image analysis software (SM04733).
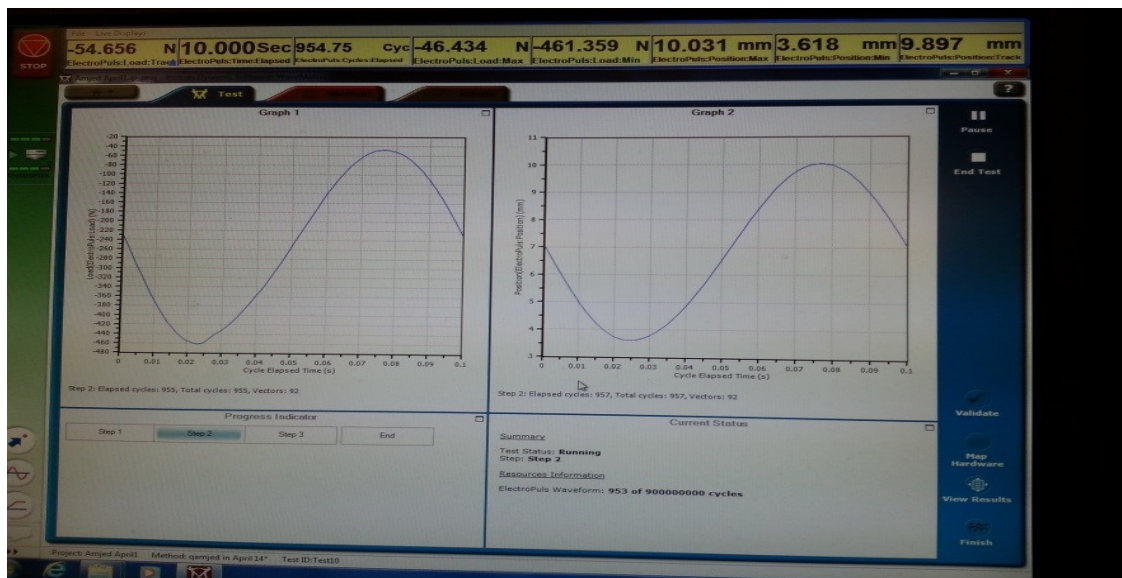
Figure B1-6: The sine wave fatigue loadings of the electro-pulse machine.

References

1. Holmes, M., Global carbon fibre market remains on upward trend. Reinforced Plastics, 2014. 58(6): p. 38-45.

2. Toll, S. and J. A. E. Manson, Elastic Compression of a Fiber Network. Journal of Applied Mechanics, 1995. 62(1): p. 223-226.

3. Toll, S. and J. A. Månson. An analysis of the compressibility of fibre assemblies. in 6th Int. Conf. Fibre Reinf. Compos. 1994.

4. Pearce, N. and J. Summerscales, The compressibility of a reinforcement fabric. Composites Manufacturing, 1995. 6(1): p. 15-21.

5. Toll, S., Packing mechanics of fiber reinforcements. Polymer Engineering & Science, 1998. 38(8): p. 1337-1350.

6. Abraham, D., S. Matthews, and R. McIlhagger, A comparison of physical properties of glass fibre epoxy composites produced by wet lay-up with autoclave consolidation and resin transfer moulding. Composites Part A: Applied Science and Manufacturing, 1998. 29(7): p. 795-801.

7. Botelho, E., Rezende, M., Mayer, S. and Voorwald, H, Evaluation of fatigue behavior on repaired carbon fiber/epoxy composites. Journal of Materials Science, 2008. 43(9): p. 3166-3172.

8. Böger, L., Sumfleth, J., Hedemann, H. and Schulte, K., Improvement of fatigue life by incorporation of nanoparticles in glass fibre reinforced epoxy. Composites Part A: Applied Science and Manufacturing, 2010. 41(10): p. 1419-1424.

9. Blanco, N., Gamstedt, E. K., Asp, L. E. and Costa, J., Mixed-mode delamination growth in carbon–fibre composite laminates under cyclic loading. International Journal of Solids and Structures, 2004. 41(15): p. 4219-4235.

10. Passipoularidis, V.A., T.P. Philippidis, and P. Brondsted, Fatigue life prediction in composites using progressive damage modelling under block and spectrum loading. International Journal of Fatigue, 2011. 33(2): p. 132-144.

11. Epaarachchi, J.A. and P.D. Clausen, An empirical model for fatigue behavior prediction of glass fibre-reinforced plastic composites for various stress ratios and test frequencies. Composites Part A: Applied Science and Manufacturing, 2003. 34(4): p. 313-326.

12. Andersson, B., A. Sjögren, and L. Berglund, Micro- and meso-level residual stresses in glass-fiber/vinyl-ester composites. Composites Science and Technology, 2000. 60(10): p. 2011-2028.

13. Guild, F.J. and J. Summerscales, Microstructural image analysis applied to fibre composite materials: a review. Composites, 1993. 24(5): p. 383-393.

14. Schell, J.S.U., Renggli, M., Van Lenthe, G. H., Muller, R. and Ermanni, P., Micro-computed tomography determination of glass fibre reinforced polymer meso-structure. Composites Science and Technology, 2006. 66(13): p. 2016-2022.

15. Snozzi, L., A. Caballero, and J.-F. Molinari, Influence of the meso-structure in dynamic fracture simulation of concrete under tensile loading. Cement and Concrete Research, 2011. 41(11): p. 1130-1142.

16. Lomov, S.V., Ivanov, D., S., Verspoest, I., Zako, M., Kurashiki, T., Nakai, H. and Hirosawa, S., Meso-FE modelling of textile composites: Road map, data flow and algorithms. Composites Science and Technology, 2007. 67(9): p. 1870-1891.

17. Boisse, P., Buet, K., Gasser, A. and Launay, J., Meso/macro-mechanical behaviour of textile reinforcements for thin composites. Composites Science and Technology, 2001. 61(3): p. 395-401.

18. Sudarisman and I.J. Davies, The effect of processing parameters on the flexural properties of unidirectional carbon fibre-reinforced polymer (CFRP) composites. Materials Science and Engineering: A, 2008. 498(1-2): p. 65-68.

19. Davies, L. W., Day, R. J., Bond, D., Nesbitt, A., Ellis, J. and Gardon, E, Effect of cure cycle heat transfer rates on the physical and mechanical properties of an epoxy matrix composite. Composites Science and Technology, 2007. 67(9): p. 1892-1899.

20. Potter, K., Khan, B., Wisnom, M., Bell, T. and Stevens, J, Variability, fibre waviness and misalignment in the determination of the properties of composite materials and structures. Composites Part A: Applied Science and Manufacturing, 2008. 39(9): p. 1343-1354.

21. Williams, G., R. Trask, and I. Bond, A self-healing carbon fibre reinforced polymer for aerospace applications. Composites Part A: Applied Science and Manufacturing, 2007. 38(6): p. 1525-1532.

22. Xu, Y. and S.V. Hoa, Mechanical properties of carbon fiber reinforced epoxy/clay nanocomposites. Composites Science and Technology, 2008. 68(3–4): p. 854-861.

23. Herring, M.L. and B.L. Fox, The effect of a rapid curing process on the surface finish of a carbon fibre epoxy composite. Composites Part B: Engineering, 2011. 42(5): p. 1035-1043.

24. Costa, M.L., S.F.M.d. Almeida, and M.C. Rezende, The influence of porosity on the interlaminar shear strength of carbon/epoxy and carbon/bismaleimide fabric laminates. Composites Science and Technology, 2001. 61(14): p. 2101-2108.

25. Chensong, D., Model development for the formation of resin-rich zones in composites processing. Composites Part A: Applied Science and Manufacturing, 2011. 42(4): p. 419-424.

26. Cartié, D.D.R., M. Troulis, and I.K. Partridge, Delamination of Z-pinned carbon fibre reinforced laminates. Composites Science and Technology, 2006. 66(6): p. 855-861.

27. Holmberg, J.A. and L.A. Berglund, Manufacturing and performance of RTM U-beams. Composites Part A: Applied Science and Manufacturing, 1997. 28(6): p. 513-521.

28. Mahadik, Y., K.A.R. Brown, and S.R. Hallett, Characterisation of 3D woven composite internal architecture and effect of compaction. Composites Part A: Applied Science and Manufacturing, 2010. 41(7): p. 872-880.

29. Hale, R.D., An experimental investigation into strain distribution in 2D and 3D textile composites. Composites Science and Technology, 2003. 63(15): p. 2171-2185.

30. Bannister, M., Herszberg, I., Nicolaidis, A., Coman, F. and Leong, K. H, The manufacture of glass/epoxy composites with multilayer woven architectures. Composites Part A: Applied Science and Manufacturing, 1998. 29(3): p. 293-300.

31. Callus, P. J., Mouritz, A. P., Bannister, M. K. & Leong, K. H, Tensile properties and failure mechanisms of 3D woven GRP composites. Composites Part A: Applied Science and Manufacturing, 1999. 30(11): p. 1277-1287.

32. Mouritz, A.P., K.H. Leong, and I. Herszberg, A review of the effect of stitching on the in-plane mechanical properties of fibre-reinforced polymer composites. Composites Part A: Applied Science and Manufacturing, 1997. 28(12): p. 979-991.

33. Aymerich, F., P. Priolo, and C.T. Sun, Static and fatigue behaviour of stitched graphite/epoxy composite laminates. Composites Science and Technology, 2003. 63(6): p. 907-917.

34. Truong, T. C., Vettori, M., Lomov, S. and Verpoest, I, Carbon composites based on multi-axial multi-ply stitched preforms. Part 4. Mechanical properties of composites and damage observation. Composites Part A: Applied Science and Manufacturing, 2005. 36(9): p. 1207-1221.

35. Garschke, C., Weimer, C., Parlevliet, P. P. and Fox, B. L, Out-of-autoclave cure cycle study of a resin film infusion process using in situ process monitoring.

Composites Part A: Applied Science and Manufacturing, 2012. 43(6): p. 935-944.

36. Mikhaluk, D. S., Truong, T. C., Borovkov, A. I., Lomov, S. V. and Verpoest, I, Experimental observations and finite element modelling of damage initiation and evolution in carbon/epoxy non-crimp fabric composites. Engineering Fracture Mechanics, 2008. 75(9): p. 2751-2766.

37. Liotier, P.-J., V. Alain, and D. Christine, Characterization of 3D morphology and microcracks in composites reinforced by multi-axial multi-ply stitched preforms. Composites Part A: Applied Science and Manufacturing, 2010. 41(5): p. 653-662.

38. Liotier, P. J., A. Vautrin, and J. M. Beraud, Microcracking of composites reinforced by stitched multiaxials subjected to cyclical hygrothermal loadings. Composites Part A: Applied Science and Manufacturing, 2011. 42(4): p. 425-437.

39. Beier, U., Fischer, F., Sandler, J. K. W., Altstädt, V., Weimer, C. and Buchs, W, Mechanical performance of carbon fibre-reinforced composites based on stitched preforms. Composites Part A: Applied Science and Manufacturing, 2007. 38(7): p. 1655-1663.

40. Tan, K.T., N. Watanabe, and Y. Iwahori, X-ray radiography and micro-computed tomography examination of damage characteristics in stitched composites subjected to impact loading. Composites Part B: Engineering, 2011. 42(4): p. 874-884.

41. Bull, D.J., et al., A comparison of multi-scale 3D X-ray tomographic inspection techniques for assessing carbon fibre composite impact damage. Composites Science and Technology, 2013. 75(0): p. 55-61.

42. Hayes, B.S., B.S. Hayes, and L.M. Gammon, Optical Microscopy of Fiber-Reinforced Composites. 2010: ASM international.

43. Summerscales, J., Microstructural characterisation of fibre-reinforced composites. 1998: Woodhead Publishing.

44. Summerscales, J., Guild, FJ., Pearce, NR. and Russell, PM, Voronoi cells, fractal dimensions and fibre composites. Journal of Microscopy, 2001. 201(2): p. 153-162.

45. Summerscales, J., D. Green, and F.J. Guild, Effect of processing dwell-time on the microstructure of a fibre-reinforced composite. Journal of Microscopy, 1993. 169(2): p. 173-182.

46. Griffin, P. R., S. M. Grove, F. J. Guild, P. Russell and J. Summerscales, The effect of microstructure on flow promotion in resin transfer moulding reinforcement fabrics. Journal of Microscopy, 1995. 177(3): p. 207-217.

47. Griffin, P. R., S. M. Grove, P. Russell, D. Short and J. Summerscales, The effect of reinforcement architecture on the long-range flow in fibrous reinforcements. Composites Manufacturing, 1995. 6(3-4): p. 221-235.

48. Pearce, N.R.L., F.J. Guild, and J. Summerscales, An investigation into the effects of fabric architecture on the processing and properties of fibre reinforced composites produced by resin transfer moulding. Composites Part A: Applied Science and Manufacturing, 1998. 29(1-2): p. 19-27.

49. Pearce, N.R.L., F.J. Guild, and J. Summerscales, The use of automated image analysis for the investigation of fabric architecture on the processing and properties of fibre-reinforced composites produced by RTM. Composites Part A: Applied Science and Manufacturing, 1998. 29(7): p. 829-837.

50. Canal, L. P., González, C., Molina-Aldareguía, J. M., Segurado, J. and Llorca, J, Application of digital image correlation at the microscale in fiber-reinforced composites. Composites Part A: Applied Science and Manufacturing, 2012(0).

51. Santulli, C., Gil, R. G., Long, A. and Clifford, M, Void content measurements in commingled E-glass/polypropylene composites using image analysis from optical micrographs. Science and Engineering of Composite Materials, 2002. 10(2): p. 77-90.

52. Stone, D. and B. Clarke, Ultrasonic attenuation as a measure of void content in carbon-fibre reinforced plastics. Non-destructive testing, 1975. 8(3): p. 137-145.

53. Mayr, G. Plank, B. Sekelja, J. and Hendorfer, G.,, Active thermography as a quantitative method for non-destructive evaluation of porous carbon fiber reinforced polymers. NDT & E International, 2011. 44(7): p. 537-543.

54. Judd, N.C.W. and W. Wright, Voids and their effects on the mechanical properties of composites- an appraisal. Sampe Journal, 1978. 14: p. 10-14.

55. Ghiorse, S., Effect of void content on the mechanical properties of carbon/epoxy laminates. SAMPE quarterly, 1993. 24(2): p. 54-59.

56. Purslow, D., On the optical assessment of the void content in composite materials. Composites, 1984. 15(3): p. 207-210.

57. Stringer, L.G., Optimization of the wet lay-up/vacuum bag process for the fabrication of carbon fibre epoxy composites with high fibre fraction and low void content. Composites, 1989. 20(5): p. 441-452.

58. Iarve, E. V., Mollenhauer, D. H., Zhou, E. G., Breitzman, T. and Whitney, T. J, Independent mesh method-based prediction of local and volume average fields in textile composites. Composites Part A: Applied Science and Manufacturing, 2009. 40(12): p. 1880-1890.

59. Singh, S. and I.K. Partridge, Mixed-mode fracture in an interleaved carbon-fibre/epoxy composite. Composites Science and Technology, 1995. 55(4): p. 319-327.

60. Chambers, A.R., et al., The effect of voids on the flexural fatigue performance of unidirectional carbon fibre composites developed for wind turbine applications. International Journal of Fatigue, 2006. 28(10): p. 1389-1398.

61. Truong, T. C., Ivanov, D. S., Klimshin, D. V., Lomov, S. V. & Verpoest, I, Carbon composites based on multi-axial multi-ply stitched preforms. Part 7: Mechanical properties and damage observations in composites with sheared reinforcement. Composites Part A: Applied Science and Manufacturing, 2008. 39(9): p. 1380-1393.

62. Chandrasekaran, V.C.S., S.G. Advani, and M.H. Santare, Influence of resin properties on interlaminar shear strength of glass/epoxy/MWNT hybrid composites. Composites Part A: Applied Science and Manufacturing, 2011. 42(8): p. 1007-1016.

63. Yudhanto, A., Watanabe, N., Iwahori, Y. and Hoshi, H, The effects of stitch orientation on the tensile and open hole tension properties of carbon/epoxy plain weave laminates. Materials & Design, 2012(0).

64. Dyer, K.P. and D.H. Isaac, Fatigue behaviour of continuous glass fibre reinforced composites. Composites Part B: Engineering, 1998. 29(6): p. 725-733.

65. Kim, K. Y. and L. Ye, Interlaminar fracture toughness of CF/PEI composites at elevated temperatures: roles of matrix toughness and fibre/matrix adhesion. Composites Part A: Applied Science and Manufacturing, 2004. 35(4): p. 477-487.

66. Liang, S., P.-B. Gning, and L. Guillaumat, Properties evolution of flax/epoxy composites under fatigue loading. International Journal of Fatigue, 2014. 63(0): p. 36-45.

67. Basford, D. M., P. R. Griffin, S.M. Grove and J. Summerscales, Relationship between mechanical performance and microstructure in composites fabricated with flow-enhancing fabrics. Composites, 1995. 26(9): p. 675-679.

68. Aziz, S.H. and M.P. Ansell, The effect of alkalization and fibre alignment on the mechanical and thermal properties of kenaf and hemp bast fibre composites: Part 1 – polyester resin matrix. Composites Science and Technology, 2004. 64(9): p. 1219-1230.

69. Gojny, F. H., M. H. G. Wichmann, B. Fiedler, W. Bauhofer and K. Schulte, Influence of nano-modification on the mechanical and electrical properties of conventional fibre-reinforced composites. Composites Part A: Applied Science and Manufacturing, 2005. 36(11): p. 1525-1535.

70. Tzetzis, D. and P.J. Hogg, Bondline toughening of vacuum infused composite repairs. Composites Part A: Applied Science and Manufacturing, 2006. 37(9): p. 1239-1251.

71. Dhakal, H.N., Z.Y. Zhang, and M.O.W. Richardson, Effect of water absorption on the mechanical properties of hemp fibre reinforced unsaturated polyester composites. Composites Science and Technology, 2007. 67(7–8): p. 1674-1683.

72. Lomov, S. V., Ivanov, D. S., Verpoest, I., Zako, M., Kurashiki, T., Nakai, H., Molimard, J. and Vautrin, A, Full-field strain measurements for validation of meso-FE analysis of textile composites. Composites Part A: Applied Science and Manufacturing, 2008. 39(8): p. 1218-1231.

73. Colin de Verdiere, M., Pickett, A. K., Skordos, A. A. and Witzel, V, Evaluation of the mechanical and damage behaviour of tufted non crimped fabric composites using full field measurements. Composites Science and Technology, 2009. 69(2): p. 131-138.

74. Liu, R. M. and D. K. Liang, Experimental study of carbon fiber reinforced plastic with embedded optical fibers. Materials & Design, 2010. 31(2): p. 994-998.

75. Heß, H. and N. Himmel, Structurally stitched NCF CFRP laminates. Part 2: Finite element unit cell based prediction of in-plane strength. Composites Science and Technology, 2011. 71(5): p. 569-585.

76. Vaughan, T.J. and C.T. McCarthy, A micromechanical study on the effect of intra-ply properties on transverse shear fracture in fibre reinforced composites. Composites Part A: Applied Science and Manufacturing, 2011. 42(9): p. 1217-1228.

77. Jeong, H. and D.K. Hsu, Experimental analysis of porosity-induced ultrasonic attenuation and velocity change in carbon composites. Ultrasonics, 1995. 33(3): p. 195-203.

78. Demers, C.E., Tension–tension axial fatigue of E-glass fiber-reinforced polymeric composites: fatigue life diagram. Construction and Building Materials, 1998. 12(5): p. 303-310.

79. Kalam, A., et al., Fatigue behaviour of oil palm fruit bunch fibre/epoxy and carbon fibre/epoxy composites. Composite Structures, 2005. 71(1): p. 34-44.

80. Kawai, M., Yajima, S., Hachinohe, A. and Kawase, Y., High-temperature off-axis fatigue behaviour of unidirectional carbon-fibre-reinforced composites with different resin matrices. Composites Science and Technology, 2001. 61(9): p. 1285-1302.

81. Ferreira, J.A.M., Costa, J. D. M., Reis, P. N. B. and Richardson, M. O. W., Analysis of fatigue and damage in glass-fibre-reinforced polypropylene

composite materials. Composites Science and Technology, 1999. 59(10): p. 1461-1467.

82. Bertin, M., F. Touchard, and M.-C. Lafarie-Frenot, Experimental study of the stacking sequence effect on polymer/composite multi-layers submitted to thermomechanical cyclic loadings. International Journal of Hydrogen Energy, 2010. 35(20): p. 11397-11404.

83. De Monte, M., E. Moosbrugger, and M. Quaresimin, Influence of temperature and thickness on the off-axis behaviour of short glass fibre reinforced polyamide 6.6 – cyclic loading. Composites Part A: Applied Science and Manufacturing, 2010. 41(10): p. 1368-1379.

84. Ferreira, J.A.M., J.D.M. Costa, and P.N.B. Reis, Static and fatigue behaviour of glass-fibre-reinforced polypropylene composites. Theoretical and Applied Fracture Mechanics, 1999. 31(1): p. 67-74.

85. Fuqiang, W. and Y. Weixing, A Model of the Fatigue Life Distribution of Composite Laminates Based on Their Static Strength Distribution. Chinese Journal of Aeronautics, 2008. 21(3): p. 241-246.

86. Caprino, G. and A. D'Amore, Flexural fatigue behaviour of random continuous-fibre-reinforced thermoplastic composites. Composites Science and Technology, 1998. 58(6): p. 957-965.

87. Epaarachchi, J.A., Effects of static–fatigue (tension) on the tension–tension fatigue life of glass fibre reinforced plastic composites. Composite Structures, 2006. 74(4): p. 419-425.

88. Clark, S.D., R.A. Shenoi, and H.G. Allen, Modelling the fatigue behaviour of sandwich beams under monotonic, 2-step and block-loading regimes. Composites Science and Technology, 1999. 59(4): p. 471-486.

89. Mao, H. and S. Mahadevan, Fatigue damage modelling of composite materials. Composite Structures, 2002. 58(4): p. 405-410.

90. Degrieck, J. and W. Van Paepegem, Fatigue damage modeling of fibre-reinforced composite materials: review. Applied Mechanics Reviews, 2001. 54(4): p. 279-300.

91. Abbadi, A., Azari, Z., Belouettar, S., Gilgert, P. and Freres, P., Modelling the fatigue behaviour of composites honeycomb materials (aluminium/aramide fibre core) using four-point bending tests. International Journal of Fatigue, 2010. 32(11): p. 1739-1747.

92. Li, H., Huang, Y., Chen, W. L., Ma, M. L., Tao, D. W. and Ou, J. P., Estimation and Warning of Fatigue Damage of FRP Stay Cables Based on Acoustic Emission Techniques and Fractal Theory. Computer-Aided Civil and Infrastructure Engineering, 2011. 26(7): p. 500-512.

93. Adden, S. and P. Horst, Stiffness degradation under fatigue in multiaxially loaded non-crimped-fabrics. International Journal of Fatigue, 2010. 32(1): p. 108-122.

94. Ferreira, J.A.M., J.D.M. Costa, and M.O.W. Richardson, Effect of notch and test conditions on the fatigue of a glass-fibre-reinforced polypropylene composite. Composites Science and Technology, 1997. 57(9–10): p. 1243-1248.

95. Gude, M., W. Hufenbach, and I. Koch, Damage evolution of novel 3D textile-reinforced composites under fatigue loading conditions. Composites Science and Technology, 2010. 70(1): p. 186-192.

96. Gagel, A., D. Lange, and K. Schulte, On the relation between crack densities, stiffness degradation, and surface temperature distribution of tensile fatigue loaded glass-fibre non-crimp-fabric reinforced epoxy. Composites Part A: Applied Science and Manufacturing, 2006. 37(2): p. 222-228.

97. Harris, B., *Fatigue in composites: science and technology of the fatigue response of fibre-reinforced plastics*. 2003: Woodhead Publishing.

98. Wu, F. and W. Yao, A fatigue damage model of composite materials. International Journal of Fatigue, 2010. 32(1): p. 134-138.

99. Baron, C., K. Schulte, and H. Harig, Influence of fibre and matrix failure strain on static and fatigue properties of carbon fibre-reinforced plastics. Composites Science and Technology, 1987. 29(4): p. 257-272.

100. Bizeul, M., Bouvet, C., Barrau, J. J. and Cuenca, R., Fatigue crack growth in thin notched woven glass composites under tensile loading. Part II: Modelling. Composites Science and Technology, 2011. 71(3): p. 297-305.

101. Quaresimin, M., L. Susmel, and R. Talreja, Fatigue behaviour and life assessment of composite laminates under multiaxial loadings. International Journal of Fatigue, 2010. 32(1): p. 2-16.

102. Azouaoui, K., Z. Azari, and G. Pluvinage, Evaluation of impact fatigue damage in glass/epoxy composite laminate. International Journal of Fatigue, 2010. 32(2): p. 443-452.

103. Pitchumani, R. and B. Ramakrishnan, A fractal geometry model for evaluating permeabilities of porous preforms used in liquid composite molding. International journal of heat and mass transfer, 1999. 42(12): p. 2219-2232.

104. Campos, K.A.d., Augusto, J. Pereira, T. A. and Hein, L. R. D. O., 3-D reconstruction by extended depth-of-field in failure analysis – Case study II: Fractal analysis of interlaminar fracture in carbon/epoxy composites. Engineering Failure Analysis, 2012. 25(0): p. 271-279.

105. Worrall, C. and G. Wells. Fiber distribution in discontinuous fiber reinforced plastics: characterization and effect of material performance. in ECCM-7:

Seventh European Conference on Composite Materials. Realising Their Commercial Potential. 1996.

106. Pearce, N.R.L., J. Summerscales, and F.J. Guild, Improving the resin transfer moulding process for fabric-reinforced composites by modification of the fabric architecture. Composites Part A: Applied Science and Manufacturing, 2000. 31(12): p. 1433-1441.

107. Summerscales, J., Russell, P. M., Lomov, S. V., Verpoest, I. and Parnas, R. S., The fractal dimension of X-ray tomographic sections of a woven composite. Advanced composites letters, 2004. 13(2): p. 113-121.

108. Picu, R. C., Li, Z., Soare, M. A., Sorohan, S., Constantinescu, D. M. and Nutu, E., Composites with fractal microstructure: The effect of long range correlations on elastic–plastic and damping behavior. Mechanics of Materials, 2014. 69(1): p. 251-261.

109. Gao, S. L., E. Mäder, and S.F. Zhandarov, Carbon fibers and composites with epoxy resins: Topography, fractography and interphases. Carbon, 2004. 42(3): p. 515-529.

110. Allen, M., G.J. Brown, and N.J. Miles, Measurement of boundary fractal dimensions: review of current techniques. Powder Technology, 1995. 84(1): p. 1-14.

111. Celli, A., Tucci, A., Espostio, L. and Palmonari, C., Fractal analysis of cracks in alumina–zirconia composites. Journal of the European Ceramic Society, 2003. 23(3): p. 469-479.

112. Biancolini, M.E., Brutti, C., Paparo, G. and Zanini, A., Fatigue cracks nucleation on steel, acoustic emission and fractal analysis. International Journal of Fatigue, 2006. 28(12): p. 1820-1825.

113. Kuznetsov, P.V., V.E. Panin, and J. Schreiber, Fractal dimension as a characteristic of deformation stages of austenite stainless steel under tensile load. Theoretical and Applied Fracture Mechanics, 2001. 35(2): p. 171-177.

114. Venkatesh, B., D.L. Chen, and S.D. Bhole, Three-dimensional fractal analysis of fracture surfaces in a titanium alloy for biomedical applications. Scripta materialia, 2008. 59(4): p. 391-394.

115. Wang, L., L. D. Wang, and W. D. Fei, Fractal analysis of fracture surfaces in aluminum borate whisker-reinforced aluminum alloy 6061 composite. Transactions of Nonferrous Metals Society of China, 2011. 21(3): p. 461-466.

116. Yuan, C. Q., Li, J., Yan, X. P. and Peng, Z., The use of the fractal description to characterize engineering surfaces and wear particles. Wear, 2003. 255(1–6): p. 315-326.

117. Pimenta, S. and S.T. Pinho, An analytical model for the translaminar fracture toughness of fibre composites with stochastic quasi-fractal fracture surfaces. Journal of the Mechanics and Physics of Solids, 2014. 66: p. 78-102.

118. Aniszewska, D. and M. Rybaczuk, Fractal characteristics of defects evolution in parallel fibre reinforced composite in quasi-static process of fracture. Theoretical and Applied Fracture Mechanics, 2009. 52(2): p. 91-95.

119. Mishnaevsky, L., Hierarchical composites: Analysis of damage evolution based on fiber bundle model. Composites Science and Technology, 2011. 71(4): p. 450-460.

120. Summerscales, J., Griffin, P. R. and Grove, S. M., Quantitative microstructural examination of RTM fabrics designed for enhanced flow. Composite Structures, 1995. 32(1-4): p. 519-529.

121. Mishnaevsky Jr, L., Hierarchical composites: Analysis of damage evolution based on fiber bundle model. Composites Science and Technology, 2011. 71(4): p. 450-460.

122. Foroutan-Pour, K., P. Dutilleul, and D. Smith, Advances in the implementation of the box-counting method of fractal dimension estimation. Applied Mathematics and Computation, 1999. 105(2): p. 195-210.

123. Buczkowski, S., Kyriacos, S., Nekka, F. and Cartilier, L., The modified box-counting method: analysis of some characteristic parameters. Pattern Recognition, 1998. 31(4): p. 411-418.

124. Li, J., Q. Du, and C. Sun, An improved box-counting method for image fractal dimension estimation. Pattern Recognition, 2009. 42(11): p. 2460-2469.

125. Chen, S.S., J.M. Keller, and R.M. Crownover, On the calculation of fractal features from images. Pattern Analysis and Machine Intelligence, IEEE Transactions on, 1993. 15(10): p. 1087-1090.

126. Jin, X. and S. Ong. Scale limits in estimating fractal dimensions of image surfaces. in Networks, 1993. International Conference on Information Engineering'93.'Communications and Networks for the Year 2000', Proceedings of IEEE Singapore International Conference on. 1993. IEEE.

127. Buczkowski, S., P. Hildgen, and L. Cartilier, Measurements of fractal dimension by box-counting: a critical analysis of data scatter. Physica A: Statistical Mechanics and its Applications, 1998. 252(1–2): p. 23-34.

128. Lacovara, B., Considering Resin Transfer Molding. Composites Fabrication Association S, 1995. 199.

129. Correia, N.C., Robitaille, F., Long. A. C., Rudd, C. D., Simacek, P. and Advani, S. G., Analysis of the vacuum infusion moulding process: I. Analytical

formulation. Composites Part A: Applied Science and Manufacturing, 2005. 36(12): p. 1645-1656.

130. Williams, C., J. Summerscales, and S. Grove, Resin Infusion under Flexible Tooling (RIFT): a review. Composites Part A: Applied Science and Manufacturing, 1996. 27(7): p. 517-524.

131. Williams, C.D., S.M. Grove, and J. Summerscales, The compression response of fibre-reinforced plastic plates during manufacture by the resin infusion under flexible tooling method. Composites Part A: Applied Science and Manufacturing, 1998. 29(1–2): p. 111-114.

132. Kim, D. W., An, Y. S., Nam, J. D. and Kim, S. W., Thermoplastic film infusion process for long-fiber reinforced composites using thermally expandable elastomer tools. Composites Part A: Applied Science and Manufacturing, 2003. 34(7): p. 673-680.

133. Woraratpanya, K., D. Kakanopas, and R. Varakulsiripunth, Triangle-box Counting Method for Fractal Dimension Estima-tion. ASEAN Engineering Journal Part D: p. 5-16.

134. FERABOLI, P.J. and K.T. KEDWARD. In search of the true interlaminar shear strength. in Nineteenth technical conference of the joint American society for composites/American society for testing and materials committee D.

135. Curtis, P., CRAG test methods for the measurement of the engineering properties of fibre reinforced plastics. 1988: Royal Aerospace Establishment.

136. Liang, S., P.B. Gning, and L. Guillaumat, A comparative study of fatigue behaviour of flax/epoxy and glass/epoxy composites. Composites Science and Technology, 2012. 72(5): p. 535-543.

137. Fibre reinforced plastics – determination of fatigue properties under cyclic loading conditions. BS ISO. 13003:2003.

138. Chawla, N., Tur, Y. K., Holmes, J. W. and Barber, J. R., High-Frequency Fatigue Behavior of Woven-Fiber-Fabric-Reinforced Polymer-Derived Ceramic-Matrix Composites. Journal of the American Ceramic Society, 1998. 81(5): p. 1221-1230.

139. Shuler, S.F., Holmes, J. W., Wu, X. and Roach, D., Influence of Loading Frequency on the Room-Temperature Fatigue of a Carbon-Fiber/SiC-Matrix Composite. Journal of the American Ceramic Society, 1993. 76(9): p. 2327-2336.

140. Staehler, J.M., S. Mall, and L.P. Zawada, Frequency dependence of high-cycle fatigue behavior of CVI C/SiC at room temperature. Composites Science and Technology, 2003. 63(15): p. 2121-2131.

141. Sun, C. and W. Chan. Frequency effect on the fatigue life of a laminated composite. in Composite Materials: Testing and Design (Fifth Conference), ASTM STP. 1979.

142. Natural Frequencies for Common Systems, University of Massachusetts Lowell, Modal Analysis and Controls Laboratory M A C L, http://faculty.uml.edu/pavitabile/22.403/web_downloads/Frequencies_of_Common_Systems.PDF.

143. Zheng, D., Cheung, Y. K., Au, F. T. K. and Cheng, Y. S., Vibration of multi-span non-uniform beams under moving loads by using modified beam vibration functions. Journal of Sound and Vibration, 1998. 212(3): p. 455-467.

144. Lee, S. H., H. Noguchi, and S.-K. Cheong, Tensile properties and fatigue characteristics of hybrid composites with non-woven carbon tissue. International Journal of Fatigue, 2002. 24(2-4): p. 397-405.

145. McDonald, J.H., Handbook of biological statistics. Vol. 2. 2009: Sparky House Publishing Baltimore, MD.

146. Dobson, A.J. and A. Barnett, An introduction to generalized linear models. 2011: CRC press.

147. Jim Frost, The Minitab Blog, 2013. Available from: http://blog.mimitab.com/blog/ adventures-in-statistics/regression-analysis-how-do-i-interpret-r-squared-and-assess-the-goodness-of-fit.

148. McDonald, J.H., Handbook of Biological Statistics (3rd ed.). Sparky House Publishing, Baltimore, Maryland., 2014.

149. Krehbiel, T.C., Correlation Coefficient Rule of Thumb. Decision Sciences Journal of Innovative Education, 2004. 2(1): p. 97-100.

150. Rice, W.R., Analyzing tables of statistical tests. Evolution, 1989: p. 223-225.